Sophie Honeder, BSc.

Activity-based proteomics: Revealing the compensatory mechanisms of an enzyme group upon activity changes of an individual enzyme

MASTER'S THESIS

to achieve the university degree of

Master of Science

Master's degree programme: Biochemistry and Molecular Biomedical Sciences

submitted to

Graz University of Technology

Supervisor

Assoz. Prof. Priv.-Doz.in Dipl.-Ing.in Dr.in. techn., Ruth Birner-Grünberger

Institute of Pathology

Medical University of Graz

Graz, September 2019

AFFIDAVIT

I declare that I have authored this thesis independently, that I have not used other than the declared sources/resources, and that I have explicitly marked all material which has been quoted either literally or by content from the sources used. The text document uploaded to TUGRAZonline is identical to the present master's thesis.

Date	Signature

Acknowledgements

First and foremost, I want to express deep gratitude to my supervisor and mentor Ruth, whose enthusiasm for science and love for life is contagious. She is not only a good and encouraging supervisor but also a great person and without question the best captain ever!

My greatest appreciation goes to the rest of the proteomics pirates, who are not only really cool people that make work a fun place, but also great scientists with lots of enthusiasm and knowledge to learn from.

I would particularly like to thank Babsi for being so patient and helpful with the topic that finally led to this thesis; Laura for her constant help and knowledge with pretty much anything concerning our lab; Jürgen for all the jokes and his help during several experiments; Christoph for the kind and patient introduction when I joined the lab; Matthias for his enthusiasm and brainstorming concerning my project amongst many things; Petra for the willingness to help and the useful input; Stefan for constantly repairing all the broken things and generating very useful tools; and Tamara for the patient guidance, her knowledge and all the helpful things she shared throughout my time in this lab – and to everyone for all the fun times and the laughter we've shared.

I want to express my gratitude to all my old as well as all the newly won friends here in Graz, who have made this time during my Master's more fun than I could have asked for. Thank you for contributing to and marking this as a very special and memorable time in my life. Additionally, I owe the utmost gratitude to all my close friends from elsewhere - friends who are there in fun times but who are also the ones that are there to pick you up when you are down.

Above all, my most heartfelt appreciation goes to my supporting and loving family, who don't fail to cheer me up when I am visiting; who have always supported me and had my back - no matter what; they have always believed in and encouraged me.

Thank You

Abstract

Lung cancer is the leading cause of cancer-related deaths worldwide and thus constitutes a severe problem of our time. As an emerging cancer hallmark altered lipid metabolism has gained in importance in recent years. In addition to the well-studied role of changes in fatty acid metabolism in cancer, the dysregulation of lipolysis has recently emerged as a novel cancer characteristic. The major triacylglycerol (TAG) hydrolase adipose triglyceride lipase (ATGL) has been associated with tumor initiation in lung tissue in mice. In recent years, ATGL has been ascribed a tumor suppressor role and several groups have investigated its role and effects in human cancers. Lack of ATGL in lung carcinoma cells causes a change in lipid profile of these cells. In addition to increased levels of TAGs the ATGL impaired lung carcinoma cells also showed higher levels of bioactive lipids such as ether- and lysophospholipids. The increase of these bioactive lipid species cannot be linked to ATGL absence directly, and thus we are investigating and searching for an enzyme that is responsible for this phenotype.

The majority of lipases and several other enzymes important in lipid metabolism belong to the enzyme group of serine hydrolases. Prominent examples are ATGL and other lipolytic enzymes such as monoglyceride lipase (MGL) and hormone sensitive lipase (HSL), all of which are important lipolytic enzymes.

To this end, the serine hydrolase profiles of ATGL impaired lung carcinoma cell lines were investigated by activity-based proteomic profiling (ABPP) in the course of this project. In ABPP small activity-based probes (ABP) are used, which bind specifically to the active site of enzymes that share the same catalytic mechanism.

In this project, ABPP workflows with different components were tested in order to determine the serine hydrolase profiles of ATGL lacking, overexpressing or control cell lines. By using a serine hydrolase-specific ABP together with a specific bio-orthogonal linker (TEV linker), we were able to enrich and detect several serine hydrolases in each of the sample sets. In addition to the successful enrichment of serine hydrolases by ABPP, we discovered a potentially interesting serine hydrolase that was found to be significantly higher abundant in ATGL overexpressing cell lines when compared to ATGL lacking cell lines. These promising results allow for further – targeted – investigation of potentially interesting enzymes.

Zusammenfassung

Lungenkrebs ist die häufigste Ursache für krebsbedingte Todesfälle weltweit und stellt somit ein schwerwiegendes Problem unserer Zeit dar. In den letzten Jahren gewann Fettstoffwechsel immer mehr an Bedeutung in der Krebsforschung. Neben der gut untersuchten Rolle von des Fettsäurestoffwechsels in Krebs hat sich in jüngster Zeit die Veränderung der Lipolyse als neues Krebsmerkmal herausgestellt. Die Triglycerid (TAG) Hydrolase adipose triglycerol lipase (ATGL) wurde mit der Tumorentstehung in Mäuse-Lungengewebe in Verbindung gebracht. In den vergangenen Jahren wurde ATGL eine Rolle als Tumorsuppressor zugeschrieben, und seine Rolle und Wirkung bei menschlichen Krebserkrankungen werden in einigen Gruppen untersucht. Das Fehlen von ATGL in Lungenkarzinomzellen führt zu einer Veränderung des Lipidprofils dieser Zellen. Neben einem erhöhten Gehalt an TAGs zeigten die Lungenkarzinomzellen mit fehlendem ATGL auch einen höheren Gehalt an bioaktiven Lipiden wie beispielsweise Ether- und Lysophospholipiden. Der Anstieg dieser bioaktiven Lipide kann nicht direkt mit der Abwesenheit von ATGL in Verbindung gebracht werden, weshalb wir das Enzym suchen, welches für diesen Phänotyp verantwortlich ist.

Die meisten Lipasen und mehrere andere für den Fettstoffwechsel wichtige Enzyme zählen zur Enzymgruppe der Serin Hydrolasen. Prominente Beispiele sind ATGL selbst und andere lipolytische Enzyme wie monoglyceride lipase (MGL) und hormone sensitive lipase (HSL), die alle wichtige lipolytische Enzyme sind.

Aus diesem Grund wurden die Serin Hydrolasen-Profile von Lungenkrebszelllinien mit mittels activity-based proteomic profiling (ABPP) untersucht. Bei ABPP werden kleine sogenannte „activity-based probes“ (ABP) verwendet, die sich spezifisch an das aktive Zentrum von Enzymen binden, welche den gleichen katalytischen Mechanismus teilen.

In diesem Projekt wurden ABPP-Workflows mit verschiedenen Komponenten getestet, um die Serin Hydrolasen-Profile von Zelllinien mit überexprimierter bzw. fehlender ATGL, sowie Kontroll-Zelllinien zu bestimmen. Durch die Verwendung einer für Serin Hydrolasen spezifischen ABP in Kombination mit einem bioorthogonalen Linker (TEV-Linker) konnten wir mehrere Serin Hydrolasen in den Proben anreichern und nachweisen. Zusätzlich zur erfolgreichen Anreicherung von Serin Hydrolasen durch ABPP entdeckten wir eine potenziell interessante Serin Hydrolase, welche im Vergleich zu Zelllinien mit fehlender ATGL häufiger in ATGL über-exprimierenden Zelllinien vorkommt. Diese vielversprechenden Ergebnisse ermöglichen die weitere – gezielte – Untersuchung potenziell interessantere Enzyme.

Table of content

Abbreviations

(HP)LC	(High Performance) Liquid Chromatography
2-AG	2-Arachidonylglycerol
ABHD	Alpha/Beta Hydrolase Domain Containing
ABP	Activity-based probe
ABPP	Activity-based proteomic profiling
ACN	Acetonitrile
AdC	Adenocarcinoma
ADIPO	Aza-dibenzocyclooctyne
APT1/2	Acyl-protein thioesterase 1/2
Asp	Aspartate
ATGL	Adipose Triglyceride Lipase
BARAC	Biarylazacyclooctynone
BG	Binding Group
Ca^{2+}	Calcium
CE	Cholesterol Ester
CEL	Carboxyl Ester Lipase
CES1	Carboxylesterase 1
CGI-58	Comparative Gene Identification 58
CID	Collision Induced Dissociation
CoA	Coenzyme A
CTC	Circulating Tumor Cells
CuAAC	Cu(I)-catalyzed alkyne-azide cycloaddition
DAG	Diacylglycerol
DAGE	Differential Activity-based Gel Electrophoresis
DAGLA/B	Diacylglycerol Lipase Alpha/Beta
DIBAC	Dibenz[b,f]azocine-5(6H)-pentanoic acid, 11,12- didehydro-δ-oxo-, methyl ester
DIBO	4-dibenzocyclooctynol
DIFO	Difluorinated cyclooctyne

DIGE	Differential Gel Electrophoresis
DIMAC	Dimethoxyazacyclooctyne
DMSO	dimethylsulfoxide
DNA	Deoxyribonucleic Acid
ECM	Extracellular Matrix
EDTA	Ethylenediaminetetraacetic acid
EGFR	Epidermal Growth Factor Receptor
ER	Endoplasmatic Reticulum
ESI	Electrospray Ionization
FA	Fatty Acid
FABP4	Fatty Acid Binding Protein 4
FASN	Fatty Acid Synthase
FBS	Fetal Bovine Serum
FT-ICR	Fourier-Transform Ion Cyclotron Resonance
G0S2	G0/G1 Switch Gene 2
GFP	Green Fluorescent Protein
HCC	Hepatocellular Carcinoma
HGP	Human Genome Project
HILIC	Hydrophilic Interaction Liquid Chromatography
HILPDA	Hypoxia-Inducible and Lipid Droplet Associated Protein
His	Histidine
HRP	Horseradish peroxidase
HSL	Hormone Sensitive Lipase
IEF	Isoelectric Focusing
IEX	Ion-Exchange
IT	Ion Trap
KO	Knock-Out
LCAT	Lecithin-Cholesterol Acyltransferase
LCC	Large Cell Carcinoma
LD	Lipid Droplet

LFQ	Label-free quantification
LG	Leaving Group
LIPC	Hepatic Lipase
LIPF	Gastric Lipase
LIPG	Endothelial Lipase
LIT	Linear Ion Trap
LPA	Lysophosphatidic Acid
LPC	Lysophospatidylcholine
LPCAT1	Lysophosphatidiylcholine acetyltransferase 1
LPL	Lipoprotein Lipase
LR	Linker Region
LYPLA1/2	Lysophospholipase ½
LYPLAL 1	Lysophospholipase like protein 1
MAG	Monoacylglycerol
MALDI	Matrix Assisted Laser Desorption Ionization
MGL	Monoacylglycerol Lipase
MMP	Metalloproteinases
mRNA	messenger Ribonucleic Acid
MS	Mass Spectrometry
NEFA	Non-esterified Fatty Acid
NNK	Nitrosamine Ketone
NP	Normal-Phase
NS	Non-Smoker
NSCLC	Non-small Cell Lung Carcinoma
OCT	Cyclooctyne
OE	Over Expressing
PBS	Phosphate Buffered Saline
PC	Phosphatidylcholine
PCA	Principle Component Analysis
PEDF	Pigment Epithelium Derived Factor

PGE2	Prostaglandin E2
PLB1	Phospholipase B
PNLIP	Pancreatic Lipase
PNPLA2	Patatin-like Phospholipase Domain containing protein 2
Q	Quadrupole
QQQ	Triple Quadrupole
RB	Retinoblastoma
RG	Reactive Group
ROS	Reactive Oxygen Species
RP	Reversed-Phase
RT	Room Temperature
S	Smoker
SCC	Small Cell Carcinoma
SCLC	Small Cell Lung Carcinoma
SDS	Sodium dodecyl sulfate
SEC	Size-Exclusion Chromatography
Ser	Serine
SH	Serine Hydrolase
SPAAC	Strain-promoted alkyne-azide cycloaddition
SqCC	Squamous Cell Carcinoma
TAG	Triacylglycerol
TBS	Tris Buffered Saline
TCA	Tricarboxyic acid cycle
TCGA	The Cancer Genome Atlas
TOF	Time of Flight
TS1/2	Transition State 1/2
VEGF	Vascular Endothelial Growth Factor
VEGFR	Vascular Endothelial Growth Factor Receptor
WHO	World Health Organization

1. Introduction

1.1. Cancer

According to the world health organization (WHO), cancer is causing approximately 9.6 million deaths per year (2018) worldwide[1]. Together with the leading death-causing group of diseases – cardiovascular diseases – it is accountable for almost half of all global deaths and therefore constitutes a severe problem of our time[2]. Environmental factors as well as behavior and lifestyle choices such as diet and physical exercise influence cancer occurrence and development. The highest risk factor for cancer development is tobacco smoking, reflected by high lung cancer occurrence in industrialized countries in the past and rising lung cancer occurrence in developing countries, where cigarette smoking has become a custom in recent years[3].

1.1.1. Lung cancer

Considering data from both females and males worldwide, lung cancer causes the highest number of new incidences (11.6%) out of all new cancer incidences. An estimated 2.1 million people have been diagnosed with lung cancer in 2018. Only breast cancer is occurring more often in women – almost one fourth of all in women diagnosed cancers is breast cancer. Nevertheless, the diagnosis of lung cancer comes with a lower chance of survival. Responsible for 1.8 million deaths in 2018, which corresponds to 18.4% of all cancer-related mortalities, lung cancer is the leading cause of cancer-related deaths (Figure 1)[1].

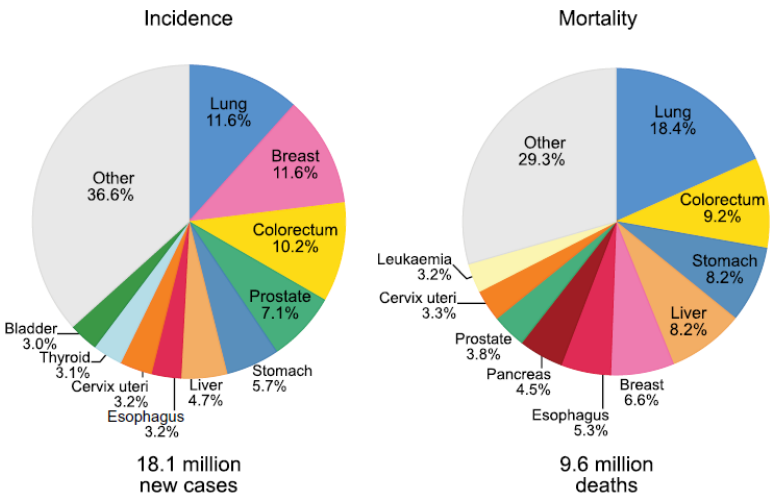

Figure 1: Cancer incidence and mortality in different cancer types worldwide in 2018 *– Combined data from males and females are represented in %. 18.1 million new cases of cancer were reported (visualized in left pie chart) while 9.6 million cancer-related deaths were reported (visualized in right pie chart) – adapted from [1]*

According to the American Cancer Society, approximately 80% of lung cancers are caused by tobacco smoking[4]. While cigarette smoking is declining in industrialized countries, in mid- to low-income countries tobacco use is still well established, which is reflected in higher numbers of lung cancer incidences[3]. Even though the predominant cause for lung cancer development is tobacco smoking, with dwindling smoking-rates but high numbers of lung cancer in total, the number of lung cancer patients who are non- or never-smokers is increasing[5]. It is oftentimes proposed to treat lung cancer occurring in never-smokers as a separate disease due to the vast amount of underlying differences in epidemiology and different clinical, pathological and molecular characteristics[5–7].

Among the epidemiological differences that have been identified, there is a globally consistent gender-bias in which lung cancer in never smokers is occurring more often in women than in men[5–8]. However, this observation may be dampened by the fact that there are generally more women who are never-smokers compared to men of similar age who have never smoked[7]. Histologically, lung cancer can be categorized into two large groups: small cell lung carcinoma (SCLC) and non-small cell lung carcinoma (NSCLC), with the latter one causing about 85% of all lung cancers[9]. The former one, however, is more strongly associated to lung cancer in smokers. Furthermore, NSCLCs can be divided into three groups: large cell carcinoma (LCC), squamous cell carcinoma (SqCC) and adenocarcinoma (AdC)[10]. Even though all histological types of lung cancer are associated with smoking, AdC is the most common type of lung cancer arising in never-smokers[6].

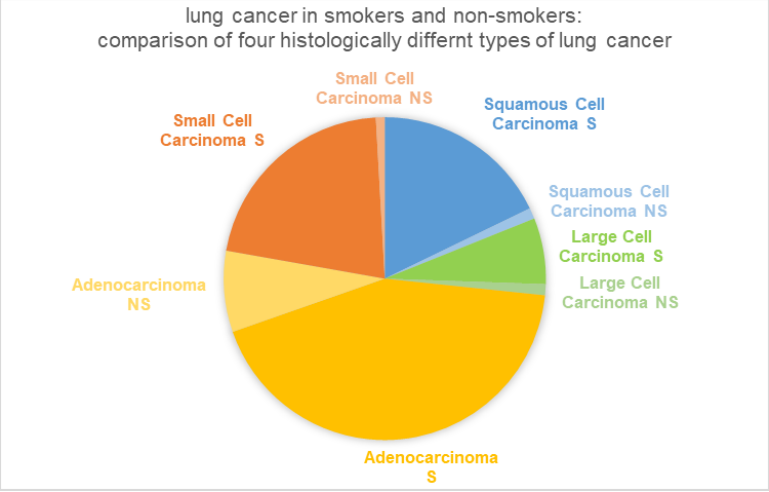

Figure 2: lung cancer in smokers and non-smokers – *Comparison of four histologically different types of lung cancer and their relative incidence based on data from Kenfield et al.11 – S: smokers, NS: nonsmokers. Yellow: adenocarcinoma (NS/S 8.1%/43%), Orange: small cell carcinoma (NS/S 0.9%/21.3%), Blue: squamous cell carcinoma (NS/S 1.1%/1.8%), green: large cell carcinoma (NS/S 1.1%/6.6%).*

This was also found in a study from 2008 on the aspects of smoking on the four best described kinds of lung cancer. In this particular study, cases of SCLC, LCC, SqCC and AdC were investigated over the course of 26 years, and the conclusion was that the type of lung cancer with the highest number of incidences in non-smokers is lung AdC (Figure 2.)[11].

Risk factors associated with lung cancer in never smokers include exposure to radon, indoor and outdoor air pollution, as well as to non-tobacco-associated carcinogens like arsenic, asbestos or others[5–8]. One possibility to explain the prevalence of AdC in never-smokers lung cancer is that non-tobacco-associated carcinogens might target the more peripheral regions of the lung, when smoke-associated carcinogens target both central and peripheral airways of the lung[6]. Tobacco-associated carcinogens including nitrosamines like nitrosamine ketone (NNK) were found to cause mutations in oncogenes KRas or TP53 in mice through reactive metabolites[12]. While oncogenes KRas and TP53 are frequently mutated in smoking-associated lung cancers, never-smokers experience epidermal growth factor receptor (EGFR) gene mutations at higher frequency, making them more susceptible for treatment with EGFR tyrosine kinase inhibitor therapy[6]. Since evidence strongly suggests that cancers of never smokers and smokers occur due to different molecular mechanisms, these diseases should be considered individual entities and treated separately.

In addition to the complexity of lung cancer concerning its heterogeneity even within histologically similar subtypes, a main problem of lung cancer remains its poor early-on diagnosis[13]. This is the most prominent reason why lung cancer is leading in cancer mortality worldwide – it often remains unnoticed at early stages. The poor early-on diagnosis desperately calls for new diagnostic tools to find lung cancer at earlier stages. Tumor markers, which are usually measured in body fluids such as urine or blood, are a promising method to diagnose or predict the prognosis of certain cancers. This, however, requires the availability of cancer-specific tumor markers. Usually, tumor markers are proteins or other substances that increase in the presence of the cancer; nowadays, however, expression patterns of tumor suppressor genes or proto-oncogenes are frequently used to test for cancer[14].

Hallmarks of cancer

Cancer cells arise from normal cells due to successive genetic alterations, which provide (growth) advantage for the cells[15]. The genes leading to advantage upon mutation are referred to as cancer genes and may be divided into tumor suppressor

genes and oncogenes. Cancer genes are oftentimes identified due to high mutation frequency in cancers[15]. While mutations in tumor suppressor genes are mostly recessive and cause loss-of-function of the gene product, mutations in oncogenes are commonly dominant and lead to gain-of-function of the gene product, and both types of mutations are contributing to an advantage in cancer cells.

Tumor suppressor genes play a role in ensuring the proper function of cell cycle replication – sometimes achieved by negatively regulating cell cycle and replication-driving oncogenes. They may also encode for DNA repair proteins, or proteins who are responsible for induction of apoptosis upon DNA damage that cannot be repaired any more[16]. Oncogenes, on the other hand, are oftentimes upregulated in cancer and contribute to cancer formation or progression. Gene products of oncogenes are associated with growth and differentiation, e.g. growth factors, growth factor receptors, or kinases regulating growth or differentiation-associated signaling pathways[17]. Other oncogenes may play a role in the inhibition of apoptosis[18].

In 2000 Hanahan and Weinberg published a thorough review in which they describe and list characteristics that are often acquired by cancer[15]. These characteristics are commonly referred to as hallmarks of cancer. The initial review was extended in 2011[19] and further revisited and updated in more recent reviews taking into consideration critical points of the initial reviews and the additional insights gained by current cancer research[20]. A summary of the cancer hallmarks is represented in Figure 3, which was adapted from Hanahan and Weinberg (2011)[19].

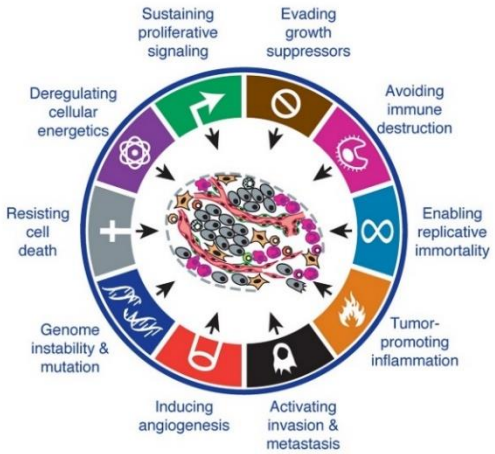

Figure 3: Summary of the main cancer hallmarks and enabling characteristics – *Hallmarks: Sustaining proliferative signaling; Evading growth suppressors; Enabling replicative immortality; Activating invasion & metastasis; Inducing angiogenesis; Resisting cell death; Deregulating cellular energetics; Avoiding immune destruction. Enabling characteristics: tumor-promoting inflammation; Genome instability & mutation. - adapted from Hanahan and Weinberg (2011)[19]*

Alteration of usually tightly-controlled growth and proliferation signaling, which is affecting growth factors, their receptors or their downstream signaling molecules is a common driver for the enhanced growth and proliferation capacity in cancer. These alterations include upregulation of growth-promoting factors, such as different growth ligands, as well as the downregulation of growth-inhibiting factors thus avoiding growth suppressors signals[20]. While growth receptors are also target of alteration, the most pronounced alterations are probably in downstream signaling molecules. A change in central signaling molecules, such as the G-protein Ras, causes maintained proliferative signaling, but through downstream signaling pathways it can furthermore influence several other hallmarks and cause apoptosis suppression or rewiring energy metabolism. This demonstrates that individual signaling pathways may be involved in several cancer hallmarks. In addition to growth signaling cell cycle control has to be circumvented in order to ensure increased proliferation. Hence, another common characteristic of cancer cells is the deregulation of cell cycle. This is reflected by the fact that key regulators of the cell cycle, like retinoblastoma (RB) or p53, are frequently mutated and inactivated in cancer[20,21]. The disruption of these regulators is often associated with other hallmarks; p53 for instance is not only arresting the cell cycle, but is also responsible for initiation of repair mechanisms or cell death if repair is not possible[20–22].

Cancer cells show a generally different response to stresses like hypoxia, DNA damage, or nutrient deficiency. The altered stress response helps in overall cancer cell survival. Apoptotic cell death is usually circumvented through numerous mechanisms, such as the frequent inactivation of major apoptosis-inducing proteins (like the already mentioned p53), or genetic alterations causing up- or downregulation of anti- or pro-apoptotic proteins respectively[20,23]. By omitting senescence, which is the irreversible exit from the cell cycle, cancer cells have acquired a strategy to maintain replicative potential and thus become immortal. This is usually achieved by the upregulation of the enzyme telomerase, which is catalyzing the addition of telomere repeat units to telomeric ends of DNA. Telomerase is found to be upregulated in the majority of human cancers[19,20,24].

In their updated review, Hanahan and Weinberg have included additional emerging hallmarks and cancer enabling characteristics, such as genomic instability, immune modulation or tumor-promoting inflammation[19]. Genomic instability is responsible for increased genomic alterations during cell division[19,25]. Mutations of the DNA repair

machinery or the DNA damage checkpoint cascade are usually underlying to genomic instability, causing limited repair of DNA due to non-functioning cell cycle arrest[26]. Similarly, mutations in the spindle assembly or mitotic checkpoint genes lead to genomic instability due to failure of ensuring the delay of mitosis onset when chromosomes are not yet properly aligned and attached to the spindle apparatus[27]. Despite immune surveillance, cancers are developing in organisms with proper immune system. In fact, cancers are often infiltrated with immune cells, mimicking inflammatory conditions. However, this interaction between malignant and immune cells might be tumor-promoting[19,20,28]. It is believed that inflammation does not always lead to tumor destruction but rather helps tumor progression by providing growth factors or other bioactive molecules[19]. Additionally, through a cancer immunoediting system, cancer cells might circumvent the tight control by the immune system. Under constant immune selection pressure, cancer cells, which generally have high genomic instability, continuously develop genetically altered cancer cell variants. Some of these cancer cells can eventually show lower immunogenicity and are able to escape the immunosurveillance[20].

A key characteristic of malignant cancers is the capability of metastasis and invasion of surrounding tissue. For invasion or metastasis, cancer cells have to first degrade the local extracellular matrix (ECM), a task that is usually fulfilled by matrix metalloproteinases (MMPs), which are often upregulated in human cancers[20,29]. After ECM degradation, cancer cells might invade local tissue or enter the lumina of vessels (intravasation). Following intravasation, circulating tumor cells (CTC) are carried to distant loci, where they can undergo the more difficult extravasation. While most organs bear a very protective layer of epithelial cell that are hard to penetrate, certain organs like bone marrow or liver possess higher permeable vessels and are thus more frequently target of metastases[20,30].

In order to metastasize, tumors need vascularization. Hence, another cancer-acquired characteristic is increased vascularization, above all, continuously active angiogenesis. Angiogenesis is the formation of new blood vessels by proliferation and assembly of endothelial cells from already existing vessels[15,19,20]. The formation of new blood vessels into malignant usually oxygen deprived tissue is aiding with oxygen and nutrient supply. One of the main factors inducing angiogenesis in tumors is hypoxia, which triggers the transcription factors of the hypoxia inducible factor (HIF) family, which change an angiogenic switch through an altered transcription of genes[31,32]. Pro-

angiogenic factors such as the vascular endothelial growth factor (VEGF) or the corresponding receptor (VEGFR) are directly activated by stable HIF. These effectors are frequently overexpressed in cancers and result in increased angiogenesis[20,31].

For faster proliferation and growth, cancer cells need more energy than their normal cell counterparts. To cope with this higher energy requirement, cancer cells have developed strategies to alter their energy metabolism. These strategies have been extensively discussed and summarized as hallmarks of cancer metabolism by Pavlova and Thompson in 2016[33]. These alterations in metabolism include upregulated uptake of glucose and amino acids such as glutamine. Already in the early 1900s Otto Warburg observed and described how cancer cells predominantly performed glycolysis with subsequent production of lactate from pyruvate, even under oxygen availability. The phenomenon of cancer cells converting pyruvate to lactate rather than using it for tricarboxylic acid (TCA) cycle, which is bioenergetically more favorable, was later termed the Warburg-effect[34]. Another metabolic alteration making use of alternative nutrients is the increased uptake of extracellular proteins, especially if insufficient vascularization causes shortage in nutrient supply. The uptake of extracellular proteins occurs through micropinocytosis, which undergo lysosomal degradation within the cells, a phenomenon induced by both oncogenes Ras and c-Src. The resulting amino acids, such as glutamine, are subsequently used for energy production in central carbon metabolism[33,35]. Another nutrient source that is used by cancer cells for energy production are lipids. Fatty acids are required by cells, not only for bioenergetic reasons but also for the generation of signaling molecules and biomembranes[36]. Next to the well-studied alterations of glucose metabolism, the change of lipid metabolism in cancer is oftentimes overlooked. The main characteristic of altered lipid metabolism in cancer is increased *de-novo* fatty acid (FA) synthesis, mirrored in the upregulation of the rate-limiting enzyme in the FA synthesis pathway - fatty acid synthase (FASN) - in several human cancers. Furthermore, cancer cells show an increase in uptake of exogenous FAs. These FAs are either incorporated into the lipogenesis pathway, generating lipids for storage or export, or are used for β-oxidation, the lipid catabolism pathway, generating energy in form of acetyl-CoA, which can be further used in the TCA cycle[37–40]. While FA metabolism and the importance of FAs in cancer is well described[37], changes in lipolysis in cancer are less well studied and remain controversial.

1.1.2. Lipolysis and ATGL in cancer

Exogenous FAs are taken up from outside of the cells, while endogenous FAs are generated from FA *de-novo* synthesis. Both endogenous and exogenous FAs can be stored as triacylglycerol (TAG). By accommodating three FAs on one glycerol backbone, TAGs constitute a major energy source for the cell. Together with other neutral lipids such as cholesteryl esters (CE) TAGs are stored within lipid droplets (LDs). These highly dynamic organelles consist of a hydrophobic core bearing neutral lipids and are enveloped with a lipid monolayer consisting of sterols and phospholipids[39]. Even though the highest presence of LDs is found in adipocytes they are also present in all other cell types. In recent years, LD accumulation has been reported for several types of cancer[39,41,42]. On the surface of LDs lipid-droplet-associated proteins are found. Dependent on cell type, different members of the perilipin-family are localized to LDs and regulate lipid metabolism on LDs (e.g. Plin1 in adipocytes and Plin5 in cardiomyocytes)[43,44]. LDs are generated by *de-novo* synthesis of TAGs within the endoplasmic reticulum (ER) bilayer forming a lens-like structure, which is subsequently budded off from the ER membrane[44–46]. LD degradation through TAG hydrolysis on the other hand occurs through a multi-step process termed lipolysis. The products of lipolysis are non-esterified fatty acids (NEFAs) and glycerol. The first step of lipolysis, cleaving one FA from TAG resulting in diacylglycerol (DAG), is mainly catalyzed by Adipose Triglyceride Lipase (ATGL), which is found on LDs upon activation[47]. This 54 kDa serine hydrolase (SH) is encoded by the gene *PNPLA2* (patatin-like phospholipase domain containing protein 2) and contains a patatin-domain. ATGL activity is positively or negatively regulated by the coactivator Comparative Gene Identification 58 (CGI-58) or G0/G1 switch gene 2 (G0S2), respectively. In unstimulated adipocytes, CGI-58 is localized to the surface of LDs and bound to perilipin-1, hence ATGL is not active. When adipocytes are activated, however, perilipin-1 is phosphorylated and dissociates from CGI-58, which is subsequently free for interaction with and activation of ATGL[47]. In cells other than adipocytes, ATGL localization to LDs and interaction with CGI-58 is most likely governed by other perilipin proteins[47]. The detailed mechanism through which ATGL is activated by CGI-58 is not fully understood[48], however, it was found that ATGL and CGI-58 interact via direct protein-protein interaction[47]. It is known that the inhibitory effect of G0S2 arises due to directly binding to the N-terminal patatin-domain of ATGL thus inhibiting its catalytic activity[47]. Under hypoxic conditions, hypoxia-inducible and LD associated protein HILPDA is inhibiting ATGL activity, causing hypoxia-induced LD formation[49]. An additional activator of ATGL was identified by investigating LD

associated proteins, such as the pigment epithelium-derived factor (PEDF) protein. PEDF was shown to bind to ATGL thereby increasing its lipolytic activity[50,51]. The involvement of ATGL in cancer development and progression is still inconclusive. While it is well-established that lipolysis and ATGL are upregulated in adipocytes in cancer cachexia[39,52–54], the role of lipolysis and ATGL in cancers themselves is controversial. It is proposed that lipolysis is exploited by cancer cells to provide more FAs for energy production and for generation of precursor molecues[55,56]. However several publications report LD accumulation in cancer cells[42,45]. Recently, decreased levels of ATGL in cancer have been described and a tumor suppressor function of this lipolytic enzyme was proposed[57–59]. Additional complexity of the role of lipolysis and ATGL in cancer arises due to the involvement of several ATGL cofactors in cancer – such as implied cancer-associated roles for the ATGL cofactors HILPDA and PEDF[47,49,51,60], as well as the interaction of cancers with its stroma.

The second step of lipolysis is mainly catalyzed by Hormone Sensitive Lipase (HSL), which was formerly believed to be the rate-limiting enzyme of the first step of lipolysis[61]. HSL, however, primarily catalyzes hydrolysis of DAG, releasing an additional NEFA and monoacylglycerol (MAG). It is worth mentioning that HSL indeed has hydrolyzing capabilities for a variety of substrates including TAG, MAG, CE and other lipids, while its main role is the hydrolysis of DAG[47]. The resulting MAG is further cleaved into glycerol and a FA, a reaction catalyzed by Monoacylglycerol Lipase (MGL). A representative scheme of lipolysis is shown in Figure 4.

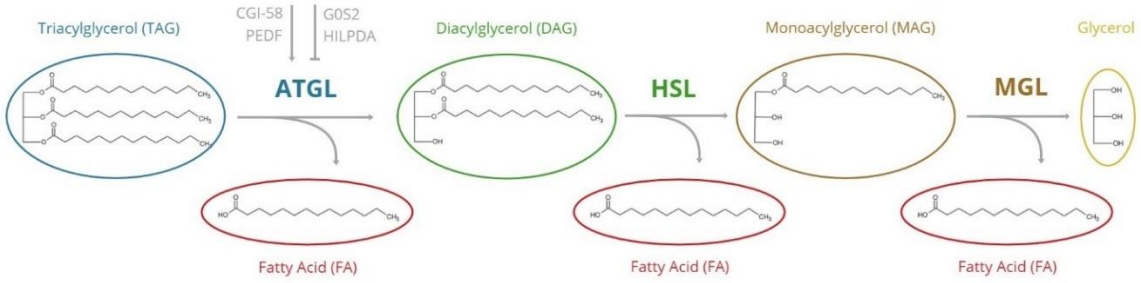

Figure 4: Schematic representation of Lipolysis *– (ATGL: adipose triglyceride lipase, CGI-58: comparative gene identification gene 58, G0S2: G0/G1 switch gene 2, HILPDA: hypoxia-induced and lipid droplet associated protein, HSL: hormone sensitive lipase, MGL: Monoglyceride Lipase, TAG: Triacylglycerol, DAG: Diacylglycerol, MAG: Monoacylglycerol, FA: Fatty Acid). ATGL catalyzes hydrolysis of TAG to DAG resulting in release of one FA, HSL catalyzes the next step, releasing the second FA by generating MAG, which is hydrolyzed to Glycerol and another FA.*

Cancer cells in general show increased lipogenesis and uptake of exogenous FAs in order to provide FAs. These FAs are usually readily incorporated into the pool of TAGs

and LDs[62]. Hence, an increase in activity of the lipolytic pathway in order to increase FA availability for the cell was suggested[55,56,62].

Nomura *et al.* studied the role of MGL in cancer and found an increased activity of this lipolytic enzyme which was associated with more aggressive types of cancer. They reported that resulting FAs are incorporated into a network of pro-tumorigenic signaling molecules such as lysophosphatidic acid (LPA) or prostaglandins, like prostaglandin E2 (PGE2), which lead to the promotion of the observed enhanced migratory potential, growth and survival[62].

As already mentioned, the role of ATGL in cancer is rather controversial. In ovarian cancer cells it was found that upon co-culture with adipocytes higher malignancy and a generally more aggressive cancer phenotype was observed. This observation was explained by an increased lipolytic activity in the adipocytes, which in turn provided more FAs for the cancer cells. These cancer cells also showed higher levels of FA uptake and transporting proteins, such as the fatty acid binding protein 4 (FABP4)[63]. In another co-culture study of breast cancer cells with adipocytes, an increased level of lipolysis and ATGL in adipocytes resulted in enhanced migration and invasion abilities of the cancer cells[64]. The role of ATGL in lung cancer cells was investigated by Zagani *et al.* in 2015 by silencing G0S2 in several cancers. The authors proposed a tumor suppressor role of this ATGL inhibiter. G0S2 expression in NSCLC cells caused elevated TAG levels and diminished cell growth. Moreover, the knockdown of ATGL in NSCLC cells resulted in slower growth and motility[65]. In the same study, it was claimed that inhibition of ATGL by the Atglistatin, a potent inhibitor of murine ATGL[66], caused a suppression of ATGL induced growth of these human cancer cells, which is a questionable result as Atglistatin is a specific target for murine but not human ATGL[67].

Contrarily, in recent years a tumor-suppressor function was proposed for ATGL[57–59,68]. In 2018, Ciriolo *et al.* found that there is, in general, a lower expression of ATGL in hepatocellular carcinoma (HCC) biopsies compared to normal tissue. Forced ATGL expression in HCC cells reduced glucose uptake and utilization leading to an overall lower proliferation[59]. In a paper from 2016, Al-Zoughbi *et al*., performed a data analysis of the cancer genome atlas (TCGA) revealing that ATGL is deleted in 25% of human cancers and a total of 38% of human lung cancers. Furthermore, they stated that the gene for ATGL, *PNPLA2*, is found in a tumor-suppressor gene region on chromosome 11. They generated mice lacking ATGL with rescued ATGL expression in the heart and found that those mice lacking ATGL in all tissues except heart spontaneously develop

lung neoplasia, which can result in lung adenocarcinoma[57]. After this initial connection between ATGL loss and lung cancer, investigations of ATGL in lung cancer were initiated. In 2018 Tomin *et al.* published a paper investigating ATGL in lung carcinoma cells. Their findings include an observation of a more aggressive phenotype of cancer cells lacking ATGL, while re-introduction of ATGL diminished this phenotype. Interestingly, their lipidomic analysis revealed an increase in not only TAG levels, but also higher levels of bioactive lysophospholipids[68]. Cancer cells profit from lipids not only in their role for providing energy, but maybe more importantly in their role as signaling molecules, which can stimulate signaling pathways contributing to cancer aggressiveness by promoting a higher migratory potential and faster growth[56].

Many of the here mentioned lipolytic enzymes that are suggested to play a role in cancer belong to or are associated with the enzyme superfamily of serine hydrolases[69].

1.2. Serine hydrolases

The serine hydrolases (SH) enzyme superfamily is a functionally diverse group of more than 200 enzymes. These enzymes can be separated into serine proteases and metabolic SHs[69]. Serine proteases have been subject of extensive studies mainly due to early investigations of proteolytic enzymes such as chymotrypsin[70], which was also the first serine peptidase with an available three-dimensional structure[71]. The three-dimensional structure aided in investigation of the catalytic mechanisms, and a catalytic triad was discovered in the active site of the enzyme, consisting of a nucleophilic serine (Ser), a histidine (His) acting as a proton-accepting base, and an aspartic acid (Asp) residue aiding in proper orientation of the His residue[72]. While all SHs share a catalytic serine in the active site of the enzyme, giving this group of enzymes its name, the participating amino acids of the catalytic core may vary. Next to the widely observed Ser-His-Asp catalytic triad, in some metabolic SHs, a Ser-Ser-Lys triad is observed and even catalytic dyads such as Ser-Lys or Ser-Asp have been observed[69]. Other catalytic dyads and triads are also observed in serine proteases[72,73].

Metabolic SHs make up a group of enzymes with varying functions and are oftentimes involved in important metabolic pathways by catalyzing the cleavage of ester-, amide-, and thioester-bonds of small molecules[69]. Several enzymes of lipid metabolism pathways, such as the enzymes of the lipolysis pathway, fall into this group.

The catalytic motif, in which the nucleophilic serine is embedded is the GXSXG motif, is common to most metabolic SHs. Another feature common to several metabolic SHs is a shared enzyme fold: the alpha/beta hydrolase fold[74]. Many lipid metabolic enzymes adopt this type of protein fold, which harbors a central beta-sheet consisting of eight beta-sheets connected by alpha helices[75]. A representation of a typical alpha/beta hydrolase fold is depicted in Figure 5. The substrates of metabolic SHs are mainly small molecules, including neutral fatty acyl esters, lipid amides, phospholipids and others. Hence, SHs play a major role in lipid metabolism.

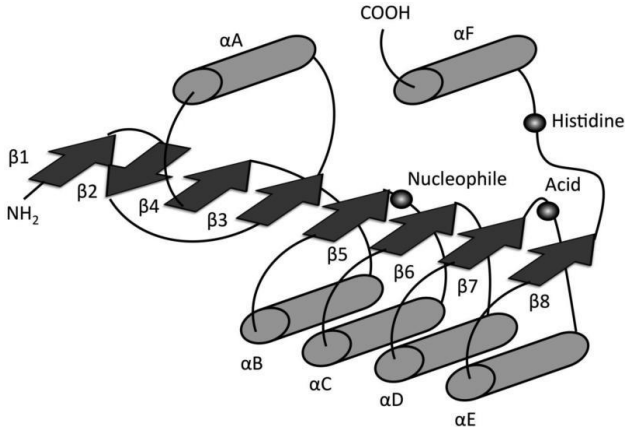

Figure 5: Alpha/beta hydrolase fold *– Eight beta-sheets connected by alpha-helices. Nucleophilic serine and components of the catalytic dyads or triads are found on connecting loops. Figure from Lord et al.* [75]

1.2.1. Serine hydrolases in lipid metabolism

Multiple SHs are responsible for the hydrolysis of intracellular lipid stores, namely the TAG and CE within lipid droplets. The major lipolytic enzymes shown in Figure 4 and mentioned in previous chapters (ATGL, HSL and MGL) all contain the GXSXG motif and nucleophilic serine in their active site, thus belonging to the group of SHs. Diacylglycerol lipases alpha and beta (DAGLA and DAGLB, respectively) are also SHs and are selective towards hydrolysis of diacylglycerol. While DAGLA is mainly expressed in brain and pancreas, DAGLB is highly expressed in bone marrow and liver[69]. Both are stimulated by calcium (Ca^{2+}) and important for generation of 2-arachidonylglycerol (2-AG), which is ligand of cannabinoid receptors in the central nervous system[76]. Another SH is the carboxylesterase 1 (CES1), which also belongs to the alpha/beta fold hydrolase family. It is highly abundant in the liver as well as in adipocytes where it is responsible for hydrolysis of xenobiotics and drugs[77]. Alpha/beta hydrolase domain containing 6 (ABHD6), another enzyme belonging to the alpha/beta hydrolase fold family, is an SH expressed in several human tissues. ABHD6 possesses

2-AG hydrolyzing capabilities and is thought to contribute to 2-AG signaling in certain areas of the brain[69,75]. Compared to MGL, which is found in the presynaptic cytosol, ABHD6 is an integral membrane protein facing the cytosol in the postsynapse[75,78]. Another ABHD family member and SH with 2-AG hydrolase activity is alpha/beta hydrolase domain containing 12 (ABHD12), whose active site faces the ER lumen. Even though MGL, ABHD6, and ABHD12 all show 2-AG hydrolyzing activity, they are expressed at different subcellular locations; the presynaptic cytosol, postsynaptic membrane and facing the ER, respectively. It is therefore proposed that they are responsible for controlling 2-AG levels in different sites of the cell[75,78]. A lipid metabolism associated protein, however not an SH is CGI-58, which is also called alpha beta hydrolase domain containing 5 (ABHD5). CGI-58 adopts the alpha/beta hydrolase fold but does not bear a catalytic serine in its active site, hence shows no enzymatic activity. Indirectly, it is responsible for the activation of ATGL, however, and thus contributes to the regulation of the lipolysis pathway. In addition to the here mentioned intracellular neutral lipases, there are several extracellular neutral lipases belonging to the family of serine hydrolases, including pancreatic lipase (PNLIP), carboxyl ester lipase (CEL), gastric lipase (LIPF), lipoprotein lipase (LPL), hepatic lipase (LIPC), lysosomal acid lipase (LIPA). There are also acyltransferases within the group of serine hydrolases, such as the lecithin-cholesterol acyltransferase (LCAT). Several phospholipase A2 (PLA2) enzymes also belong to the group of metabolic SHs. They catalyze the formation of lysophospholipids from phospholipids by hydrolyzing their sn-2 acyl chain. Some PLA2 are Ca^{2+} dependent and they show specificity for certain acyl chains. Additionally, they vary in expression in different tissues. Several other phospholipases, such as endothelial lipase (LIPG), phospholipase B (PLB1), or alpha/beta hydrolase domain containing 4 (ABHD4) also belong to the group of SH[69]. More members of the SH lipase, acyltransferase and the ABHD family have been described[69,75,79].

1.2.2. Catalytic reaction mechanism of serine hydrolases

SHs share the same catalytic mechanism, in which a nucleophilic serine in the active site of the enzyme performs a nucleophilic attack at the carbonyl carbon of an amide, ester or thioester bond, causing two subsequent nucleophilic substitution reactions, resulting in the regeneration of the nucleophilic serine. The cleaved amide, ester or thioester bond results in the formation of an amine, alcohol or thiol respectively, and the generation of a carboxylic acid.

The core catalytic machinery of SHs usually consisting of a catalytic Ser-His-Asp triad, and the proposed catalytic reaction are depicted in Figure 7. In the active site of the enzyme the O_γ atom of serine (Figure 6) and the non-protonated nitrogen in ε-position in the imidazole ring of histidine in $N_\varepsilon 2$ coordination (Figure 6) are found in close proximity, while an aspartate serves for stabilization of the histidine.

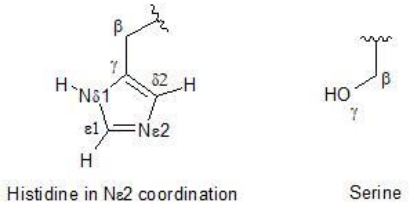

Figure 6: Nomenclature of atoms in Histidine in the N-epsilon-2 coordination and Serine

The reaction mechanism is initialized by a nucleophilic attack of the catalytic active-site serine on the carbonyl group of the substrate (ester, thioester or amide), while histidine accepts the leaving proton of the hydroxy group of serine. The resulting tetrahedral transition state (TS1) oxyanion fits in the oxyanion hole of the enzyme containing an oxyanion binding site. This oxyanion binding site is made up of two backbone amine groups that donate their hydrogens for hydrogen bonding with the resulting negatively charged oxygen of the oxyanion, thus stabilizing the transition state. From TS1 a more stable acyl-enzyme intermediate is obtained by electron rearrangement and release of an amine, thiol or alcohol group, depending on the bond that is cleaved. In the case of a lipolytic reaction (Figure 7), the fatty acid group is esterified with the active site serine at this step, while the reduced glycerol, di- or mono- acyl-glycerol (=alcohol group) is released. In the following step, an activated water molecule undergoes a nucleophilic attack on the carbonyl group of the acyl-enzyme while histidine accepts the resulting proton. This results in the second tetrahedral transition state (TS2) oxyanion. TS2 oxyanion is readily converted back into the enzyme, and serine O_γ accepts back the proton from histidine, while a carboxylic acid is released – in the case of lipolysis a fatty acid. The reaction results in the net regeneration of the enzyme with the nucleophilic serine, while the ester, amide or thioester bond is cleaved into a carboxylic acid and the corresponding alcohol, amine or thiol[69,72,80]. The mechanistic reactions of serine hydrolases with different catalytic site triads or dyads are likely proceeding in similar ways to the here represented scheme of the Ser-His-Asp catalytic triad[73].

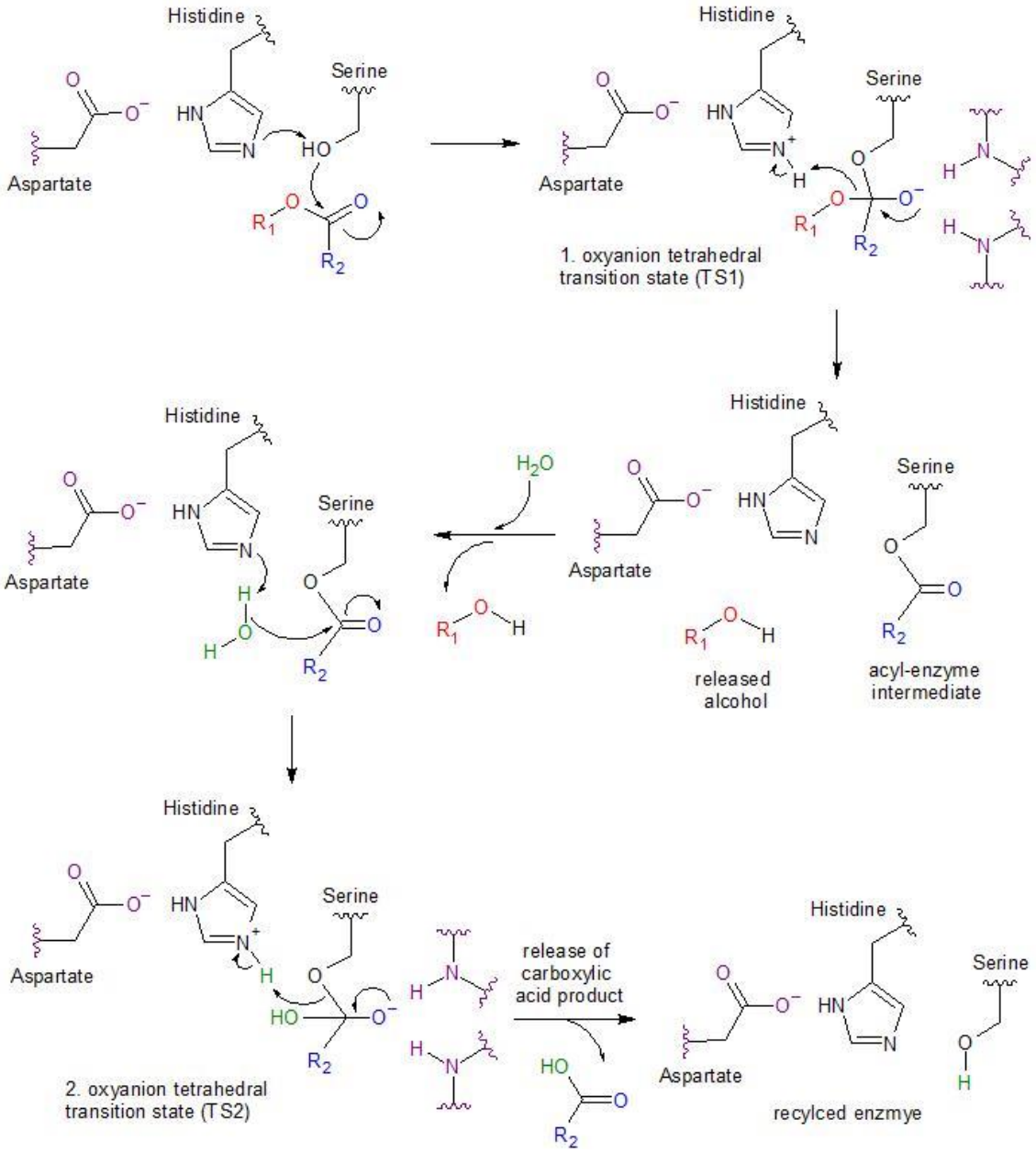

Figure 7: catalytic reaction mechanism of serine hydrolases based on Ishida and Kato[80]

Due to the shared catalytic mechanisms and the high reactivity of the active site serine, inhibitors can be used to bind covalently and specifically to active SHs. This can be exploited for the determination of the functionality of SHs by activity-based proteomic profiling (ABPP)[69,81].

1.3. Proteomics

Proteomics is the study of the proteome, which is the set of all proteins expressed by an organism, cell or tissue at a given time[82]. The post-genomic era started with the completion of the human genome project (HGP) in 2001, and together with this historic landmark the proteomics era emerged[83]. While the genome contains all the information that is needed to build an organism, it is mainly a source of information. In order for an organism to function, however, this information needs to be processed and turned into proteins, which are the molecules that do most of the work in cells.

While the human genetic code consists of an estimated 19,000-21,000 protein-coding genes[84], the number of mRNA transcripts making up the transcriptome is higher with an estimated 100,000 mRNA transcripts. This increase in complexity is arising mainly due to alternative splicing[85]. Through the process of translation of these gene products into proteins additional complexity is achieved. The increase in complexity at the proteome level is especially arising due to post-translational modifications (PTMs), which are covalent chemical modifications on proteins. Individual proteins can thus occur in several variously modified forms, which results in functional diversity. PTMs are crucial in regulating the activation or deactivation of certain proteins and thus alter protein function. It is therefore a widely accepted view that the complexity of the proteome is beyond the complexity of the genome and transcriptome (Figure 8)[86,87].

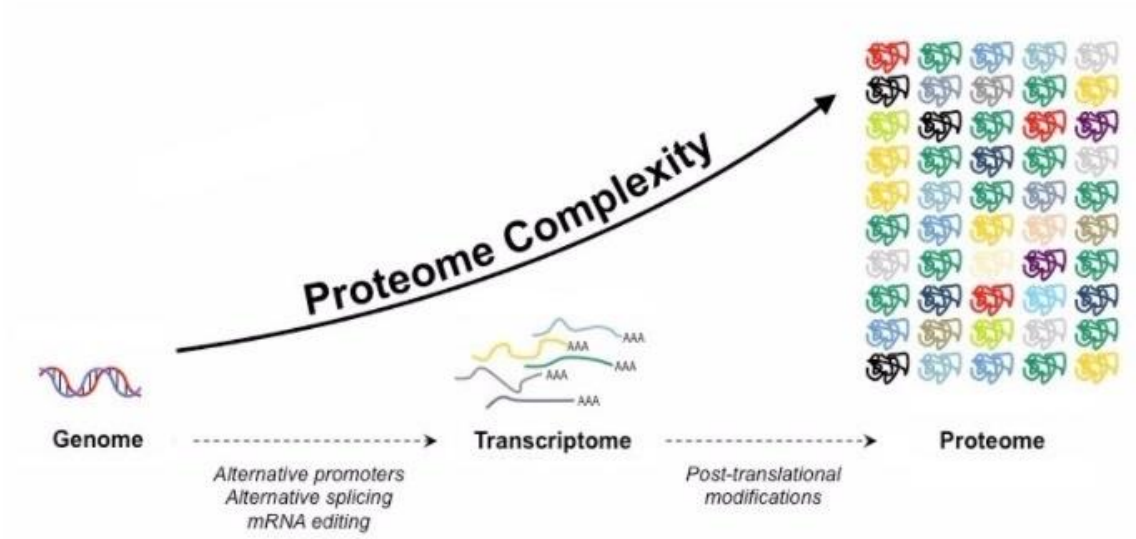

Figure 8: The proteome complexity *– A scheme of the genome, transcriptome and proteome and the associated increase in complexity due to alternative RNA formation and processing in the first step of gene expression, as well as post-translational modifications during the second step of protein formation – adapted from Thermo Fisher Scientific*[88]

The knowledge of the proteome and protein expression levels is fundamental to understanding changes in biological processes that are not reflected by mRNA abundance. The proteome is highly dynamic and varies over time. Especially between different tissues the proteome varies, while the genome is rather stable. Protein content and abundance often differs between cells, depending on their condition[89]. Proteomic analysis has thus emerged as an important method in biomedical research.

Nowadays, proteomic analysis is mainly mass spectrometry (MS) based, which is oftentimes preceded by liquid chromatography (LC), especially for the widely used “bottom-up” proteomics approach. Due to technological advances, MS instrument performance and bioinformatics computational tools have improved, and MS has become the prevailing method for proteomic analysis[90]. The use of LC-MS techniques allows for on-line separation of complex samples, thus is used for high throughput analysis of hundreds or thousands of proteins, providing quantitative protein information[90,91]. The quantification of proteins by means of MS is not easily done, however, thus several labelling and non-labelling techniques have been developed to improve this issue[92]. While some challenges of MS-based proteomics have been improved by technological developments, several challenges remain to be advanced further.

One of the most challenging problematics in MS-based proteomic analysis is the dynamic range of protein concentrations. With certain proteins highly abundant in the cell and others that are several orders of magnitude lower in abundance, the dynamic range is rather extensive. These lower abundant proteins are oftentimes the proteins of interest; however, they are harder to detect. In order to deal with this problem, fractionations or enrichment steps are frequently incorporated into the proteomics workflow[92].

Activity-based proteomic profiling (ABPP) is a special proteomics approach in which the activities of proteins of a certain enzyme group are targeted, enriched and measured. This technique improves the problem of the usually vast dynamic range of protein concentrations due to the enrichment based on the activity of the enzymes. The proteins that belong to this enzyme class may be low abundant compared to other proteins, but they are enriched while other more abundant proteins, which do not share the same reaction mechanism, are lost. Since this technique works by targeting active enzymes, this proteomics approach falls into a group of techniques termed functional proteomics, which infers information of the proteins functionality rather than mere abundance[92].

1.3.1. Activity-based proteomic profiling (ABPP)

Activity-based proteomic profiling (ABPP) is an approach for the functional analysis of proteins. The principle of ABPP is the covalent attachment of a small molecular probe termed activity-based probe (ABP) to the active site of a group of enzymes with shared catalytic mechanism. For the probe to covalently attach to the active site the enzymes are required to be in their active state[93]. Most enzymes are transcriptionally as well as post-translationally regulated. While transcriptional regulation affects the abundance of a protein, post-translational modifications do not change the protein's abundance, but usually affect the protein's function and activity. This functionality is usually not measurable by regular proteomics approaches, however, activity-based proteomics allows for the determination of the activity of a protein rather than its mere abundance[92]. When an appropriate reporter tag (such as biotin) is incorporated in the ABP, the probe-tagged proteins can be enriched (e.g. by use of streptavidin). This provides an additional advantage of this method as it allows for the detection of proteins that are low in abundance because target protein concentration is increased and sample complexity is decreased upon enrichment.

ABPP can be very useful for the identification and characterization of novel proteins of enzyme classes, which are sometimes not identified based on sequence homology with other members of the same enzyme group[94]. Furthermore, new covalent inhibitors for enzyme groups can be tested by ABPP that can be potentially interesting pharmaceutical targets, making ABPP a useful tool in early drug discovery[93]. Another ABPP approach is the combination of differential gel electrophoresis (DIGE) with functional proteomics by the use of ABPs containing fluorophores. This method was termed DABGE (differential activity-based gel electrophoresis) and allows for the visualization of expression patterns of enzyme groups[92]. Relative quantification can be performed by this method by image analysis of the expression pattern followed by MS-based identification of the protein spots. Due to the limited resolution of DIGE and advances in MS performance, nowadays proteins are usually directly measured by LC-MS methods following probe treatment and sample preparation. Additionally, bulky and/or charged reporter groups on the ABPs often interfere in DIGE with isoelectric focusing (IEF). On the other hand, DIGE is able to resolve protein isoforms which is very challenging in shotgun proteomics. Another application of ABPP is the subcellular imaging of the target proteins when using an ABP with fluorescent reporter tags. With this method the localization of enzymes can be resolved *in-vivo*, which provides

important information of the enzymes of interest in physiological or pathophysiological processes[95]. Bulky reporter groups on the ABPs also interfere with *in-vivo* studies as they oftentimes do not readily diffuse across cell membranes. One method to circumvent this problem is the use of bio-orthogonal chemistry, in which a small and chemically inert tag on the probe is attached to the reporter via a coupling reaction[91]. This way, smaller probes can be employed that allow for *in-vivo* treatment of the cells or tissue. Enabling the treatment of samples with the probe prior to homogenization is of advantage. In this case the enzymes are in their active state, which is a pre-requisite for probe recognition[93]. While some enzymes are partially deactivated by homogenization, others require cofactors or co-localization to specific sub-cellular compartments in order to be in their active form[92]. *In-vitro* labelling thus often leads to a loss of otherwise positive signals, even if an appropriate probe is used[92]. Hence, the employment of bio-orthogonal chemistry has been a very useful improvement in the development of *in-vivo* ABPP methods.

1.3.1.1. Activity based probes (ABP)

Activity-based probes make up excellent tools to examine the diversity of enzyme activities at different conditions or stimuli[95]. ABPs are oftentimes developed from potent covalent inhibitors for a certain enzyme[93]. The core and most important part for the selectivity of a typical ABP is the enzyme class-specific reactive group (RG). The RG is usually designed to mimic the transition state of the first reaction step that is catalyzed by these enzymes, and it binds covalently to the active site of the enzyme. For the first time in 1999, the Cravatt group published a novel covalent inhibitor of serine hydrolases which consisted of a fluorophosphonate and a non-radioactive biotin reporter tag[91,93]. In order to target different groups of enzymes, other inhibitor structures have been used, like epoxide electrophiles for cysteine proteases[96] or α-bromobenzyl-phosphonates for tyrosine phosphatases[97]. In addition to the selectivity achieved by the RG, the binding group (BG) of an ABP can be altered to allow for additional selectivity. Depending on the desired application, the probes can be tuned to target the whole enzyme class, specific subpopulations, or even individual enzymes within a group. Schmidinger *et al.* developed a panel of p-nitrophenyl phosphonates with different BGs that allow for the discrimination of lipases and esterases within the group of serine hydrolases[98]. For visualization, enrichment and detection, the ABP needs to contain a reporter tag (RT). RTs are either radioactive, fluorescent or affinity tags that are chosen based on the

application[92]. Radioisotope tags, however, have been mostly replaced by fluorophores or affinity-tags like biotin[91]. Bulky and/or charged RTs interfere with techniques like DIGE or may be unable to permeate the cell membrane. Thus, it is of advantage to use a small ABP to which a linker or RT can be attached at a later step. This is made possible by click-chemistry reactions, which are often applied in ABPP. Additionally, the RT can be spatially separated from the probe by a linker region (LR) to further decrease the effect of the RT on the enzyme. The LR can be designed in a way to be cleavable, which can be employed after affinity enrichment steps to elute specifically the isolated active enzymes. Through attaching the linker or RT after the initial probe binding, the choice of reporter tags is virtually unlimited since there is no interference while the probe binds to the active enzyme[95].

1.3.1.2. ABP for serine hydrolases

As thoroughly discussed above, SHs share a catalytic triad in their active site consisting of a nucleophilic serine, a histidine acting as an acid/base, and usually an aspartic acid residue. The catalytic mechanism of SHs allows for the covalent attachment of a properly designed ABP.

When the substrate is attacked by the nucleophilic serine, the tetrahedral transition state (TS1) is formed (Figure 7)[92], which is converted to the acyl-enzyme intermediate upon kicking out the alcohol, amine, or thiol group from the substrate. Inhibitors of serine hydrolases mimic this tetrahedral transition state resulting in their covalent attachment to the serine of the enzyme. The reactive group of the ABP for SHs is a tetrahedral phosphonate, containing fluoride or p-nitrophenol which act as the leaving group (LG), enabling covalent binding to the enzyme[92]. The binding group (BG) is chosen for specific selectivity according to the application. For functional lipase or lipid associated protein analysis the BG can be chosen to be different alkyl chains, TAG analogues, or other lipid analogues (Figure 9)[92]. In order to identify, visualize or enrich the SH based on the ABP, the ABP has to bear some kind of reporter tag (RT) or linker moiety to which a RT can be attached[92].

The main structure of phosphonate inhibitors for SHs with the most common leaving groups (fluoride or p-nitrophenyl) as well as possible binding groups for lipid-associated protein targets and commonly used reporter tags are listed and shown in Figure 9.

In Figure 10, the reaction mechanism of SH inhibitors covalently attaching to SH enzymes is represented.

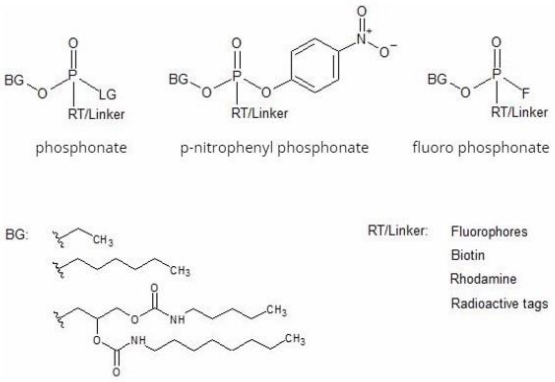

Figure 9: Design of serine hydrolase (SH) activity-based probes *– Phosphonates with either fluoride or p-nitrophenyl as leaving group (LG). Possible binding groups (BG) are depicted below the SH inhibitor structures, as well as possible reporter tags (RT). Contents of the figure adapted from Schittmayer* et al. [92]

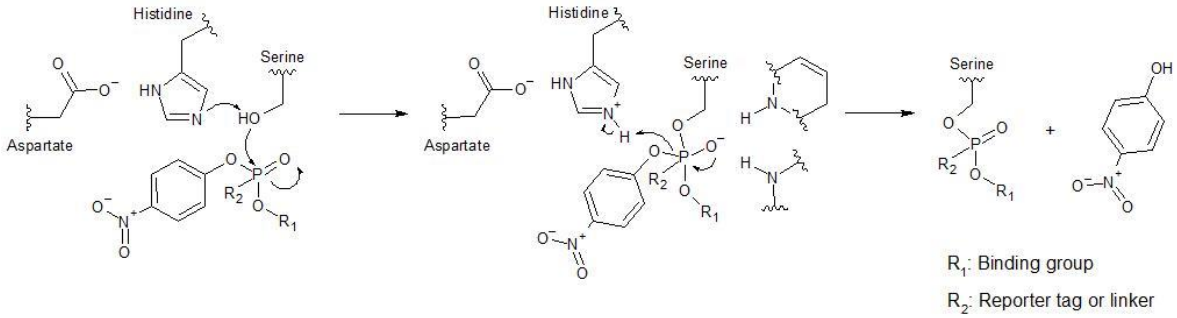

Figure 10: Proposed mechanism of serine hydrolase (SH) inhibition by SH inhibitors *– the inhibition occurs via covalent attachment of the SH inhibitor to the active serine in SHs; the SH inhibitor in this case bears a p-nitrophenol as a leaving group.*

The covalently linked ABP can subsequently be used for identification, visualization or affinity purification of the active SHs. Since it became evident that large reporter tags directly on the probe can interfere with probe recognition or cause other problems, click chemistry has been employed to attach the RT after probe recognition has occurred.

1.3.2. Click-chemistry

In 2001, Sharpless and coworkers coined the term click-chemistry when they published a collection of highly reliable and selective reactions based on carbon heteroatom bond formation, which can be employed for the synthesis of new compounds[99]. Their aim was to copy nature, by joining together small chemical units through heteroatom links[99] in a facile, selective, high-yield reaction under mild water-tolerant conditions[100]. In their

review, they mention an important cycloaddition reaction - the Huisgen dipolar cycloaddition of azides and alkynes[99].

Thereafter, the Sharpless group developed the copper catalyzed Huisgen alkyne-azide [3+2] cycloaddition (CuAAC), published in an additional paper in 2002[101]. In the same year the Meldal group reported the same Cu(I) catalysis of this reaction, independently from Sharpless. As reviewed in Liang *et al.*, 2011[100], the CuAAC reaction shortly became one of the most used click-chemistry reactions due to its easy use and wide application. It has had important impact on drug design and development, organic synthesis as well as on polymer chemistry[100]. CuAAC has also been used frequently for bioconjugations, aided by its bio-orthogonality. The reacting components azide and alkyne are not reacting with functional groups found in nature; besides, the reaction can undergo under physiological conditions[102].

However, one major drawback to CuAAC for *in-vivo* applications is the cytotoxicity of the Cu(I) catalyst. The toxicity of copper is mainly ascribed to its contribution to form reactive oxygen species (ROS), leading to oxidative damage and changes in cellular metabolism[103]. This makes CuAAC non-compatible for most *in-vivo* applications.

In order to emphasize this problem, Bertozzi and colleagues have coined the term bio-orthogonal chemistry which excludes reactions with toxic components[104].

1.3.3. Bio-orthogonal chemistry

Bio-orthogonal chemistry is defined to include all chemical reactions that can take place within living cells or organisms while not interfering or interacting with the biological system[105]. These types of reactions are especially useful for *in-vivo* applications, as another criterium for bio-orthogonal reactions is that they have to be functional under physiological conditions while not being toxic[104]. Bertozzi *et al.* describe a two-step process in which first a bio-orthogonal functional moiety is placed onto the probe or substrate and introduced into the living cell or organism. In a second step, a reporter tag can be added and is attached through a bio-orthogonal reaction[104].

Two outstanding bio-orthogonal reactions include the chemically inert azide moiety. One is the modified Staudinger (Bertozzi) reaction in which an azide group is reacted with a phosphine[104,106], while the other reaction is termed strain-promoted azide alkyne cycloaddition in which the driving force is the relieve of strain from a cyclic alkyne[107]. The azide group is appreciated for its chemical inertness as is the capability to react it in a very selective manner.

1.3.3.1. Staudinger Ligation

Bertozzi and Saxon first described the modified Staudinger ligation in 2000 based on the original Staudinger reaction, which was developed by Hermann Staudinger as early as 1919. The original reaction includes a tertiary phosphine that reacts with an azide moiety. Then, the intermediate product is hydrolyzed to yield a phosphine oxide and an amine[108]. In the modified Staudinger ligation reaction, the tertiary phosphine is modified in a way to contain an electrophilic trap, which prevents the hydrolysis of the intermediate aza-ylide forming an amide bond. This amide bond links the two molecules together (Figure 11)[106]. However, the Staudinger ligation does not come without limitations. One problem is the low kinetics of the reaction, another issue is the high susceptibility of phosphines to oxidation[107].

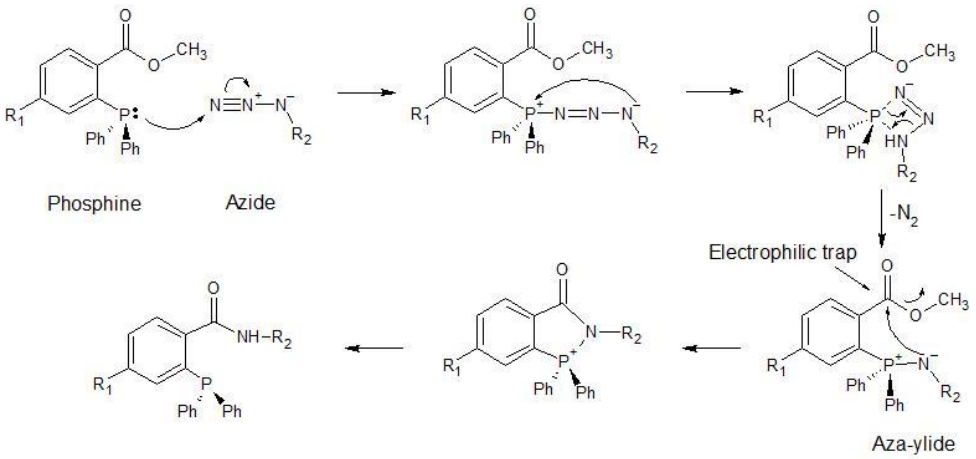

Figure 11: Reaction mechanism of the modified Staudinger reaction *- the Staudinger (Bertozzi) ligation*

1.3.3.2. Strain promoted alkyne-azide cycloaddition (SPAAC)

In order to prevent some of the disadvantages of the Staudinger ligation, a new reaction was considered by the Bertozzi group in 2004, giving up on using the highly oxidizable phosphine[107]. They re-considered the alkyne-azide cycloaddition reaction described by Huisgen but aimed at omitting the cytotoxic Cu(I) catalyst[107]. Since at ambient temperature the azide and alkyne do not react at a reasonable rate, the alkyne has to be activated to react with the azide group, which is the purpose of the Cu(I) catalyst in the first place. Bertozzi and colleagues found that they can activate the alkyne elsewise, namely by introducing the alkyne into a ring and thereby generating a considerable ring strain[107]. By using cyclooctyne derivatives that include a highly strained – thus activated

– alkyne group, the [3+2] alkyne-azide cycloaddition occurs readily at ambient temperature without the use of any catalyst[107]. The reaction was termed strain-promoted alkyne-azide cycloaddition (SPAAC) and is depicted in Figure 12.

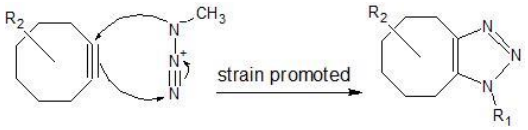

Figure 12: Reaction mechanism of the strain-promoted alkyne-azide cylcoaddition reaction

While the use of cyclooctyne eliminates the need for cytotoxic Cu(I) catalysts or poor performing phosphine reactive groups, the first generation of cyclooctynes showed poor reactivity as well. Thus, a number of cyclooctyne derivatives were generated in an attempt to improve reaction rates and hydrophilicity of the reactive group. Some of the second generation developed cyclooctynes are depicted in Figure 13 together with the initially used first generation cyclooctyne (OCT), which was initially described in 2004[107].

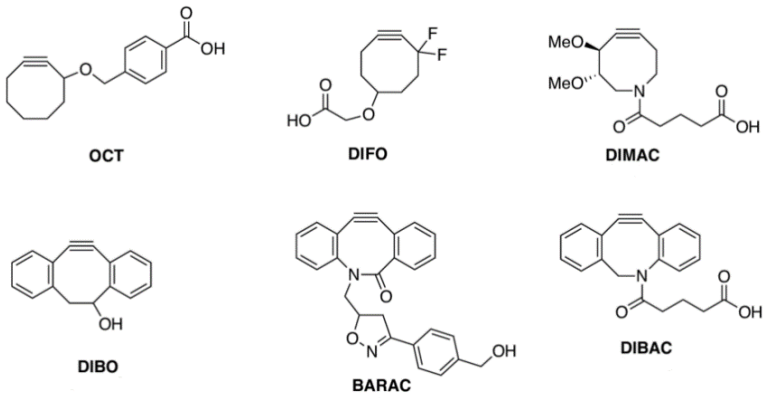

Figure 13: several generations of cyclooctynes for SPAAC bioconjugation reactions *- adapted from Shadmehr*[109]

One of the first improvements was the incorporation of electron withdrawing fluorine atoms at the propargylic positions of the alkyne which aided in lowering the activation barrier for the SPAAC reaction, generating rates comparable to the Cu(I) catalyzed reaction. The difluorinated cyclooctyne (DIFO) showed the best reaction rate[110]. In a different attempt, two aryl rings were introduced on either side of the cyclooctyne ring, leading to higher rates, as the aromatic rings impose additional ring strain on the alkyne while the *ortho* hydrogen atoms shield the alkyne from nucleophilic attack[111]. In their attempt, Ning *et al.* also attached an hydroxy group to the dibenzocyclooctyne generating 4-dibenzocyclooctynol (DIBO) providing a functional group that enables facile incorporation of tags[111]. To further improve DIBO by increasing its stability, an amide group was incorporated into the dibenzocyclooctyne ring making it an

azacyclooctyne, namely biarylazacyclooctynone (BARAC)[112]. Sletten *et al.* from Bertozzi group used another different approach to incorporate polarity donating methoxy groups into the cyclooctyne ring together with a nitrogen group making it an azacyclooctyne termed dimethoxyazacylcooctyne (DIMAC)[113]. In 2012, Yao *et al.* screened a panel of five different cyclooctyne structures and found that the best conjugation occurred with an aza-dibenzocyclooctyne termed ADIPO[114], which is also termed DIBAC for the systematic name Dibenz[b,f]azocine-5(6H)-pentanoic acid, 11,12-didehydro-δ-oxo-, methyl ester. Cyclooctynes can further be labelled with desired affinity tags or fluorophores to enable enrichment or visualization.

A protein mixture of interest can be subjected to an ABP containing an azide functional group, and subsequently the mixture can be reacted with a SPAAC cyclooctyne. After generation of the link between the proteins and an enrichment tag on the cyclooctyne the desired proteins can be affinity enriched. Finally, the protein mixture can be used for proteomic analysis. A frequently used analysis technique in proteomics is liquid chromatography (LC) coupled with mass spectrometry (MS).

1.3.4. Liquid Chromatography (LC)

One of the most widely used techniques for chemical analysis in which samples can be separated, analyzed and/or purified is liquid chromatography (LC)[115]. In proteomics analysis, LC is widely used to separate complex sample mixtures of intact proteins or peptides prior to mass spectrometric analysis[116]. It is well appreciated for its high resolving power, reproducibility and compatibility with MS, and it can be used to separate both complex mixtures of intact proteins or peptides[117].

The main principle of any type of chromatography is based on the differential partitioning of the analytes between a stationary and a mobile phase based on their physical properties[118]. In LC, the separation is based on the interactions of dissolved analytes in a liquid mobile phase with the functional groups of a stationary phase. The liquid mobile phase together with the dissolved analyte molecules is pumped through a column packed with stationary phase material under high pressure (HPLC)[118]. The vast selection of different stationary as well as mobile phases makes LC a very versatile tool for proteomic analysis[117]. A number of LC types can be classified based on the chemistry of the stationary phase e.g. reversed-phase (RP), normal-phase LC (NP), ion-exchange (IEX) or size-exclusion (SEC). Other combinatory types of LC have been developed such as hydrophilic interaction chromatography (HILIC).

Even though a variety of LC methods have been developed, reversed-phase LC (RP-LC) remains one of the most commonly used methods in proteomics[117]. In RP-LC, the stationary phase is usually silica-based with conjugated non-polar residues such as C-8, C-18 or phenyl groups. The mobile phase is in general a mixture of highly diluted volatile acid in water and a water-miscible organic solvent such as acetonitrile (ACN)[117].

With the help of electrospray ionization (ESI) LC can be directly coupled to the mass spectrometer allowing for an on-line analysis[116].

1.3.5. Mass Spectrometry (MS)

Mass spectrometry (MS) is an extremely sensitive and specific analytical technique that separates ions based on their difference in mass to charge (m/z) ratio[90]. A typical mass spectrometer consists of an ion source, a mass analyzer, and an ion detector[90]. By means of the ion source the analytes are converted into gas-phase ions, which is a prerequisite for MS analysis[119]. The mass analyzer separates the gas-phase ions based on their m/z ratio in a high vacuum while the detector records the number of ions at the individual m/z values and thus gives an intensity information about every m/z species[90,119].

The two ionization techniques that are most commonly used in proteomics are electrospray ionization (ESI) and matrix assisted laser desorption ionization (MALDI), both soft ionization techniques that can be used to ionize intact proteins or peptides[90,119].

The central part of the mass spectrometer, the mass analyzer, is key to the sensitivity, resolution and mass accuracy of the instrument[90]. The main function of a mass analyzer lies in the separation of the ions based on their m/z ratio. There are several basic mass analyzers: quadrupole (Q), Ion Trap (IT), time-of-flight (TOF), Fourier-transform ion cyclotron resonance (FT-ICR) and Orbitrap[90]. The mass analyzers differ in their analytical performance and physical principles, hence oftentimes combinations of mass analyzers are utilized to combine the advantages of the different mass analyzers. Combinations of mass analyzers are also used for tandem-mass spectrometry (tandem-MS). Prominent examples are quadrupole–time-of-flight (Q-TOF) mass analyzers, Triple Quadrupole mass analyzers or linear ion trap (LIT)-Orbitrap mass analyzers[90,119–121].

1.3.5.1. Electrospray Ionization (ESI)

For the development of the electrospray ionization method, John Fenn was awarded the 2002 Nobel prize in chemistry, which points out the importance of this ionization method for the analysis of biological macromolecules like proteins[122]. The development of the ESI ionization method revolutionized LC-MS-based proteomics analyses[119].

Since the ESI method can be directly coupled to LC, it provides an important connection between LC and MS. As a soft ionization method it keeps peptides and proteins intact[90]. The dissolved analytes arriving from the LC column are fed into a small high-voltage capillary tube together with a nebulizer gas (usually N_2). The high electric field at the tip of the capillary causes the formation of small charged droplets, which form the so-called Taylor cone. In most proteomic experiments the ionization is set to positive mode, hence positively charged droplets form, emerging as an aerosol spray from the capillary into the ESI chamber. Aided by heated N_2 gas they are subsequently evaporated in the ESI chamber while travelling to a negative potential which is applied on the entry of the mass analyzer. During evaporation, electrostatic repulsion forces grow and once they overcome the surface tension (Rayleigh limit) charged molecules break free from the droplet until eventually positively charged single molecules are generated[90,121,123]. These charged single molecules are delivered from atmospheric pressure into the mass analyzer which is operated under vacuum[90,121,123]. A schematic representation of the electrospray ionization run in positive mode is depicted in Figure 14.

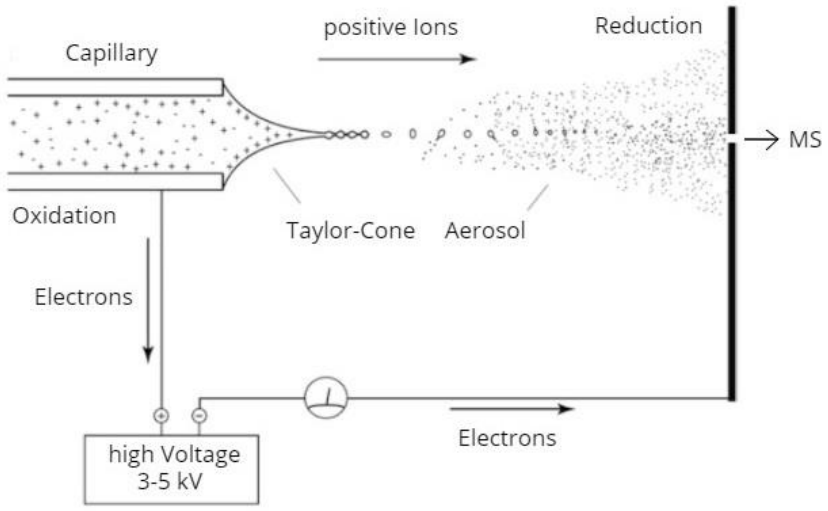

Figure 14: Electrospray ionization in positive mode *- schematic representation, adapted from Jürgen H. Gross*[121]

1.3.5.2. Mass Analyzers

Mass analyzers differ not only in their performance but also in the physical principles underlying their separation capability. However, all mass analyzers are based on static or variable electric or magnetic fields[121]. Furthermore, all mass analyzers are operated under high vacuum between 10^{-5} and^{-10} mbar[121].

Quadrupole - Q

A Quadrupole mass analyzer consists of four parallel metal rods. Each pair of diagonal rods is subjected to a certain radio frequency voltage and to a DC voltage. The ions drift along the z-axis of the quadrupole and oscillate between the polarity-changing rods. If ions hit a rod they are neutralized and lost. Depending on the ratio of the applied voltages only certain m/z make it through the quadrupole and are detected. This feature enables the quadrupole to detect only certain m/z values or scan through a range of values by changing the applied voltage[121]. Many hybrid systems contain one or more quadrupoles, e.g. the widely used triple quadrupole (QQQ) or the Q-TOF mass analyzer. Besides, quadrupoles can be filled with an inert gas (He, N_2, or Ar) and thus allow fragmentation experiments by collision induced dissociation (CID)[121].

Time of flight - TOF

Time of flight (TOF) mass analyzers are based on the temporal separation of ions with different m/z values. The ions are accelerated with the same kinetic energy into an evacuated tube. The time it takes for an ion to arrive at a detector that is a known distance away depends on its m/z value. The flight times are measured and correspond to different m/z[121].

Orbitrap

The orbitrap mass analyzer is a type of ion trap available since 2005[121]. The separation is based on ions oscillating in an electric field[124]. The frequencies of the ions ions' axial movement is recorded and like in FT-ICR the mass spectrum is subjected to Fourier-transformation to yield signal intensity over m/z[121].

1.3.6. General proteomics workflow

In MS-based proteomics analysis there are two major approaches – bottom-up or "shotgun" proteomics and top-down proteomics. In top-down proteomics, the proteins

are separated without prior digestion to peptides and introduced into the mass spectrometer while still intact[116]. In the more commonly applied shotgun or bottom-up proteomics approach the samples are digested prior to separation and introduced into the mass spectrometer as peptides[125]. A schematic view of the two main proteomics approaches is depicted in Figure 15.

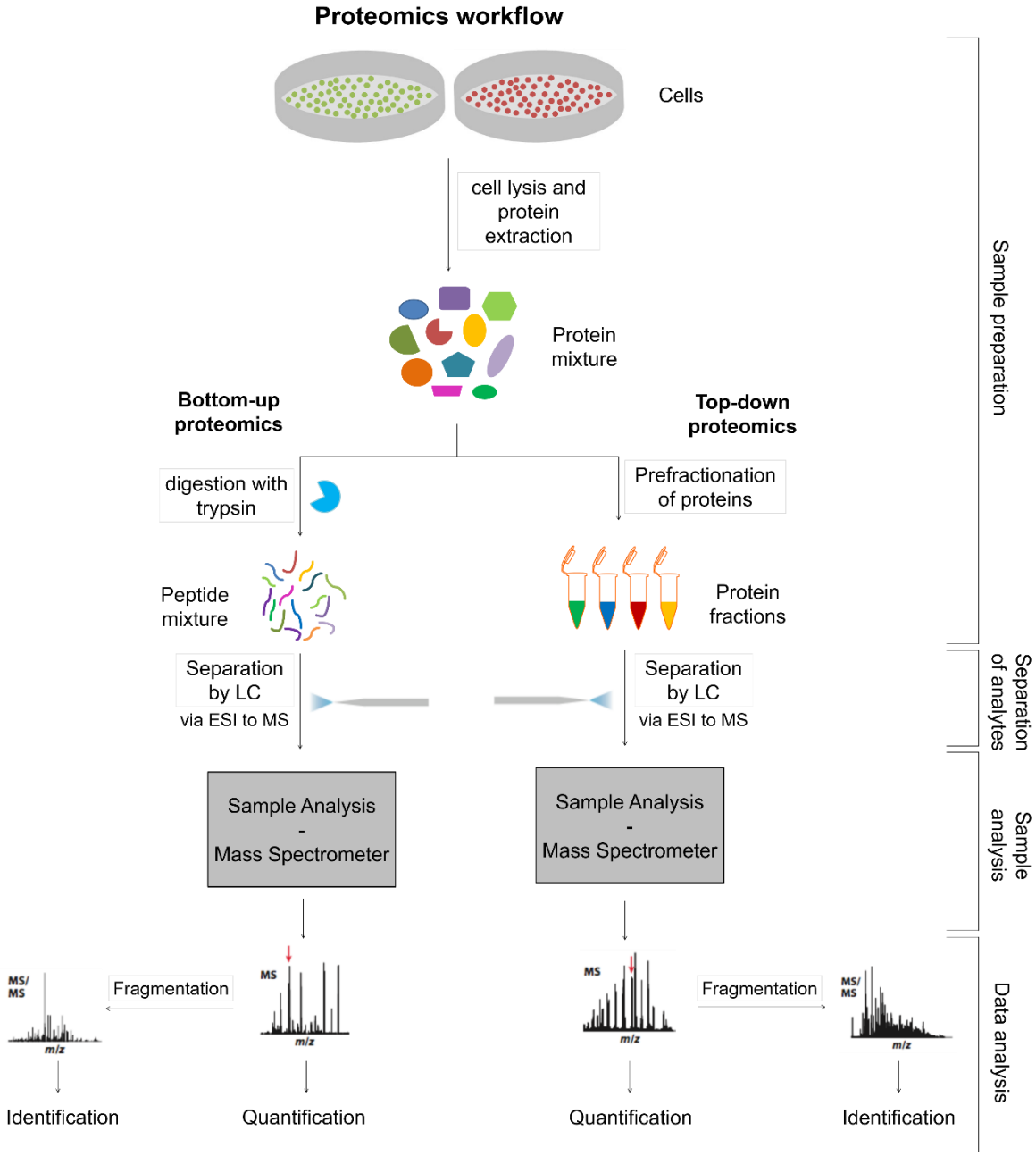

Figure 15: Proteomics workflow *- bottom up vs. top down approach, adapted from Zhang et al.*[126]

Both workflows can be divided roughly into four parts – the sample preparation, the separation of the complex mixture of analytes (usually by LC), the sample analysis and the data analysis. For both proteomics approaches, the sample preparation starts with

protein extraction from cells, tissue or other sources to yield a protein mixture. In the top-down approach this is oftentimes followed by a prefractionation method like isoelectric focusing (IEF), or gel-electrophoresis prior to LC separation. In bottom-up proteomics, the obtained protein mixture is exposed to digestion enzymes to generate peptides, which are then usually separated by LC followed by MS analysis. Protein identification is achieved by tandem-MS in which proteins and peptides are fragmented to infer the amino acid sequence from the obtained fragments.

1.3.7. Activity-based proteomic profiling workflow

Activity-based proteomic profiling is a variation of the general MS-based proteomics analysis. The workflow of how ABPP is performed in our lab is depicted in Figure 16 and explained in more detail in *Materials and Methods* (3.7.5.).

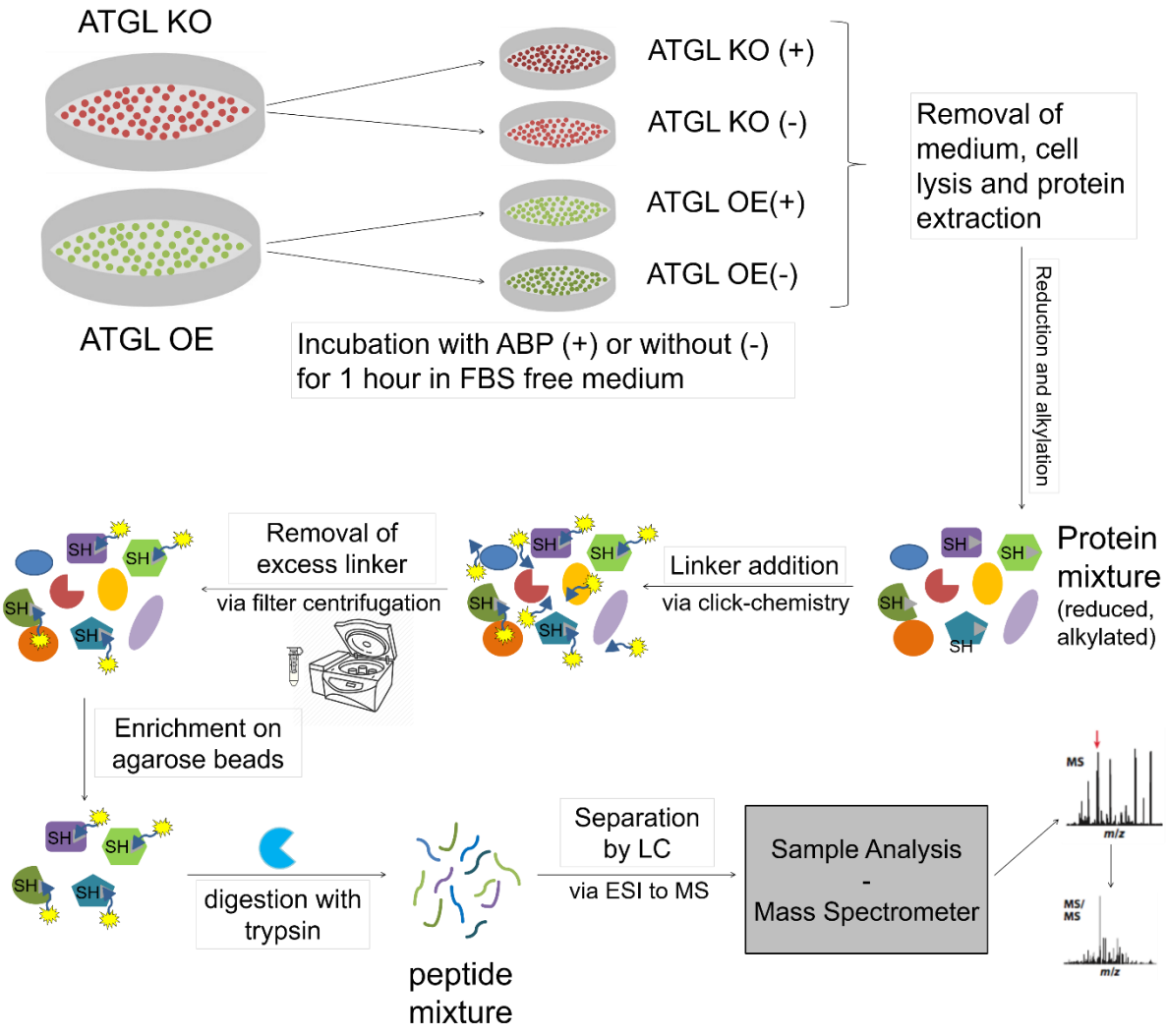

Figure 16: Activity-based proteomic profiling workflow

In short, the cells are either incubated with the ABP ((+) sample set) or not ((-) sample set) followed by lysate preparation. After cell harvest (+) and (-) samples are subjected to the same workflow: First, the proteins are reduced and alkylated (with N-ethylmaleimide (NEM)) before a linker with reporter tag (biotin) is added. The linker reacts via bio-orthogonal chemistry with the ABP, resulting in proteins covalently linked with biotin. Excess of linker is removed via centrifugal filters and the resulting lysate is used for enrichment on streptavidin-agarose beads. The biotin on the linker interacts with the streptavidin on the beads and ABP-tagged proteins are retained on the beads. After removal of non-bound proteins, the enriched proteins are digested with trypsin and the peptide samples are analyzed by HPLC-MS. For the identification and label-free quantification (LFQ) of the peptide samples MaxQuant[127,128] is employed and statistical analysis is performed with Perseus[129].

1.3.7.1. Data Analysis

The output from LC-MS/MS measurements consists of chromatograms and MS spectra, which contain the peptide mass and intensity information. Besides, the output includes tandem MS (MS/MS) spectra for the most intense peptides. The peptides are identified by matching their MS/MS spectra with predicted MS/MS spectra of *in-silico* peptides by a peptide search engine (Andromeda in MaxQuant). The *in-silico* peptides are generated by *in-silico* digest of proteins from a protein database.

For appropriate peptide matching, the *in-silico* generated peptides need to be processed like the experimentally derived peptides, hence the digestion enzyme used in the experiment needs to be specified for the *in-silico* digest. The most commonly used digestion enzyme is trypsin, as the cost of trypsin is relatively low and digestion is specific and efficient. Trypsin cleaves C-terminal to lysine and arginine (with exception of Proline being present N-terminally)[130]. The average peptides that are generated from tryptic digest are suitable in length and charge for LC-MS[130]. Typically, some missed cleavages occur[130], thus a certain number of missed cleavages per peptide can be allowed[127]. Since trypsin itself contains several lysine and arginine residues it is subjected to autolysis, which leads to a high number of tryptic peptides in the samples. Therefore, it is of importance to include trypsin in the protein database.

The database for *in-silico* MS/MS spectra generation should contain all proteins that can be expected in the experiment, i.e. the entire protein database of the organism of interest[131]. The proteins can be retrieved from protein databases like UniProt

(www.uniprot.org) and if possible, manually annotated and reviewed proteins should be chosen (Swiss-Prot). In addition to the proteins from the organism of interest, common contaminants should be included in the database – one example is the inclusion of porcine trypsin. Other examples are bovine serum albumin (frequently present in cell culture) or human keratin. The Global Proteome Machine has generated a list of common contaminants termed the common Repository of Adventitious Proteins (cRAP) protein sequences, which should be included into the database (https://www.thegpm.org/crap/).

Modifications on amino acids lead to mass changes and thus have to be included in the search in order to properly identify peptides containing modified amino acids. Fixed as well as variable modifications on specific amino acids can be applied in MaxQuant settings. For instance, reduction and alkylation of cysteins to prevent re-folding is performed experimentally, resulting in a fixed modification on all cysteins. This modification is specified in MaxQuant as fixed modification on all cysteins and selenocysteins with a mass change corresponding to the used alkylating agent (e.g. 125.05 Da for NEM). Variable modifications like oxidation on methionine or acetylation on the N-terminus of the protein can be set as well. The so-called search space contains all spectra of the (modified) peptides from the database and should contain all proteins possibly occurring in the samples, while kept as small as possible in order to prevent long run times and random peptide matches.

In order to identify proteins from the peptides, the peptide hits are assembled into protein hits. Peptides are either unique for a protein (unique peptide), or assigned to the protein group with the highest number of identified peptides (razor peptide)[127]. If a set of peptides is the same for two or more proteins, these proteins are united into one protein group[127]. For higher protein confidence quantification can be set to be based on unique and razor peptides only. Additionally, settings can include that a minimum of a certain number of independent peptides have to be confidently measured per protein.

For each sequence matching the peptide MS/MS spectra in the database search a peptide score is obtained and the best scoring sequence is kept[127]. The peptide matches are statistically tested based on the probability of false positives. To this end, a decoy database is generated. In general, the decoy database contains peptides in reverse or randomized order. The experimental MS/MS spectra are matched against *in-silico* spectra from the decoy database and matches are recorded as false positive hits that are used to calculate the posterior error probability (PEP), given the peptide

score and peptide length[127]. For each individual peptide a PEP is calculated, which gives the probability of a peptide being identified incorrectly[127]. The matched peptides are listed according to the PEP scores, starting with the best PEP score (low probability of wronge identification). The FDR is set to a certain threshold (cutoff score) e.g. 1% and all peptides are accepted until the threshold is reached at which e.g. 1% of the total hits are false positives. Hence, the FDR is defined as the ratio of false positive matches to the total number of matches. To each protein group a PEP can be assigned by multiplication of the peptide PEPs, allowing for an FDR of protein groups[127].

The quantification of the peptides in MaxQuant is based on extracted ion chromatograms (XIC)[128]. XIC analysis allows for a more accurate readout of peptide-ion intensity, however, pre-requisite for accurate determination of XICs of peptides is a high mass resolution of the peptides[128].

The in MaxQuant incorporated match-between-runs feature further allows for an increased peptide identification by matching peptides identified in adjacent samples by their m/z and retention time. This feature leads to an overall higher number of identified peptides after retention time alignment[127].

2. Aims

It was shown by Tomin *et al.* that ATGL loss from lung carcinoma cells leads to an altered lipid profile. Not only did they observe that TAGs are increased in cell lines lacking ATGL, but more strikingly, the lysophospholipid levels were increased as well[68].

Lysophospholipids are neither substrates nor products of ATGL directly, thus it is hypothesized that ATGL loss from lung carcinoma cells leads to the up- or downregulation of a different lipase or acyltransferase, which causes these altered lysophospholipid levels.

The main aim of this study was to discover the suspected up- or downregulated lipase or acyltransferase in lung carcinoma cells by activity-based proteomic profiling with a serine hydrolase probe followed by bio-orthogonally linking the ABP-tagged proteins to a biotin moiety. The biotin was finally be used for affinity enrichment and subsequent proteomic analysis of the enriched proteins.

To this end, a serine hydrolase-specific ABP was employed on A549 lung carcinoma cell lines lacking ATGL (ATGL knock-out (KO) cells) and on A549 wild-type (WT) cell lines. Additionally, an ABPP experiment was performed on ATGL KO cell lines together with their ATGL overexpressing (OE) counterpart cell lines. The used ABP was a p-nitrophenyl-phosphonate with a six-carbon alkyl chain as binding group and a propylazide as the linker-reactive group and was termed C_6-probe. Additionally, two different linkers were tested. Both contained a strain-promoted azide-reactive alkyne group and a biotin as reporter tag for affinity purification. In one linker, the RT and alkyne group were connected via an amino acid sequence, while the other was linked via a DNA sequence. Both linkers were designed to be cleavable, making them applicable for elution of the enriched proteins on the affinity columns.

The first aim of this project was to achieve efficient enrichment and identification of serine hydrolases upon ABP treatment of the cells compared to non-treated cells.

The second and main aim was to use this established activity-based proteomic profiling technique to find the hypothetically up- or downregulated serine hydrolase, which may be responsible for the altered lysophospholipid profile in ATGL lacking cells.

3. Material and Methods

If not stated otherwise chemicals were obtained from Sigma Aldrich. Human A549 lung carcinoma cells were obtained from CLS (Eppelheim, Germany).

3.1. Cell culture

3.1.1. Material

- Roswell Park Memorial Institute (RPMI) 1640 Medium with 2 g/L glucose, sodium bicarbonate, without L-glutamine, liquid, sterile-filtered, suitable for cell culture (Sigma-Aldrich, Product #R0883)
- Fetal bovine serum (FBS), qualified (Thermo Fisher Scientific, Product #10270-106)
- L-Glutamine 200 mM (Sigma Aldrich, Product #G7513)
- Dulbecco's Phosphate Buffered Saline (PBS) (Sigma Aldrich, Product #D8537)
- Trypsin-EDTA solution, 0.25 %, sterile-filtered, suitable for cell culture – 2.5 g porcine trypsin and 0.2 g EDTA • 4Na per liter (Sigma Aldrich, Product #T4049)
- Gentamycin (Sigma Aldrich, Product #G1397)
- Cell culture-grade dimethylsulfoxide (DMSO) (Sigma Aldrich, Product #D2438)
- BioLite 75 cm^2 flasks, vented (Fisher Scientific, Product #11884235)
- Tissue culture plates, 12 wells (VWR, Product #734-2324)
- Tissue culture dish, 10 cm (TPP, Switzerland, Product #93100)
- CASY ton (Omni Life Science, Product #5551808)

For the preparation of the cell medium 500 ml RPMI medium were supplemented with 50 ml FBS and 5 ml 200 mM L-glutamine solution generating 10 % FBS and 0.3 g/L L-glutamine final concentration.

For initial thawing of the ATGL KO* and ATGL OE cell lines, in addition to the 10 % FBS and 0.3 g/L L-glutamine 4.44 ml of 50 mg/ml gentamycin was added to obtain a final concentration of 0.4 mg/ml gentamycin.

For the preparation of freezing medium 1 ml of 95 % cell medium with 5% cell-culture grade DMSO was prepared for each sample.

3.1.2. Cells

Cell line	Short Name
A549 ATGL KO (CRISPR/Cas9 knock-out)	ATGL KO
A549 wild type (WT) (control)	WT (control)
A549 ATGL KO with introduced GFP overexpression	ATGL KO*
A549 ATGL KO with reintroduced ATGL overexpression	ATGL OE

Table 1: Cell lines

The A549 lung carcinoma cells lacking ATGL were previously established in our lab using CRISPR/Cas9 technology. The A549 cells overexpressing ATGL or green fluorescent protein (GFP) were established previously by lentiviral transfection of ATGL or GFP into the ATGL KO cells.

All experiments were carried out using three biological replicates if not otherwise stated.

The cells were generally kept in an incubator at 37°C and humidified 5% CO_2 atmosphere. For counting of the cells 50 µl of cell suspension was added to 10 ml of CASY ton (1:200 dilution) and cells were counted on a CASY Innovatis cell counter.

3.1.3. Splitting of cells

Cells were kept in 75 cm^2 cell culture flasks (T-75) and split at 60-80% confluency. For splitting, the culture medium was removed and the cells were washed with 5 ml PBS. In the next step 2 ml trypsin-EDTA was added and incubated at 37°C for 6 minutes. The cells were checked under the microscope to confirm the detachment from the flask. The trypsin activity was stopped by adding 4 ml of cell medium to the flasks and cells were taken up from the flask and transferred into a 15 ml Sarstedt tube. Depending on the application the cells were split either 1:4 or 1:8, hence one fourth or one eight of the cell suspension was transferred back into a T-75 flask filled with 10 ml of working medium. The flasks were reused for up to 2 weeks.

3.1.4. Thawing of cells

The frozen cells were thawed in the cryo-vials in a 37°C water bath. Once the cells were thawed, they were transferred into a fresh T-75 flask filled with 10 ml of cell medium. After 4-5 hours or after the cells were allowed to settle, the medium was exchanged to

dispose of the remaining DMSO from the freezing medium. The cells were generally kept at 37°C under a 5% CO_2 atmosphere.

3.1.5. Freezing of cells

For preparing stocks of the cells, the cells were harvested as described above (3.1.3.) and again transferred into a 15 ml Sarstedt tube. The cells were centrifuged at 800 rpm for 5 min at room temperature (RT). The supernatant was removed and the cells were resuspended in an appropriate amount of freezing medium (1 ml for each frozen sample). 1 ml of the cell suspension was transferred into a cryo-vial and placed into a -20°C freezer before putting the vials in -80°C.

3.2. Protein determination

3.2.1. Material

- Pierce™ BCA Protein Assay kit (Thermo Fisher Scientific, Product #23227)
    - BCA reagent A (containing sodium carbonate, sodium bicarbonate, bicinchoninic acid and sodium tartrate in 0.1M sodium hydroxide)
    - BCA reagent B (containing 4% cupric sulfate)
- BSA (Sigma Aldrich, Product #A6003)
- BSA stock solution (10 mg/ml) prepared by dissolving 50 mg of BSA in 5 ml H_2O

The BSA standard solutions were prepared according to table 2.

Vial	Volume of diluent [µl]	Volume of BSA Source [µl]	Final BSA conc. [mg/ml]
Stock			10.000
A	800	200 (stock)	2.000
B	125	375 (A)	1.500
C	375	375 (A)	1.000
D	175	175 (B)	0.750
E	325	325 (C)	0.500
F	325	325 (E)	0.250
G	325	325 (F)	0.125
Blank	300	0	0.000

Table 2: BCA protein estimation - standard solutions

3.2.2. Protein estimation for Western blot

Western blot lysates were diluted either 1:10 or 1:20 with lysis buffer prior to the protein estimation. Therefore, lysis buffer was also used as a diluent for the protein determination. 25 µl of diluted lysate sample and BSA standard solutions were transferred in duplicates to a 96-well plate. 1 part of BCA reagent B was added to 50 parts BCA reagent A generating the working BCA reagent. 200 µl of BCA reagent was added to the wells with sample and BSA standard solutions and incubated at 37°C for 30 min. Afterwards a colorimetric detection was performed on a plate reader at 562 nm wavelength. From the standard solutions a standard curve was generated and from the obtained equation the concentrations of the samples were calculated.

3.2.3. Protein estimation for Activity-based proteomic profiling

ABPP lysates were diluted 1:8 with PBS prior to protein estimation. PBS was used as the diluent for the standard solutions. 9 µl of diluted sample and BSA standard solutions were transferred in duplicates to a 96-well plate. BCA working reagent was prepared as described above (3.2.2). 260 µl of BCA reagent was added to each well and incubated for 30 min at 37°C. The remaining procedure was performed as described in chapter 3.2.2.

3.3. Western Blot

3.3.1. Material

Solutions and Buffers

- 10x TBS
- 1x TBS-T
- Transfer Buffer
- Lysis Buffer
- Tween 20 (Sigma Aldrich, Product #P2287)
- NuPAGE™ MOPS SDS Running Buffer (20X) (Thermo Fisher Scientific, Product #NP0001)
- Protease Inhibitor cocktail (Sigma Aldrich, Product #P8340)

- Phosphatase Inhibitor cocktail 3 (Sigma Aldrich, Product #P0044)
- Ponceau S (1 g/L in 5% acetic acid)
- NuPAGE™ LDS Sample Buffer (4X) (Thermo Fisher Scientific, Product #NP0007)
- NuPAGE™ Sample Reducing Agent (10X) (Thermo Fisher Scientific, Product #NP0009)
- Pierce™ ECL Plus Western Blotting Substrate (Thermo Fisher Scientific, Product #32132)
- Restore™ Western Blot Stripping Buffer (Thermo Fisher Scientific, Product #21059)
- Protein Standard: Novex™ Sharp Pre-stained Protein Standard (Thermo Fisher Scientific, Product #LC5800)

10x Tris-buffered saline (TBS) (pH 7.6)		
Concentration	**Substance**	**Amount per liter**
200 mM	Tris-base	24.2 g
1.37 M	NaCl	78.8 g
	H_2O dest.	Fill to 900 ml
Adjust pH to 7.6	37% HCl	
	H_2O dest.	Fill to 1 liter

Table 3: Composition of 10x TBS buffer

1x Tris-buffered saline with Tween20 (TBS-T)	
Substance	**Amount per liter**
10x TBS	100 ml
Tween 20	1 ml
H_2O dest.	Fill to 1 liter

Table 4: Composition of 1x TBS-T

Transfer buffer (pH 9.2)		
Concentration	**Substance**	**Amount per liter**
48 mM	Tris-base	5.82 g
39 mM	Glycine	2.93 g
0.0375 %	SDS	0.375 g
20 %	MeOH	200 ml
	H_2O dest.	Fill to 1 liter

Table 5: Composition of Transfer buffer

Lysis buffer		
Concentration	**Substance**	**Amount per 10 ml**
1%	TritonX-100	100 µl
50 mM	Tris-HCl (pH 8)	50 µl (of 1 M Tris-HCl pH 8)
150 mM	NaCl	0.08775 g
0.1 %	SDS	50 µl (of 20% SDS)
1:100	Protease inhibitor cocktail	100 µl
1:200	Phosphatase inhibitor cocktail 3	50 µl

Table 6: Composition of Lysis Buffer

Enzymes

Primary antibodies	Company	kDa
Anti-ATGL, rabbit, 1:1000 in 5% skim milk	Cell Signaling Technology	54
Anti-β-Actin, mouse, 1:5000 in 5% skim milk	Sigma Aldrich	42

Table 7: Primary antibodies for Western Blot

Secondary antibodies	Company
Anti-rabbit IgG HRP-linked, 1:5000 in TBS-T	Cell Signaling Technology
Anti-mouse IgG HRP-linked, 1:5000 in TBS-T	Cell Signaling Technology

Table 8: Secondary antibodies for Western Blot

Equipment

- NuPAGE™ 4-12% Bis-Tris (Midi) Protein Gels
    - 12+2-well (Thermo Fisher Scientific, Product #WG1401BOX)
    - 20-well (Thermo Fisher Scientific, Product #WG1402BOX)
    - 26-well (Thermo Fisher Scientific, Product #WG1403BOX)
- Criterion™ Vertical Electrophoresis Cell (BioRad, Product #1656001)
- Nitrocellulose Blotting Membrane 0.2µm (GE Healthcare Life science, Product #10600001)

For the preparation of lysates for western blots, the cells were seeded into 10 cm dishes and grown to 80-90% confluency. When appropriate confluency was reached, the plates

were transferred on ice, the medium was removed and the cells were washed twice with cold PBS. 200 µl of lysis buffer was added onto the cells and incubated for 20 minutes on ice. The cells were detached using a cell scraper, transferred into 1.5 ml Eppendorf tubes and sonicated at 70% amplitude for a maximum of 10 seconds. The suspension was centrifuged at 14,000 g for 5 minutes and the supernatant was used for protein estimation using Pierce™ BCA Protein Assay Kit (chapter 3.2.2). An appropriate amount of the lysate was transferred to a fresh 1.5 ml tube and diluted with water, LDS Sample Buffer (4X) and Reducing Agent (10X) to obtain a 2 µg/µl protein concentration. Denaturation of the proteins was achieved by heating up the lysates to 95°C for 5-10 minutes. The lysates were then used directly or stored at -20°C. For later usage the lysates were re-heated shortly to 95°C after storage at -20°C.

15-20 µl (=30-40 µg) of the denatured protein samples and 6 µl of protein standard were loaded onto an SDS-PAGE (sodium dodecyl sulfonate poly acrylamide gel electrophoresis) gel. Electrophoresis was performed for approximately 60 minutes at 200 V (constant voltage). After separation of the proteins based on their mass by SDS-PAGE, they were blotted onto a nitrocellulose membrane using a Trans-Blot® SD Semi-Dry Cell for a minimum of 60 minutes at 180 mA (constant current) in the following setup: anode plate – blotting paper immersed in transfer buffer – nitrocellulose membrane – SDS gel – blotting paper immersed in transfer buffer – cathode plate. After blotting the membrane was rinsed with Milli-Q water and suspended in Ponceau-S staining solution briefly for visualization of proteins. After de-staining with tap water the membrane was blocked using 5 % skim milk in TBS-T buffer for at least 1 hour. After blocking the membrane was incubated with anti-ATGL primary antibody for 1-2 hours at room temperature or overnight at 4°C. The membrane was then washed with TBS-T 5 times for 5 minutes and incubated with anti-rabbit secondary antibody for 1 hour. After washing 3 times with TBS-T for 5 minutes the membrane was treated with ECL substrate and reactive protein bands were visualized using chemiluminescence on a ChemiDoc™. Afterwards, the membrane was stripped with stripping buffer and the same procedure was performed using anti-β-actin primary antibody and anti-mouse secondary antibody.

Western blot with anti-ATGL primary antibody was performed three times with ATGL KO* and ATGL OE cell lines.

3.4. Growth Curve Analysis

For growth analysis, the cells were grown in duplicates in a 12-well plate. 80,000 cells were seeded into each well. The plate was thoroughly shaken for even distribution of the cells in the well. The cells were allowed to settle down over night before the analysis was started. For the analysis, the cells were observed under the Cell Observer microscope for up to 96 hours. Seven positions in each well were chosen and images were acquired hourly. Each image was then subjected to an analysis tool kindly provided by Jürgen Gindlhuber, a PhD student in my group. The analysis tool counts the numbers of pixels that are occupied by the cells in each image. From the output of all the positions in one well a mean was calculated that was plotted for each timepoint. From the plot, linear slopes of the exponential growth phase were determined and the slopes were compared giving information on the growth behavior comparing the two conditions.

Growth Curve Analysis was performed two times for ATGL KO* and ATGL OE cell lines and once for ATGL KO and WT cell lines.

3.5. Cell Proliferation (MTT) Assay

3.5.1. Material

- Cell Proliferation Kit I (MTT) (Roche, Product #11465007001)
    - MTT labeling reagent (containing MTT (3-[4,5-dimethylthiazol-2-yl]-2,5-diphenyl tetrazolium bromide) labeling reagent (1x) 5 mg/ml in PBS)
    - Solubilization solution (1x) (containing 10% SDS in 0.01 M HCl)

3.5.2. Procedure

For the cell proliferation assay 4 x 10^3 cells (A540 ATGL KO* and OE cell lines) in 100 µl of working medium were seeded in triplicates into 96-well plates and allowed to settle overnight. Timepoints t = 0 hours, 24 hours, 48 hours and 72 hours were investigated and for each timepoint a separate plate was prepared. Upon addition of 10 µl of MTT labeling reagent timepoint 0 is denoted and subsequently over the next three days MTT labeling reagent was added to the cells in one after the other plates at the same timepoint. After 4 hours of incubation of MTT on the cells at 37°C and 5% CO_2

atmosphere the cells were treated with 100 µl of solubilization agent. The cells were then incubated for 24 hours before the solubilized formazan product generated from MTT by living cells can be detected on a microplate reader. The emission of the solutions was detected once at 555 nm and once at 655 nm for a blank test. Additionally, three wells on each plate without cells were treated like the other wells, first incubation with MTT and subsequently with solubilization agent. These values were used as a blank.

The MTT assay experiment was performed twice on ATGL KO* and OE cell lines. In the first MTT experiment the cell lines were kept in gentamycin containing cell medium while the second time the experiment was performed the cells were kept in regular cell medium.

3.6. Gap Closure ("Scratch") Assay

The scratch assay – also referred to as wound healing or gap closure assay – is used to study cell migration. To this cause, the cell lines were seeded into a 12-well plate in duplicates. Into each well 1 x 10^5 cells were seeded and allowed to grow to confluency. Once the cells were confluent each well was subjected to a manually performed scratch. The scratch in the cell monolayer was performed with a sterile 200 µl pipette tip, which was run down in a 90° angle from the top point of the well to the bottom point in a straight line. Particular attention was paid to ensure that the pipette tip slided as smoothly as possible over the cell layer without any interruption. After performing the scratch, the cells were washed with PBS and supplied with fresh medium. The obtained gaps in the cell layer were observed under an inverted microscope at 4 x magnification and images were taken ($t = 0$). The exact area in the well where an image was taken was marked on the plate for each well in order to be able to retake images at the same position. The gaps were observed again at timepoints $t = 15$, $t = 25$, $t = 39$, $t = 48$ and $t = 63$ hours and images were obtained for each timepoint and each well. The images were analyzed using the open source software package Fiji (Fiji Is Just ImageJ) version 1.50d. The gap area was estimated using a "wound-healing" plugin kindly provided by Jürgen Gindlhuber. By estimating the gap area, the gaps of later timepoints were compared to the initial gap and by this method the percentage of the gap closure was calculated.

The scratch assay experiment was performed once on ATGL KO* and ATGL OE cell lines.

3.7. Activity-based proteomic profiling

3.7.1. Material

- N-ethylmaleimide (NEM) (Fluka Analytical, Product #04260-5G-F, CAS #128-53-0)
- Dithiothreitol (DTT) (Sigma Aldrich, Product #43815-5G, CAS #3483-13-3)
- Ethylenediaminetetraacetic acid (EDTA) (Fluka Analytical, Product #100949486)
- TEV protease (Sigma Aldrich, Product #T4455)
- Tris(2-carboxyethyl)-phosphine hydrochloride) (TCEP) (Sigma Aldrich, Product #C4706, CAS #51805-45-9)
- C_6 activity-based probe (synthesized by Marko Kljajic (Institute of Organic Chemistry, University of Technology, Graz) according to Rengachari, Aschauer, Schittmayer *et al.*[132])
- DIBAC-Biotin peptide linker (piCHEM, customary made, batch #AZ9-160501)
- DBCO-N-hydroxysuccinimidyl ester (Sigma Aldrich, Product #761524)
- DNA oligo (biotin and amine functional groups) (Sigma Aldrich, customary made)
- DIBAC-Biotin DNA linker (synthesized from DBCO-N-hydroxysuccinimidyl ester and biotin-DNA-amine)
- Deoxyribonuclease (DNAse) I from bovine pancreas (Sigma Aldrich, Product #D5025)
- Dibenzylcyclooctyne (DBCO)-Amine (Jena Bioscience, Product #CLK-A103)
- Atto 633 NHS-Ester (Atto Tec, Product #AD 633-31)
- DIBAC-Atto 633 dye (synthesized from DBCO-Amine and Atto 633 NHS-Ester)
- Mark12$_{TM}$ Unstained Standard (Thermo Fisher Scientific, Product #LC5677)
- Amicon® Ultra – 4 Centrifugal Filters Ultracel® – 3K (Merck Millipore, Product #UFC800324)
- Amicon® Ultra – 4 Centrifugal Filters Ultracel® – 10K (Merck Millipore, Product #UFC801024)
- Pierce™ Spin Columns – Screw Cap (Thermo Fisher Scientific, Product #69705)
- Pierce™ Micro-Spin Columns (Thermo Fisher Scientific, Product #89879)
- Streptavidin Agarose Resin (Thermo Fisher Scientific, Product #20347)
- Sequencing Grade Modified Trypsin (Promega, Product #V5111)
- Solid Phase Extraction Disc – Empore™ Styrene Divinyl Benzene (SDB-RPS) Extraction discs (Supelco, Product #66886-U)
- Aurora Series Emitter nanocolumn with CSI fitting (C18, 1.6µm, 120Å, 250 x 0.075mm) (IonOpticks, Melbourne, Australia)

3.7.2. Stock Solutions and Buffers

125.13 mg (= 1 mmol) of N-ethylmaleimide (NEM) was weighed into a 5.0 ml Eppendorf tube and dissolved in 4 ml H_2O yielding a 250 mM NEM stock solution. The stock solution was aliquoted into 500 µl portions and kept frozen at -20°C. Once thawed the stock solution was discarded after usage.

A Dithiothreitol (DTT) stock solution was prepared by dissolving 15.43 mg of DTT in 1 ml of H_2O yielding a 100 mM DTT stock solution. The stock solution was prepared fresh for every experiment.

An EDTA stock was prepared by dissolving 1.46 g EDTA in 10 ml of H_2O adjusted to pH 8.0 with NaOH, yielding a 0.5 M stock solution. The EDTA stock solution was kept at RT and reused.

The click buffer and urea buffers were always prepared fresh just before usage. For some experiments 0.5 M NaCl salt was added to the urea buffers.

For the preparation of a 0.1 µg/µl TEV protease stock 1 µl of 2 µg/µl stock was diluted to 20 µl with TEV buffer.

Click Buffer		
Concentration	**Substance**	**Amount per 100 ml**
100 mM	Tris-HCl (pH 8.5)	10 ml (of 1 M Tris-HCl)
1 %	SDS	5 ml (of 20% SDS)
10 mM	TCEP	28.665 mg
	H_2O	Fill up to 100 ml

Table 9: Composition of Click Buffer

2 M Urea Buffer		
Concentration	**Substance**	**Amount per 100 ml**
100 mM	Tris-HCl (pH 8.5)	10 ml (of 1 M Tris-HCl)
2 M	Urea	12.012 g
(0.5 M	NaCl*	2.922 g)
	H_2O	Fill up to 100 ml

Table 10: Composition of 2 M Urea Buffer

8 M Urea Buffer		
Concentration	**Substance**	**Amount per 100 ml**
100 mM	Tris-HCl (pH 8.5)	10 ml (of 1 M Tris-HCl)
8 M	Urea	48.048 g
(0.5 M	NaCl*	2.922 g)
	H_2O	Fill up to 100 ml

Table 11: Composition of 8 M Urea Buffer

TEV Buffer		
Concentration	**Substance**	**Amount per 10 ml**
50 mM	Tris-HCl (pH 8.5)	50 µl (of 1 M Tris-HCl)
0.5 mM	EDTA	10 µl (of 0.5 M stock)
1 mM	DTT	100 µl (of 100 mM stock)
	H_2O	Fill up to 10 ml

Table 12: Composition of TEV Buffer

3.7.3. Activity-based probe

The serine hydrolase activity-based probe that is used in all activity-based proteomic profiling experiments of this project was available in the lab. The hexyl-(p-nitrophenyl)-(azidopropyl)-phosphonate contains the p-nitrophenyl group as a leaving group, the azidopropyl group as the bio-orthogonal functional moiety and the hexyl chain for binding selectivity. It was termed C_6 ABP and is depicted in Figure 17.

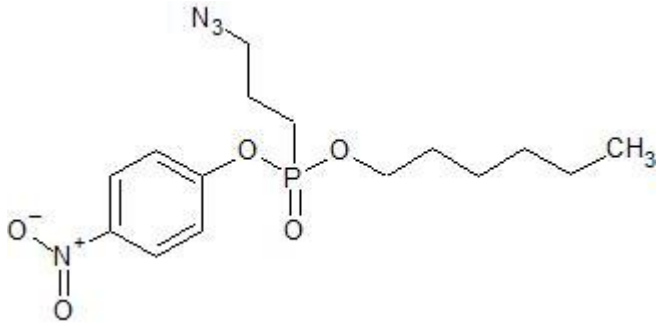

Figure 17: C_6 activity-based probe *– hexyl-(p-nitrophenyl)-(azidopropyl)-phosphonate*

The probe was synthesized and purified according to Rengachari, Aschauer, Schittmayer *et al.*[132]. 1 µmol dry aliquot of the probe was dissolved in 100 µl of cooled chloroform ($CHCl_3$). The 100 µl were aliquoted into 10 x 10 µl into 0.5 ml Eppendorf tubes and dried in a vacuum concentrator centrifuge yielding 100 nmol per Eppendorf

tube. To one 100 nmol stock 100 µl of chloroform was added generating a 1 nmol/µl or 1 mM stock solution. For each sample 60 µl (= 60 nmol) of probe was aliquoted into a 2.0 ml Eppendorf tube. Additionally, 12 µl (= 12 nmol) of the probe was aliquoted into 1.5 ml Eppendorf tubes for each sample. The probe was dried in a vacuum concentrator centrifuge and kept at -20°C until used. The remaining aliquots of the probe were also stored at -20°C.

3.7.4. Bio-orthogonal Linkers

The TEV and DNA linkers are depicted in Figures 18 and 19, respectively.

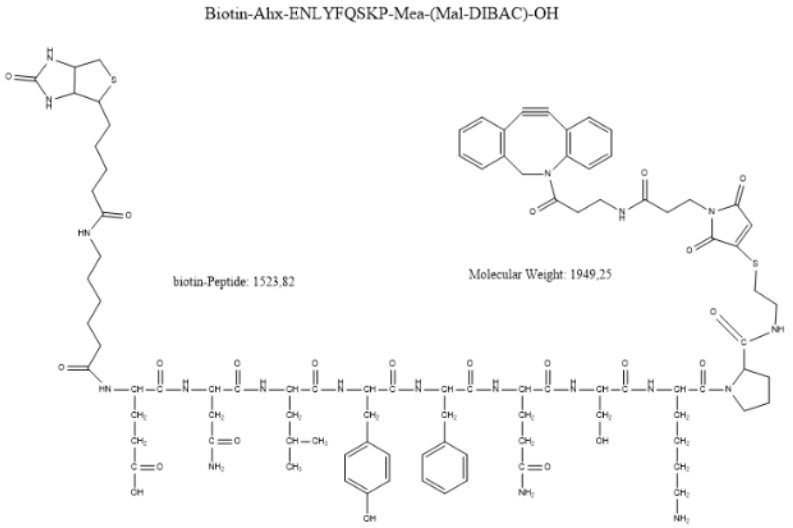

Figure 18: TEV linker *– Biotin coupled to DIBAC via a peptide sequence*

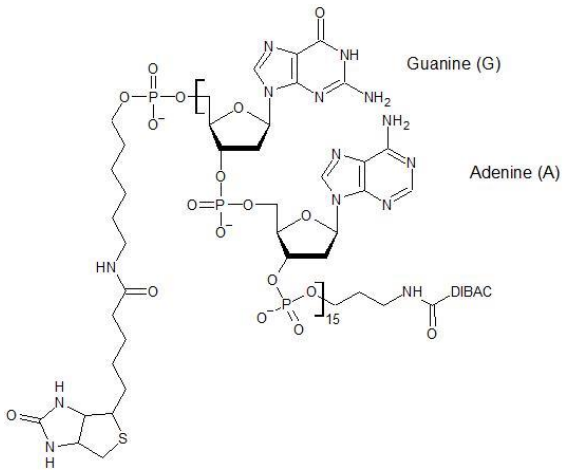

Figure 19: DNA-linker *– Biotin coupled to DIBAC via a 30 nucleotide long single stranded DNA oligonucleotide of alternating Guanine and Adenine* $[GA]_{15}$

The TEV linker was customary made by piCHEM. 50 µg corresponds to approximately 25 nmol of the linker. Dry aliquots of 50 µg were dissolved in 50 µl of 1:1 H_2O/ACN yielding a 1 µg/µl solution. The DNA linker was synthesized in the lab from DBCO-N-hydroxy-succinimidyl ester and customary made single strand (ss) DNA with biotin and amine functional groups. A 0.3 mM stock solution of the DNA-linker was used, which is a concentration of approximately 600 pmol/µl.

3.7.5. ABPP Workflow

Cell culture and lysate preparation

For activity-based proteomic profiling cells were seeded and grown until almost confluent in 10 cm dishes. For each cell line two plates were seeded. When the cells were almost confluent the medium of the cells was removed. The previously prepared 60 nmol of C_6 ABP was dissolved directly in the Eppendorf tube with 2 ml of FBS-free RPMI medium. The ABP-containing FBS-free medium was added to one set of the cell lines. To the second plate of each cell line FBS-free medium without ABP was added. The plates were then incubated at 37°C and under CO_2 atmosphere for 1 hour. After the incubation, the cells were placed on ice and the medium was removed. The cells were washed twice with 5 ml cold PBS. 400 µl of PBS was added to each plate. The cells were then scraped off the plates by a cell scraper and transferred to a 1.5 ml Eppendorf tube. The cells that were not treated with the ABP were transferred to an empty 1.5 ml Eppendorf tube, while the cells that were incubated with C_6 probe were transferred to a 1.5 Eppendorf tube containing 12 nmol of the C_6 probe, yielding a 30 µM probe concentration in 400 µl cell suspension. The suspensions were incubated at 37°C for 1 hour. The cells were then briefly sonicated on a Sonoplus mini20 hand sonicator while they were kept on ice. After sonication, the cells were centrifuged at 600 g for 5 minutes at 4°C and the supernatant was transferred to a 1.5 ml Eppendorf Protein LoBind tube. Subsequently, protein estimation was performed (according to 3.2.3).

Reduction and alkylation of lysates

Acetone protein precipitation was performed with 500 µg of protein by adding a minimum of 4-times the volume of ice-cold acetone to the lysates followed by incubation at -20°C overnight. The following day, the acetone precipitations were centrifuged at 18,000 g for 10 minutes at 4°C. The supernatant was removed and the pellet was

dissolved in 350 µl of click buffer containing TCEP. Sonication was performed to aid with dissolving of the pellet. TCEP in the click buffer was needed for reduction of disulfide bonds of the proteins to thiol groups. The samples were heated to 95°C for 10 minutes. Subsequently, 48 µl of 250 mM NEM stock was added to the samples to yield a 30 mM NEM concentration. NEM was used as an alkylating agent of the free thiol groups on the proteins. The samples were then heated to 37°C for 30 minutes.

Linker addition

Before linker addition an aliquot of 10 µg of each sample was taken for the linker addition test.

For DNA linker experiments, 1 µl of the 600 pmol/µl DNA linker solution was added to each sample. The samples were subsequently incubated at 37°C overnight.

For TEV linker experiments 1.2 µl of the 1 µg/µl TEV linker solution, which corresponds to approximately 600 pmol, was added to each sample. The samples were subsequently incubated at 37°C overnight.

After linker addition, another aliquot of 10 µg was taken from each sample to test for the efficiency of the linker addition.

Linker addition test

For the linker addition test, a DIBAC-Atto dye solution was prepared from dry 25 nmol DIBAC-Atto stocks by addition of 25 µl of DMSO yielding a 1 nmol/µl DIBAC-Atto dye solution. To the aliquots taken before and after linker addition 1 µl DIBAC-Atto dye solution was added and the samples were incubated for 1 hour at 37°C under light exclusion. As a positive control a C_6-labeled lipoprotein lipase (LPL) was also subjected to the same amount of DIBAC-Atto dye and incubated together with the samples.

After the incubation 4 µl of SDS sample buffer (containing 4X LDS sample buffer and 10X sample reducing agent) was added to each sample and the samples were then boiled for 10 minutes at 95°C. The samples were loaded onto an SDS gel. 6 µl of Mark12 unstained protein standard was loaded onto the gel and used as loading control. Electrophoresis was performed for 1 hour at 200 V constant voltage.

The bands were visualized by a molecular imager with an external laser (excitation wavelength 635 nm). Probe-treated samples had an exposed azide group that should

have reacted with the DIBAC-Atto dye and therefore create fluorescent bands. The non-probe-treated samples were expected to show no bands. Bands in the samples after linker addition indicate that there are still unreacted C_6-probes, hence more of the linker was added in this case.

Removal of excess linker and SDS

Before the enrichment on streptavidin agarose beads was performed, the excess of linker and SDS was removed. To this end centrifugal filters with 10 kDa or 3 kDa molecular weight cut-offs were used for DNA-linker or TEV-linker experiments, respectively. The samples were diluted 1:10 in 8 M urea buffer and transferred to the appropriate cut-off filters prior to centrifugation at 7830 rpm for 30 minutes (3 kDa) or 10 minutes (10 kDa). The filters were washed once with 8 M urea buffer and once with 2 M urea buffer. The protein retentate in 2 M urea buffer (approx. 200 µl) was used for enrichment on streptavidin-agarose beads.

Enrichment

To the spin columns 12 µl of streptavidin-agarose resin was added and the beads were washed twice with 150 µl of 2 M urea buffer. The retentate was added to the beads and incubated on an overhead-shaker at RT for 4 hours. After incubation the non-bound proteins were collected and kept at -20°C. The beads were washed twice with 2 M urea buffer and once with TEV buffer in TEV linker experiments or three times with 2 M urea buffer for DNA linker experiments.

Digestion and sample preparation of LC-MS

Both the DNA and the TEV linker were designed to allow for cleavage by DNAse or TEV protease, respectively. Cleavage of the linker allows for elution of only those proteins that are bound to the beads via the linker. Therefore, the beads were incubated with TEV protease or DNAse overnight. 200 µl TEV protease buffer containing 0.1 µg of TEV protease (= 1 µl of 0.1 µg/µl stock) was added to the beads and incubated overnight at 30°C. For DNA-linker experiments, 200 µl 2 M urea buffer containing 0.1 U of DNAse (= 0.1 µl of 1 U/µl DNAse) was added to the beads and incubated overnight at 37°C.

The proteins were collected in 1.5 ml LoBind Eppendorf tubes and termed “E” for eluates. 0.1 µg of Trypsin was added to the eluted proteins. To the beads 0.1 µg

containing 2 M urea buffer was added to perform on-bead digest. The eluates and on-bead digests were incubated at 37°C overnight. The on-bead digests were collected in 1.5 ml LoBind Eppendorf tubes and termed “O” for on-bead.

Desalting of the peptide samples

For desalting of the peptide samples, the 200 µl of sample were brought to 1 % TFA. The samples were loaded onto an SDB-RPS Stage Tip (200 µl pipette tip with two layers of SDB-RPS material). The stage tip was placed into a 2 ml Eppendorf tube in an appropriate adapter and centrifuged at 1500 g for 5 minutes. The tip was washed with 100 µl of 0.2 % TFA and eluted with 100 µl of 5 % ammonium hydroxide in 80 % ACN into a 2 ml Eppendorf tube equipped with a glass vial insert. The samples were dried in a vacuum concentrator centrifuge. The dried samples were then dissolved prior to LC-MS measurement in 16 µl of 0.1 % FA and 2 % ACN in H_2O.

3.7.6. Chromatography and Mass Spectrometry

The samples were analyzed by nano High-Performance Liquid Chromatography (nano-HPLC) (Dionex Ultimate 3000) equipped with an Aurora Series Emitter nanocolumn with CSI fitting (C18, 1.6 µm, 120 Å, 250 x 0.075 mm). Separation was carried out at 35°C at a flow rate of 300 nl/min. Solvent A (0.1 % FA in water) and solvent B (0.1 % FA in acetonitrile) were used in a 133 min chromatography gradient depicted in Table 13. Chromatorgraphy was coupled either to a Thermo Orbitrap Velos Pro MS (Thermo Scientific, USA) for ATGL KO and WT samples, or to a Bruker maXis II ETD Q-TOF MS for ATGL KO* and ATGL OE samples. The samples were ionized by nano-ESI.

Time [min]	Solvent
0 – 18	2 % B
18 – 100	2 – 25 % B
100 – 107	25 – 35 % B
107 – 108	35 – 95 % B
108 – 118	95 % B
118 – 118	95 – 2 % B
118 – 133	2 % B

Table 13: Chromatography gradient

The maXis II ETD Q-TOF MS was operated with nano-ESI source in positive mode with the following settings: mass range: 150 – 2200 m/z; 4 Hz; capillary 1600 V; dry gas flow 3 L/min with 150°C; nanoBooster 0.2 bar. Fragmentation of the parental ions (peptides) to obtain MS2 spectra was achieved by collision-induced dissociation (CID). Fragmentation was induced for the most intense (top 20) ions of the MS spectrum in a data-dependent acquisition (DDA) mode.

The Thermo Orbitrap Velos Pro MS was operated with a nanospray source in positive mode, applying alternating full scan MS for a mass range of 300 – 2000 m/z in the ICR cell. Fragmentation was performed in a DDA mode by CID of the 20 most intense peaks in the ion trap with dynamic exclusion enabled.

3.7.7. Data Analysis

Label-free quantification (LFQ) of the MS/MS data was performed using MaxQuant (version 1.6.0.16)[127]. For database search the integrated peptide search engine Andromeda was employed. For the peptide search a reference database was generated with data from a public database (UniProt) with taxonomy homo sapiens (downloaded on Feb 25th, 2019) and common contaminants (cRAP protein sequences) form the global proteome machine.

Oxidation on methionine and acetylation on the N-terminus of proteins were set as variable modifications and NEM modification on cysteines and selenocysteins was set as fixed modification. Trypsin was chosen as the digestion enzyme and a maximum of two missed cleavages per peptide was allowed. The match-between-runs feature was enabled with a retention time window of 0.7 min and an alignment window of 20 min. A minimum of two peptides (unique or razor) per protein had to be confidently measured to allow for protein identification. The false discovery rate (FDR) was set to 1 % for the database search.

The analysis of the LFQ dataset from MaxQuant was performed using Perseus software (version 1.6.6.0)[129].

The LFQ intensity data of protein groups was subjected to statistical analysis in Perseus. First, the contaminants and proteins that were only identified by site were excluded, resulting in a reduced matrix. The samples were then divided into two groups (ATGL OE samples were separated from ATGL KO* samples and ATGL KO samples were separated from WT samples in the respective experiments) in order to compare

ABP (+) with ABP (-) sample sets within the cell lines with the same condition. For each group, a principle component (PCA) analysis was performed and the individual samples were assigned to the corresponding group (KO* (+) was compared to KO* (-) and OE (+) to OE (-); in the other experiment KO (+) and KO (-) were compared as well as WT (+) and WT (-)). The values were log_2 transformed and the data was filtered to contain at least three valid values in at least one group, resulting in further matrix reduction. The missing values were imputed based on a downshifted normal distribution (down shift: 1.6; width: 0.4 if not otherwise stated). A t-test was performed and a volcano plot based on the t-test outcome was generated (p-values (from t-test) were plotted against the difference of the means of the log_2 LFQ intensities between two groups). A permutation-based FDR multi-test correction was performed and the threshold was set to 1%.

3.8. Equipment

CASY Innovatis (Roche)

Cell Observer Microscope (Zeiss)

Centrifuge 5430 R (Eppendorf)

ChemiDoc® (BioRad)

Dionex UltiMate 3000 HPLC (Thermo Fisher Scientific)

maXis II ETD Q-TOF Mass Spectrometer (Bruker Daltonics)

Molecular Imager® FX and External Laser (BioRad)

Orbitrap Velos Pro Mass Spectrometer (Thermo Fisher Scientific)

SpectraMax Plus 384 (Molecular Devices)

Inverse Microscope IX51 (Olympus)

Sonoplus mini20 (Bandelin)

Thermomixer comfort (Eppendorf)

Trans-Blot® SD Semi-Dry Cell (BioRad)

Univapo 100 ECH (UniEquip)

4. Results

4.1. Protein Estimation

In order to use the appropriate amount (µg) of lysates for each experiment and for the cell line samples to be comparable, protein estimation was performed using the BCA Protein Assay kit. The protein content was estimated for lysates of ATGL KO* and ATGL OE cell lines for Western Blot analysis and ABPP, as well as for ATGL KO and WT cell lines for ABPP.

The ATGL KO* and OE cell lines were initially kept in gentamicin containing cell medium, which probably caused additional stress for the cells. After three months of experiments the cells were kept in cell medium without gentamicin to relieve some of the stress on the cells. Unless otherwise stated, the experiments and data are shown for the ATGL KO* and OE cell lines kept in cell medium without gentamicin.

The calibration curves obtained from measuring the absorbance of the standard solutions prepared fresh for each experiment are depicted in Figure 20.

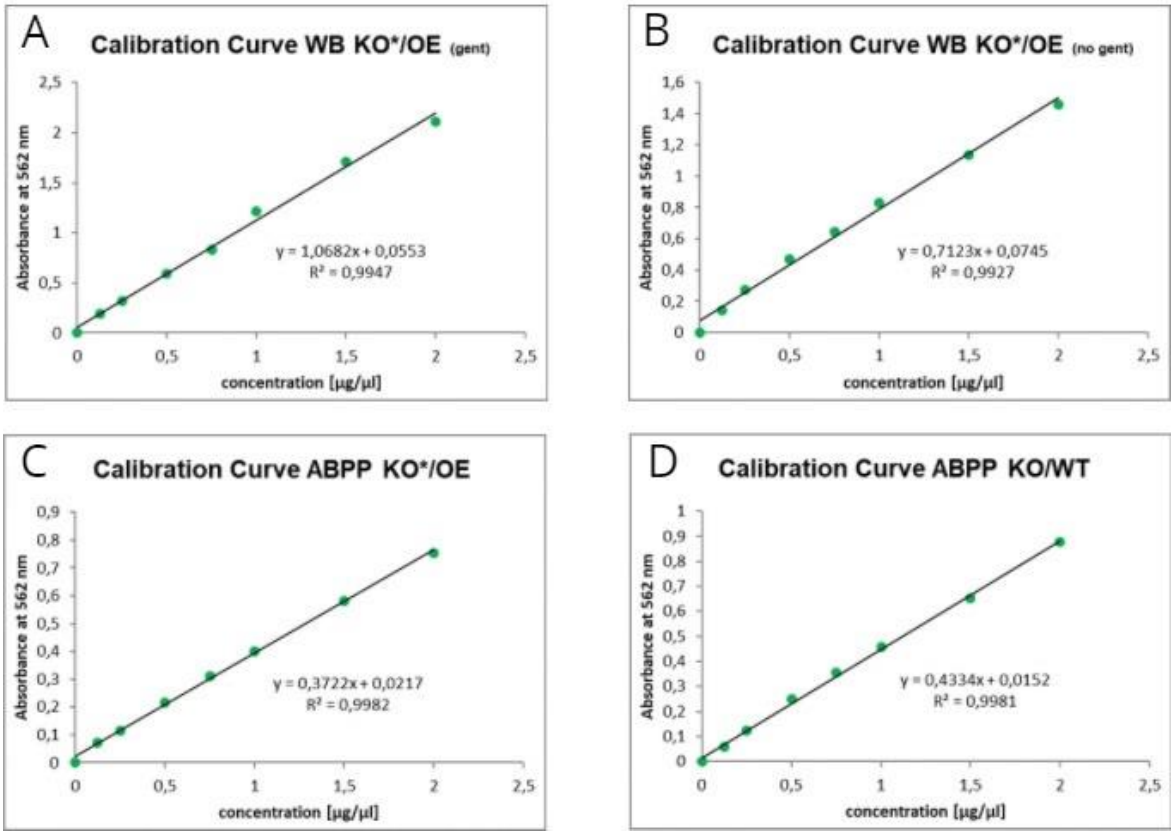

Figure 20: Calibration curves of BCA protein estimation *– Concentration of the standard solutions are plotted against the absorbance (mean of two measurements) at 562 nm – A: western blot lysates of ATGL KO* and OE cell lines grown in gentamicin (gent) containing cell medium; B: western blot lysates of ATGL KO* and OE cell lines grown in regular cell medium (without gentamicin); C: activity-based proteomic profiling (ABPP) lysates of ATGL KO* and OE cell lines; D: ABPP lysates of ATGL KO and WT cell lines.*

The equations were obtained from fitting a linear regression line through the points on the blot, which directly linked the absorbance to the concentration. The equations are listed in Table 14 for the corresponding experiments.

Experiment	**Calibration curve equation**	**R^2**
WB ATGL KO*/OE (gent)	y = 1.0682x + 0.0553	0.9947
WB ATGL KO*/OE (no gent)	y = 0.7123x + 0.0745	0.9927
ABPP ATGL KO*/OE	y = 0.3722x + 0.0217	0.9982
ABPP ATGL KO/WT	y = 0.4334x + 0.0152	0.9981

Table 14: Calibration curve equations –*the calibration curve equations from the BCA protein estimations with their corresponding correlation coefficient for the shown experiments*

The concentrations of the protein lysates were calculated from the corresponding equations and are shown for each experiment in the corresponding table (Tables 15-18). For western blot experiments, lysates with a concentration of 2 µg/µl were prepared by diluting appropriate amounts of lysate with H_2O and SDS NuPAGE™ buffers (Table 15, Table 16). Since the samples were diluted 1:20 for the BCA measurement, a dilution factor of 20 was used for the calculation of the concentrations from the absorbances.

	Absorbance	Concentration [µg/µl]	V(lysate) [µl]	V(diluent) [µl]	V(sample buffer) [µl]	V(reducing buffer) [µl]	final conc. [µg/µl]
KO* 1	0,4972	4,39	182	78	100	40	2
KO* 2	0,5186	4,59	174	86	100	40	2
KO* 3	0,5219	4,61	173	87	100	40	2
OE 1	0,5728	5,07	158	102	100	40	2
OE 2	0,6332	5,62	142	118	100	40	2
OE 3	0,4628	4,08	196	64	100	40	2

Table 15: KO*/OE (gent) lysate preparation for western blot - *calculated concentrations of the samples (taking into account the 1:20 dilution) and calculation of needed diluent, sample and reducing buffer to generate a 2 µg/µl protein solution*

	Absorbance	Concentration [µg/µl]	V(lysate) [µl]	V(diluent) [µl]	V(sample buffer) [µl]	V(reducing buffer) [µl]	final conc. [µg/µl]
KO* 1	0,3470	7,65	105	155	100	40	2
KO* 2	0,3016	6,38	125	135	100	40	2
KO* 3	0,3309	7,20	111	149	100	40	2
OE 1	0,2883	6,00	133	127	100	40	2
OE 2	0,3333	7,27	110	150	100	40	2
OE 3	0,3476	7,67	104	156	100	40	2

Table 16: KO*/OE (no gent) lysate preparation for western blot - *calculated concentrations of the samples (taking into account the 1:20 dilution) and calculation of needed diluent, sample and reducing buffer to generate a 2 µg/µl protein solution*

For ABPP experiments, the appropriate concentrations of the protein lysates were calculated based on the equations, and a dilution factor of 8 was used due to the 1:8 dilution of the samples prior BCA measurement.

	Absorbance	Conc. [µg/µl]	V(lysate) [µl]
KO* 1 (+)	0,2440	4,78	105
KO* 1 (-)	0,2432	4,76	105
KO* 2 (+)	0,1997	3,82	131
KO* 2 (-)	0,1914	3,65	137
KO* 3 (+)	0,2423	4,74	105
KO* 3 (-)	0,2299	4,48	112
OE 1 (+)	0,1916	3,65	137
OE 1 (-)	0,1701	3,19	157
OE 2 (+)	0,1856	3,52	142
OE 2 (-)	0,1813	3,43	146
OE 3 (+)	0,2010	3,85	130
OE 3 (-)	0,2083	4,01	125

	Absorbance	Conc. [µg/µl]	V(lysate) [µl]
KO 1 (+)	0,2175	3,73	134
KO 1 (-)	0,2154	3,70	135
KO 2 (+)	0,2289	3,94	127
KO 2 (-)	0,1895	3,22	155
KO 3 (+)	0,2065	3,53	142
KO 3 (-)	0,1869	3,17	158
B8 (+)	0,2919	5,11	98
B8 (-)	0,2545	4,42	113
B9 (+)	0,1297	2,11	237
B9 (-)	0,1393	2,29	218
C7 (+)	0,3117	5,47	91
C7 (-)	0,2737	4,77	105
C8 (+)	0,18355	3,11	161
C8 (-)	0,1557	2,59	193

For ABPP a total of 500 µg of protein was used. The appropriate amount of ABP-labeled lysate was transferred into an Eppendorf tube and acetone precipitation with a minimum of four-fold amount of acetone was performed at -20°C overnight.

4.2. Western Blot

In order to verify that ATGL was successfully re-introduced by lentiviral transfection into the A549 ATGL KO cell lines, immunoblotting was performed. 30 µg of the cell lysates was loaded into the well of an SDS gel and SDS-PAGE was performed. ATGL primary antibody was used to verify ATGL presence or absence from the cell lines and actin primary antibody was employed as a loading control. HRP-conjugated secondary antibodies were used for visualization on a ChemiDoc. The western blot image of the three biological replicates that were used throughout the project (KO* 1-3, OE 1-3) are visualized in Figure 21.

It is confirmed that ATGL is present in ATGL OE cell lines – clear bands were visible at 54 kDa on the membrane, corresponding to ATGL – while ATGL is not present in ATGL

KO* cell lines – no bands were visible in the wells loaded with ATGL KO* cell line lysates.

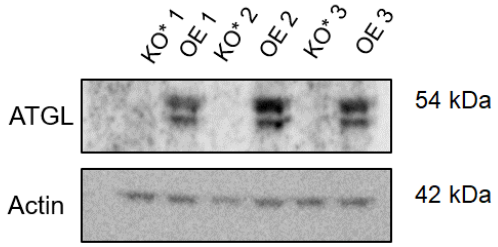

Figure 21: Protein expression analysis – *30 µg of protein lysates were loaded into each well of an SDS gel and immunoblotting was performed. The cell lysates of ATGL KO* and ATGL OE samples were tested for ATGL expression and actin as loading control (representative image of one of three similar experiments)*

The lentiviral introduction of GFP into the CRISPR-generated ATGL KO cell lines was checked by fluorescence microscopy. These cell lines were accordingly termed ATGL KO* - the asterisk (*) symbolizes the GFP overexpression. The GFP was introduced to generate stress from lentiviral protein overexpression in the ATGL KO cell lines, as this stress is also experienced by ATGL overexpression in the ATGL OE cell lines. Thus, the introduction of GFP was important in order for the two cell lines to be comparable.

Immunoblotting of the ATGL KO and WT cell lines that were used – ATGL KO 1-3 and WT cell lines B8, B9, C7, C8 – was not performed in the course of this project as the absence of ATGL in A549 KO cell lines as well as the presence of ATGL in the WT cell lines was previously verified by Tamara Tomin[133].

4.3. Growth Curve

In order to assess whether there is a phenotypic difference between the A549 ATGL KO* cell lines and the ATGL OE cell lines, the growth of these cell lines was investigated. To this end, a cell proliferation (MTT) test and a growth curve analysis was performed. The growth curve analysis experiments are based on imaging of cells over time and subsequent estimation of the area occupied by cells. Several spots in each well of a 12 well plate seeded with cells were selected and images of these spots were generated every hour for up to 96 hours. The images were subsequently subjected to the image analysis tool and the obtained values correspond to the area being taken up by the cells. Hence, larger numbers corresponded to higher confluency of the cells. A mean value from all numbers of the two wells seeded with the same cell line was calculated. The obtained values were then normalized on the value at timepoint *t = 0*

hours generating relative values in percent. From the obtained graphs, the time period in which the cells grew most steady was used to calculate slopes. In general, the cells grew steadily within the first 30-35 hours of the experiment. At later timepoints, the growth of some of the cell lines started slowing down and they reached a plateau phase. Thus, later timepoints had to be excluded from further calculations. The slopes of the cell lines in their linear growth phase were calculated, representing the speed of growth. From the slopes a mean value for each condition (ATGL KO* or ATGL OE) was calculated and subjected to a student's t-test.

Growth curve experiments were performed for cell lines ATGL KO* and ATGL OE twice and are visualized in Figures 22-23.

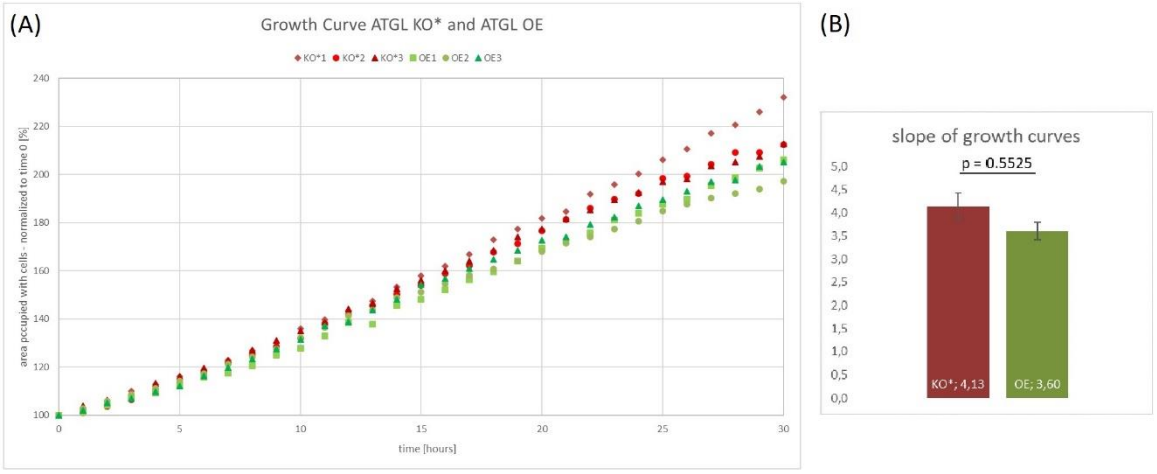

Figure 22: Growth Curve experiment ATGL KO* and ATGL OE (1) *- A: Dot plot of normalized values corresponding to the area taken up by cells over a time-span of 30 hours; B: mean slopes of the ATGL KO* cell lines and ATGL OE cell lines – error bars represent standard deviation – significance was determined by student's t-test (* p < 0.05, ** p < 0.01)*

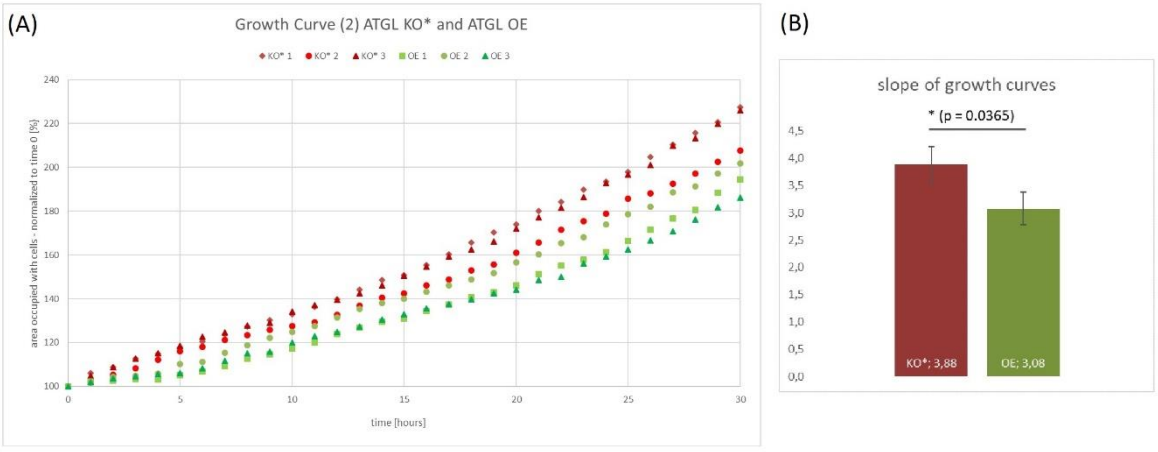

Figure 23: Growth Curve experiment ATGL KO* and ATGL OE (2) *- A: Dot plot of normalized values corresponding to the area taken up by cells over a time-span of 30 hours; B: mean slopes of the ATGL KO* cell lines and ATGL OE cell lines – error bars represent standard deviation – significance was determined by student's t-test (* p < 0.05, ** p < 0.01)*

In the first of the two experiments, the difference in cell growth between ATGL KO* and ATGL OE cell lines is not significant. However, a trend towards higher proliferation in ATGL KO* cell lines can be observed. In the second experiment, the difference in growth is significant ($p \leq 0.05$), and from the graph it can be seen that the ATGL KO* cell lines (in shades of red) show faster growth.

In this type of growth curve experiments it was necessary to find an appropriate time span during which all cell lines grow comparably and the slopes can be determined. One of the problems with this experiment and the A549 cell line was that in general, A549 cells grow very fast. Thus, most of the later timepoints had to be excluded, as the cells soon reached confluency and the cells growth started to slow down. An additional problem was cell line ATGL KO* 1, which grew disproportionately faster than the remaining cell lines (Figure 22). Another problem with the first experiment was that at this point the cells were still kept on antibiotics, which caused additional stress for the cells, which can lead to the cells showing less of the expected typical phenotype.

For cell lines ATGL KO and WT the growth curve experiment was performed once in order to verify the previously observed growth difference between those cell lines. The result from this experiment is visualized in Figure 24.

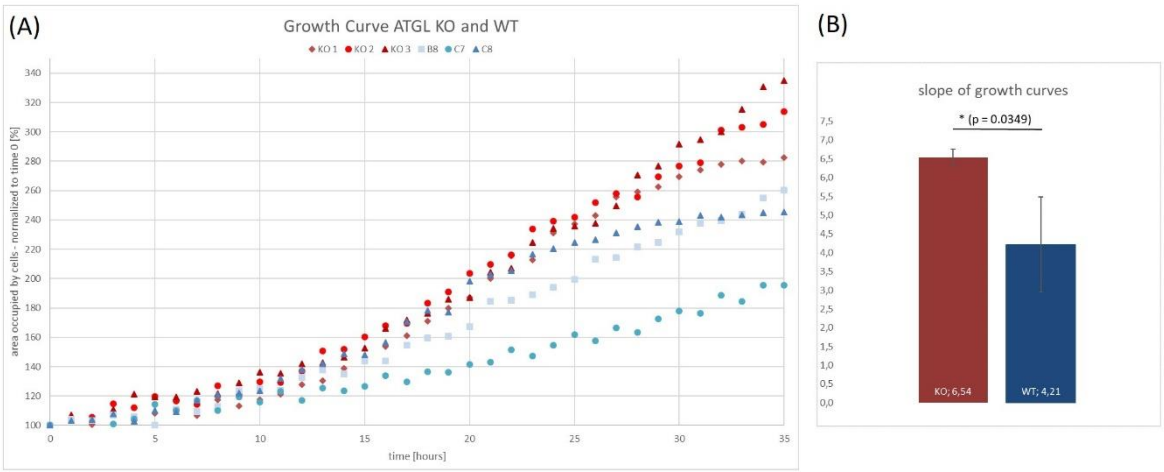

Figure 24 Growth Curve experiment ATGL KO and WT *- A: Dot plot of normalized values corresponding to the area taken up by cells over a time-span of 35 hours; B: mean slopes of the ATGL KO cell lines and WT cell lines – error bars represent standard deviation – significance was determined by student's t-test (* p < 0.05, ** p < 0.01)*

In the timeseries graph in Figure 24 it can clearly be seen that the A549 WT cells did not grow as uniformly as the ATGL OE and ATGL KO* cell lines in the previous experiments. However, it can be seen that upon normalization, which allows for all the cell lines to start at 100%, the ATGL KO cell lines (shades of red) seem to grow faster

than the WT cell lines (shades of blue). Unfortunately, the big difference in between the WT cell lines causes a rather high standard deviation and thus the difference is not significant. However, even with the rather high standard deviation, the mean slope of ATGL KO cell lines is significantly larger than the mean slope of the WT cell lines. Hence, it can be assumed that ATGL KO cells grow faster than the respective control cells.

Overall, the growth curve experiment shows that loss of ATGL in lung carcinoma cell lines leads to an altered phenotype, namely an increase in growth and thus a first step towards a more aggressive cancer phenotype.

4.4. Cell proliferation (MTT) assay

Cell proliferation was additionally assessed by cell proliferation (MTT) assay for ATGL KO* and ATGL OE cell lines. The MTT assay is based on the cleavage of the yellow tetrazodium salt MTT to the purple formazan crystals by metabolically active cells. Metabolically active cells produce reducing equivalents like NADH, H^+ that catalyze the aforementioned reaction while being converted to the respective oxidized species (NAD^+) (Figure 25).

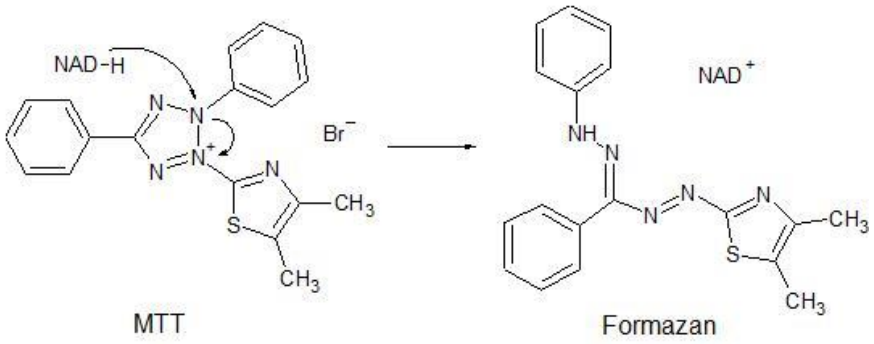

Figure 25: MTT assay reaction *- conversion of MTT (yellow) to Formazan (purple) by metabolically active cells due to the presence of NADH*

The produced Formazan crystals were solubilized in 10% SDS in acidic solution (solubilization agent). The resulting formazan solution was subjected to absorption measurement at excitation wavelength 555 nm. More metabolically active cells produced more formazan, which finally lead to higher absorption values. The absorption values were assessed every 24 hours in a time-span of 72 hours (*t = 0*, *t = 24*, *t = 48* and *t = 72* hours). Additionally, absorption at 655 nm (reference wavelength) was measured. The values obtained from 555 nm and 655 nm measurement were

normalized on cell free blanks that were subjected to the same treatment. Finally, the values obtained from 655 nm were subtracted from those at 555 nm. The resulting differences were plotted against time.

The results of the MTT assay are described and visualized below (Figures 26-27).

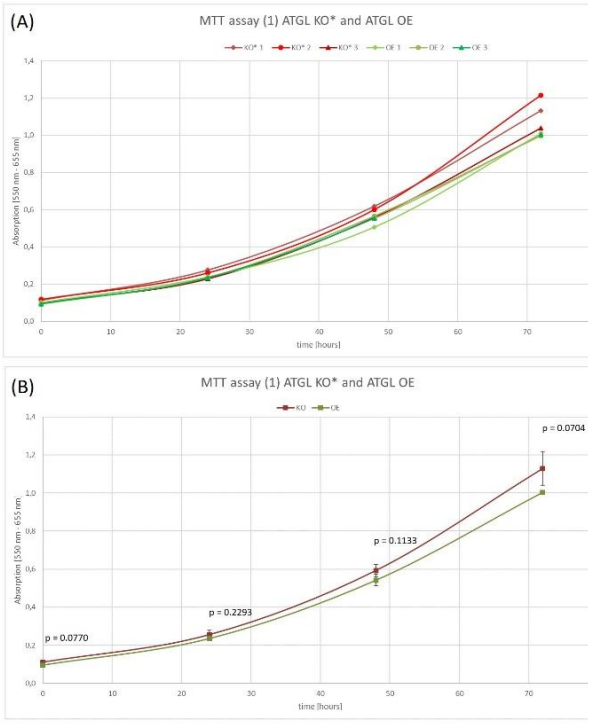

Figure 26: MTT assay (1) *- A: three biological replicates of both conditions (ATGL KO* and ATGL OE) visualized in one dot plot with interpolated lines; ATGL KO* cell lines in shades of red and ATGL OE cell lines in shades of green; B: the means of the biological replicates plotted for each condition – error bars represent standard deviation – significance was determined by student's t-test (* p < 0.05, ** p < 0.01)*

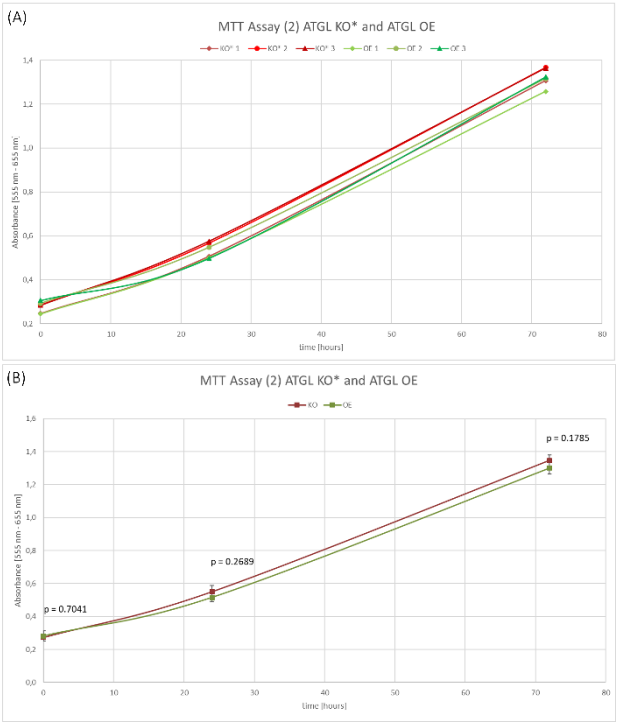

Figure 27: MTT assay (2) *- A: three biological replicates of both conditions (ATGL KO* and ATGL OE) visualized in one dot plot with interpolated lines; ATGL KO* cell lines in shades of red and ATGL OE cell lines in shades of green; B: the means of the biological replicates plotted for each condition – error bars represent standard deviation – significance was determined by student's t-test (* p < 0.05, ** p < 0.01)*

In the first MTT experiment, no significant difference between the growth of ATGL KO* and ATGL OE cell lines was observed, however, a clear trend (p = 0.0704) towards ATGL KO* cell lines growing faster than ATGL OE cell lines can be seen. The trend increases towards later timepoints; therefore, the growth difference might become more distinct in longer experiments. However, keeping the cells for longer than 72 hours for MTT tests generated complications. With longer time spans the limit of absorbance that is reliably measured by the microplate reader was reached before the end of the measurement. Another problem with longer experiments is the inadequate supplementation of new medium that is required by the cells to sustain normal growth.

In the second MTT experiment, no significance and no trend was observed. It seems like the ATGL KO* cells were less initially (*t = 0*), and grew faster for the first 24 hours. However, this trend is not met for the measurement at *t = 48*, where one of the ATGL OE cell lines (ATGL OE 3) shows a surprisingly high value, while two of the ATGL KO* cell lines (ATGL KO* 3 and 1) show rather low values. Overall, none of the cell lines seem to show a normal growth according to the plot. One problem of this type of proliferation measurement is that there are only a few timepoints measured during a rather long span of time.

Taken these findings into consideration, the MTT proliferation assay might be well suitable for experiments in which a strong growth difference is expected, while it is rather difficult to obtain a significant growth difference for small growth differences. Additionally, more repetitions of this experiments need to be performed in order to be able to conclude about the growth difference based on MTT assay experiments.

4.5. Gap Closure (“Scratch”) assay

The gap closure or “scratch” assay was performed to determine whether a migration difference can be observed between the ATGL KO* and ATGL OE cell lines. The scratch assay is based on generation of a scratch across cells that are grown to confluency in a well. The percentage of the initial gap that is overgrown again with cells (% of gap closure) is determined by measuring the area of the gap over a time span of 48 hours, during which at least every 15 hours an image of the gap is taken. Cells with a higher migratory potential migrate towards the empty space of the gap and hence close the gap faster. The rate of gap closure is therefore an estimation of the cells’ migratory potential.

For this assay, ATGL KO* and ATGL OE cell lines were allowed to grow to confluency and scratches were made. Images were taken of the scratches in the timespan of 48 hours and the gap closure was estimated based on the area that was grown over with cells after the scratch.

The results are visualized in Figure 28. Unfortunately, one of the cell lines (ATGL KO* 1) had to be excluded from the scratch assay experiment, as in both wells seeded with this cell line the gaps were unable to be quantified as most of the gap was grown over already after the first 15 hours of growth. An unproportionally fast growth in the ATGL KO* 1 cell line was previously noticed, especially upon keeping the cells in culture for

weeks. Nevertheless, there were still 4 wells with ATGL KO* cell lines (2 technical replicates of ATGL KO* 2 and two technical replicates of ATGL KO* 3) as well as 6 wells with ATGL OE cell lines.

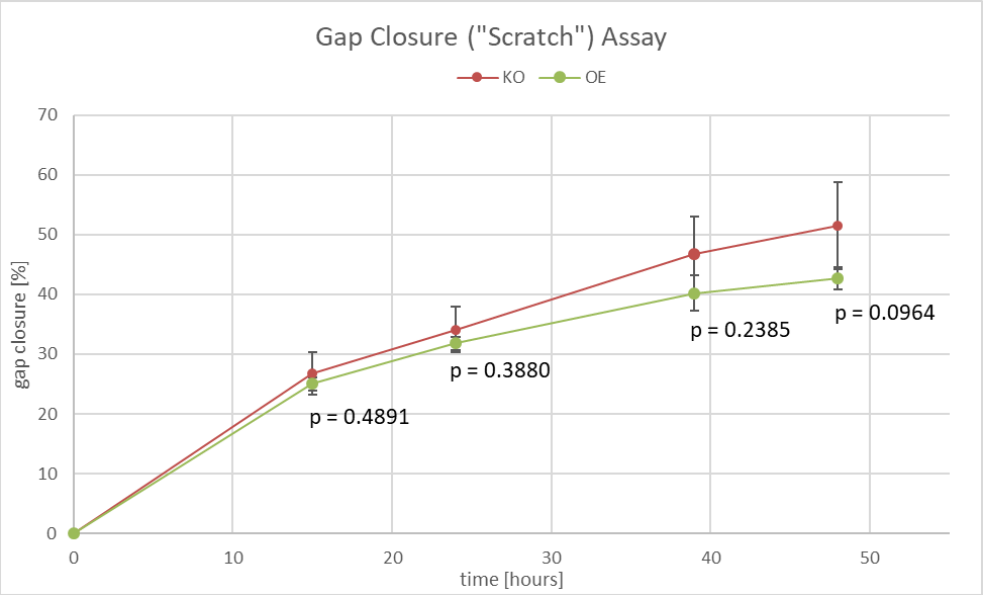

Figure 28: Gap closure (scratch) assay *– gap closure after 15, 24, 39 and 48 h determined from scratch assay (N=2-3 biological replicates per condition, N=2 replicates per cell line); significance was determined by student's t-test (* p < 0.05, ** p < 0.01)*

The scratch assay experiment suggests a higher migratory potential in the ATGL KO* cell lines compared to the ATGL OE cell lines. However, the results are not significant and the experiment has to be repeated. Taken into account that ATGL KO* 1 closed the gap even faster, it can be assumed that the ATGL KO* cell lines do show faster migration.

Even though the scratch assay is a convenient and inexpensive technique to compare migration of different cells, there are several limitations to this test. The manually created scratch might lead to gaps that are inconsistent in size and depth, and cells can be damaged at the border of the scratch. Additionally, in non-automated experiments it is hard to keep the same position on the gap for each measured timepoint. Therefore, scratch assay experiments can give an important insight into the migratory behavior of cells, nevertheless, the results of such experiments have to be used carefully.

Even though the results of this experiment show a minor trend towards ATGL KO* cell lines migrating faster, the results are inconclusive and the experiment requires to be repeated.

4.6. Activity-based proteomic profiling

Activity-based proteomic profiling experiments were performed to determine the serine hydrolase profiles of ATGL lacking, overexpressing or control A549 lung carcinoma cell lines. For the experiment with ATGL KO* and ATGL OE cell lines three biological replicas of each genotype were used, while for the ATGL KO and control experiment four control cell lines were used. In the ABPP experiments, the cells were incubated with the respective activity-based probe (+) or not (-) and subsequently treated according to Figure 16 and chapter 3.7.5. (ABPP workflow). In the course of this thesis project, two different bio-orthogonal linkers were tested (chapter 3.7.4.) for their efficiency to enrich serine hydrolases via their biotin moiety on the streptavidin-agarose beads. From each experiment, two fractions were obtained: on-bead trypsin digests and eluates that were subjected to TEV-protease or DNAse (in the respective experiment) and eluted from the spin columns prior to digestion with trypsin.

The data analysis was performed as described in the material and methods section (3.7.7.). In short, the peptides were quantified and assigned to according protein groups by MaxQuant. The label-free quantification intensity values of the protein groups were used for statistical analysis in Perseus. For the evaluation of the enrichment based on treatment with ABP (+) or without (-), the samples were grouped into respective sample sets (e.g. ATGL KO*) and compared to each other. To this end probe-treated samples were compared to non-treated samples of the same genotype to identify enriched serine hydrolases. In experiments where several serine hydrolases were found, they were compared between the different conditions (e.g. KO* and OE).

Initially, experiments were performed on ATGL KO* and OE cell lines to test which of the linkers and digests (on-bead (O) or eluate (E)) allows for the most efficient enrichment of serine hydrolases.

4.6.1. DNA linker experiment

4.6.1.1. Elution prior digestion with trypsin

Initially, the DNA linker was tested on samples from the ATGL KO* and ATGL OE cell lines. The initial protein group matrix consisted of 2656 identified protein groups. First, this matrix was separated into the two sample sets: ATGL KO* samples (containing both (+) and (-) samples) and ATGL OE samples (containing both (+) and (-) samples). In order to check for the serine hydrolase enrichment due to the ABPP workflow the

ABP treated samples (+) were compared with the non-treated (-) samples in each of the genotypes. The individual samples in each sample set were therefore assigned to the corresponding group ((+) or (-)), and the values were log_2 transformed. Prior to statistical testing, missing values had to be removed or imputed. Therefore, a protein group was removed unless it contained at least three valid values in at least one group. This reduced the the matrix to 738 protein groups in the ATGL KO* sample set and 421 protein groups in the ATGL OE sample set. After filtering, the log histogram was checked and the remaining missing values were imputed based on a downshifted (1.6 downshift, 0.4 width) normal distribution.

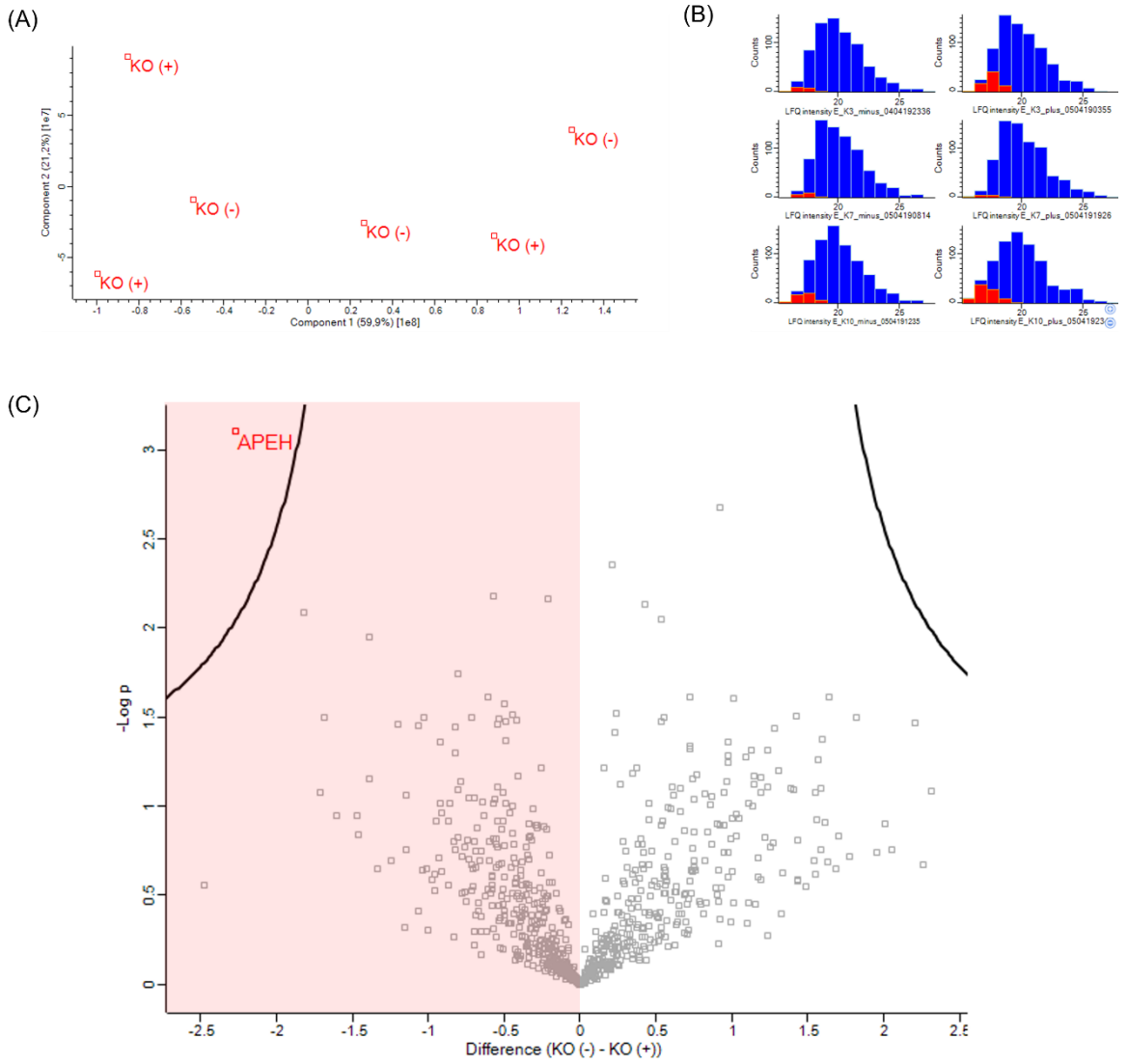

Figure 29: ABPP with DNA linker and eluted ATGL KO* samples with (+) or without (-) ABP *- (A) principle component analysis (PCA) of KO*(+) and KO*(-) samples; (B) log histograms of the log_2 transformed LFQ intensity values (blue) and the imputed values in red; (C) volcano plot: plotted are the log fold changes of the means of the samples in the two conditions (+) and (-) against the negative log of the p-value of the performed student's t-test – the protein in red is significantly higher in (+) samples compared to (-) samples – proteins higher in treated samples are found in the space colored in red; significance determined by permutation based FDR: FDR 5% and s0 = 1*

Finally, a volcano plot was generated, visualizing the proteins significantly enriched in either of the two groups: ABP-treated or non-treated samples. Volcano plots depict the statistical significance of the performed t-test (-log(p-value) on the y-axis) plotted against the difference of the mean values of the log_2 transformed and imputed LFQ intensities between the two groups (Difference between (-) and (+) on the x-axis). A permutation-based FDR multi-test correction was performed and the threshold was set to 5 % and the s0 value was set to 1. The results of the test are represented in Figures 29 and 30 for the ATGL KO* and ATGL OE sample sets, respectively. The figures contain the volcano plot showing the significant protein groups in red (KO) or green (OE) (C), the log histograms of each sample in blue with the imputed values in red (B), and a principle component analysis (PCA), which visualizes the similarity between the individual samples (A).

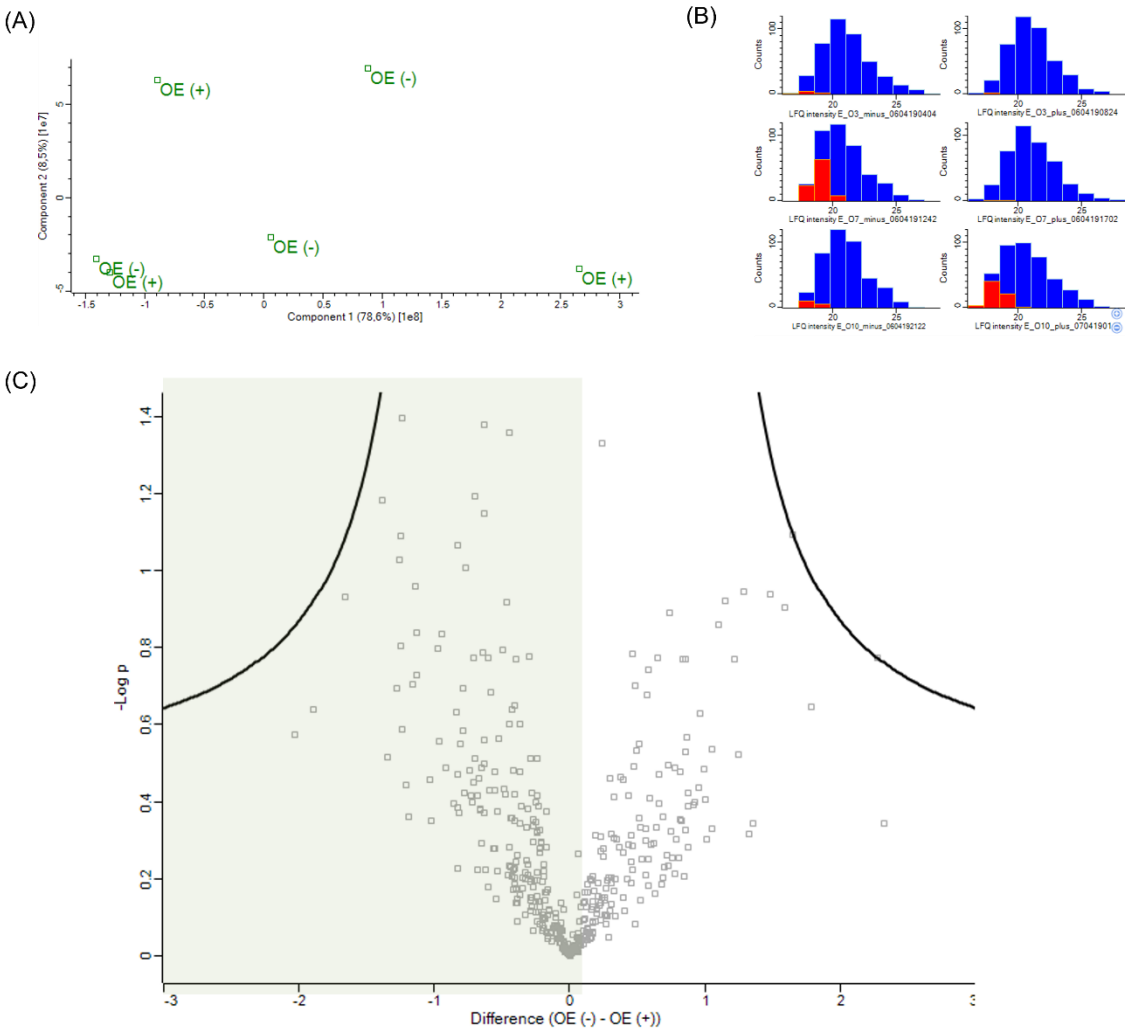

Figure 30: ABPP with DNA linker and eluted ATGL OE samples with (+) or without (-) ABP *- (A) principle component analysis (PCA) of OE(+) and OE(-) samples; (B) log histograms of the log₂ transformed LFQ intensity values (blue) and the imputed values in red; (C) volcano plot: plotted are the log fold changes of the means of the samples in the two conditions (+) and (-) against the negative log of the p-value of the performed student's t-test – proteins higher in treated samples are depicted in the space colored in green; significance determined by permutation based FDR: FDR 5% and s0 = 1*

As seen in the PCA plots, the probe-treated and non-probe treated samples do not cluster according to their treatment, which implies that the samples within one group are not more similar to each other than to samples outside their group. We expected to see that at least the ABP-treated samples cluster together, since they should contain similar serine hydrolases enriched in all of them but not in the non-treated controls. In the volcano plots, however, only one (Figure 29) or no (Figure 30) significantly different proteins could be detected even with an FDR of 5%. Interestingly enough, the one detected protein acylamino-acid-releasing enzyme (APEH) belongs to the group of serine hydrolases. However, this enzyme is a peptidase that releases acyl groups from N-acetylated proteins, and does not seem to be involved in hydrolysis of lipids.

Since the enrichment of serine hydrolases using the DNA linker did not work as expected, control experiments were conducted. In order to rule out that the DNAse simply did not cleave the DNA linker sufficiently and hence the bound proteins were not released the on-bead digested proteins of the same samples were also analyzed.

4.6.1.2. On-bead digest with trypsin

ABP-treated ATGL KO* and OE samples clicked to the same DNA linker but released from the beads by on-bead digest with trypsin after enrichment on the streptavidin-agarose beads were subjected to the same analytical protocol and statistical analysis procedure (as described more extensively in 4.6.1.1). From initially 2556 protein groups in the protein group matrix, 1318 protein groups remained in the ATGL KO* sample set after filtering for three valid values in at least one group, and 1110 protein groups in the ATGL OE sample set, respectively. Again, PCA plots were generated and the missing values were imputed from a downshifted (1.6 downshift, 0.4 width) normal distribution. For generation of the volcano plot, t-test analysis was performed and the multi-test correction permutation-based FDR was set to 5 % with the s0 value at 1.

The results of the statistical analyses of ATGL KO* and ATGL OE on-bead digested samples are shown in Figures 31 and 32, respectively.

Unfortunately, the PCA plots of on-bead digested samples also showed no clustering in the ABP-treated or non-treated samples in either one of the two sets. Additionally, one of the samples in the ATGL OE sample set contained an unproportionally high amount of missing values that had to be imputed (Figure 32 (B)), adding uncertainty to the results.

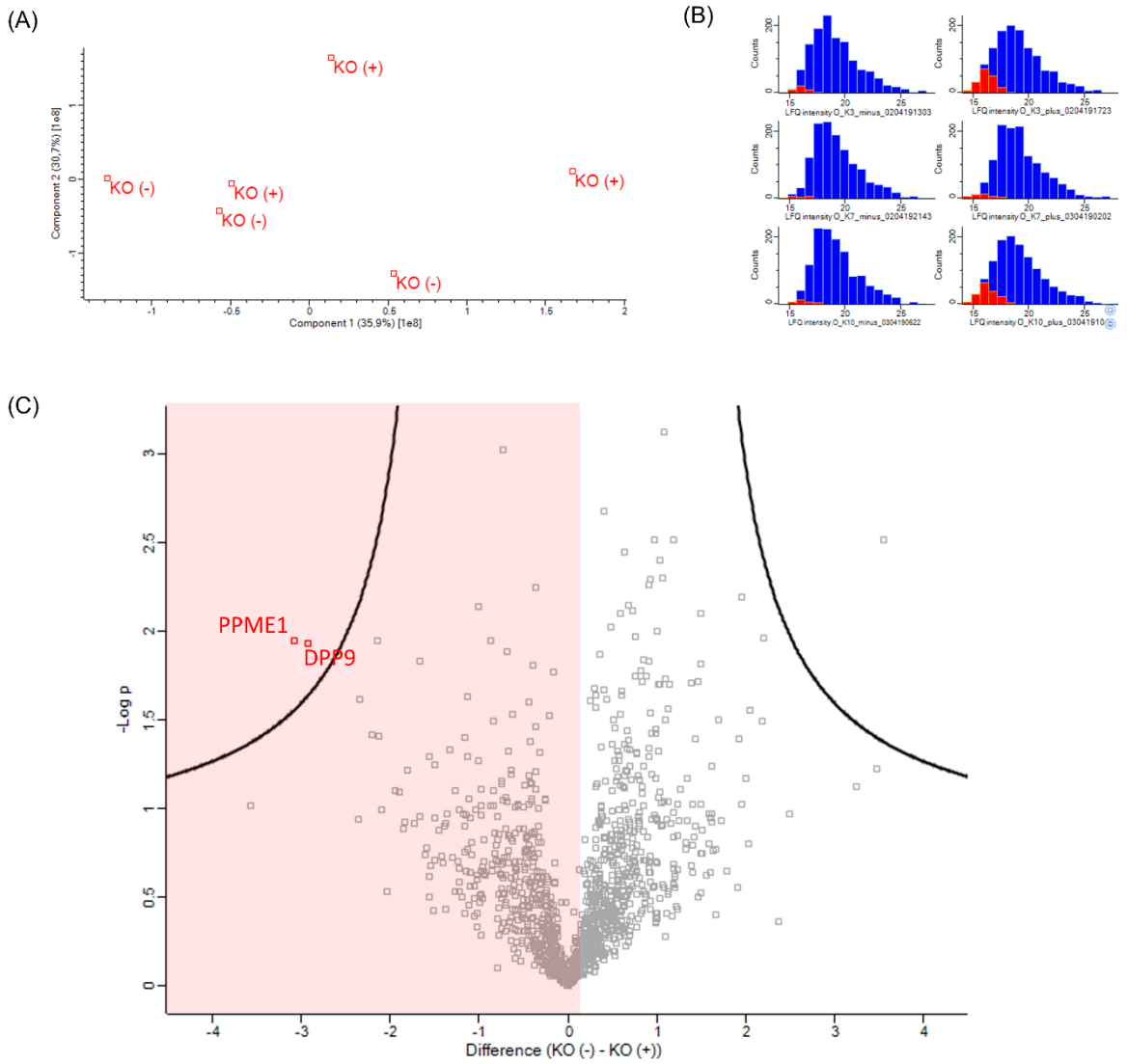

Figure 31: ABPP with DNA linker and on-bead ATGL KO* samples with (+) or without (-) ABP *- (A) principle component analysis (PCA) of KO*(+) and KO*(-) samples; (B) log histograms of the log_2 transformed LFQ intensity values (blue) and the imputed values in red; (C) volcano plot: plotted are the log fold changes of the means of the samples in the two conditions (+) and (-) against the negative log of the p-value of the performed student's t-test – the proteins in red are significantly higher in (+) samples compared to (-) samples – proteins higher in treated samples are found in the space colored in red; significance determined by permutation based FDR: FDR 5% and s0 = 1*

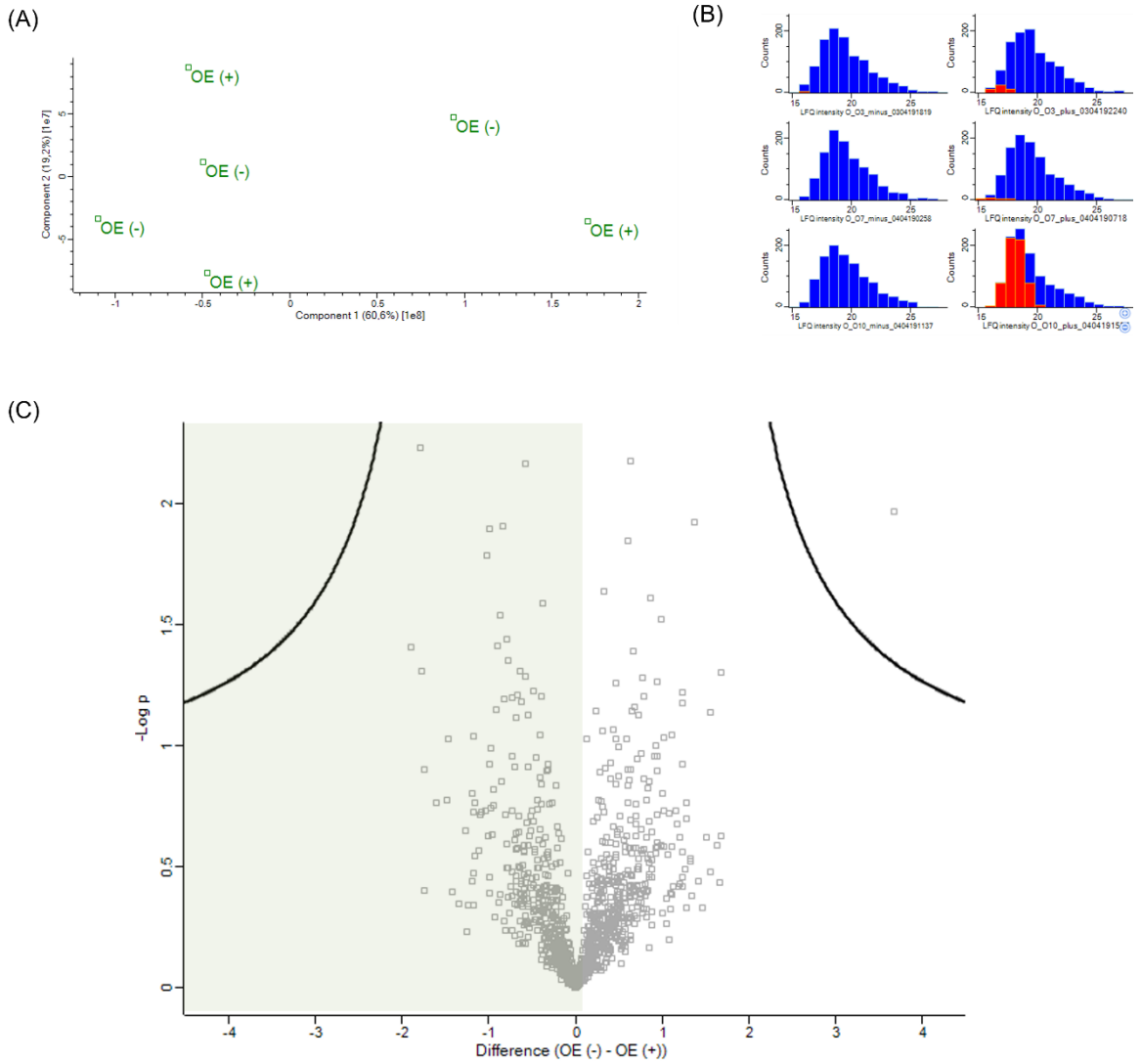

Figure 32: ABPP with DNA linker and on-bead ATGL OE samples with (+) or without (-) ABP *- (A) principle component analysis (PCA) of OE(+) and OE(-) samples; (B) log histograms of the log₂ transformed LFQ intensity values (blue) and the imputed values in red; (C) volcano plot: plotted are the log fold changes of the means of the samples in the two conditions (+) and (-) against the negative log of the p-value of the performed student's t-test – proteins higher in treated samples are found in the space colored in green; significance determined by permutation based FDR: FDR 5% and s0 = 1*

The volcano plot depicting the proteins in the ATGL OE sample set does not show any protein significantly higher in the probe-treated samples.

In the ATGL KO* sample set, however, two proteins higher in (+) samples passed the significance test. Additionally, both of these proteins belong to the group of serine hydrolases: Dipeptidyl peptidase 9 (DPP9) and Protein phosphatase methylesterase 1 (PPME1). The only two proteins significantly higher in (+) samples are serine hydrolases, which suggests that the enrichment worked to some extent but was very inefficient using the DNA-linker. To this end, the TEV linker was used on the same probe-treated samples, and again, tryptic on-bead digests were checked in addition to TEV released eluate samples.

4.6.2. TEV linker experiments

4.6.2.1. Elution prior digest with trypsin

In the initial protein groups matrix in the ABPP experiment using the TEV linker on ATGL KO* and ATGL OE samples with elution by TEV cleavage prior to digestion with trypsin contained 2377 protein groups. After filtering for at least three valid values in at least one group the ATGL KO* sample set consisted of 174 protein groups, while 183 protein groups remained in the ATGL OE sample set. The PCA plots and log histograms with imputed values as well as the volcano plots (FDR = 5 %; s0 = 1) of the ATGL KO* and ATGL OE sample sets are visualized in Figures 33 and 34, respectively.

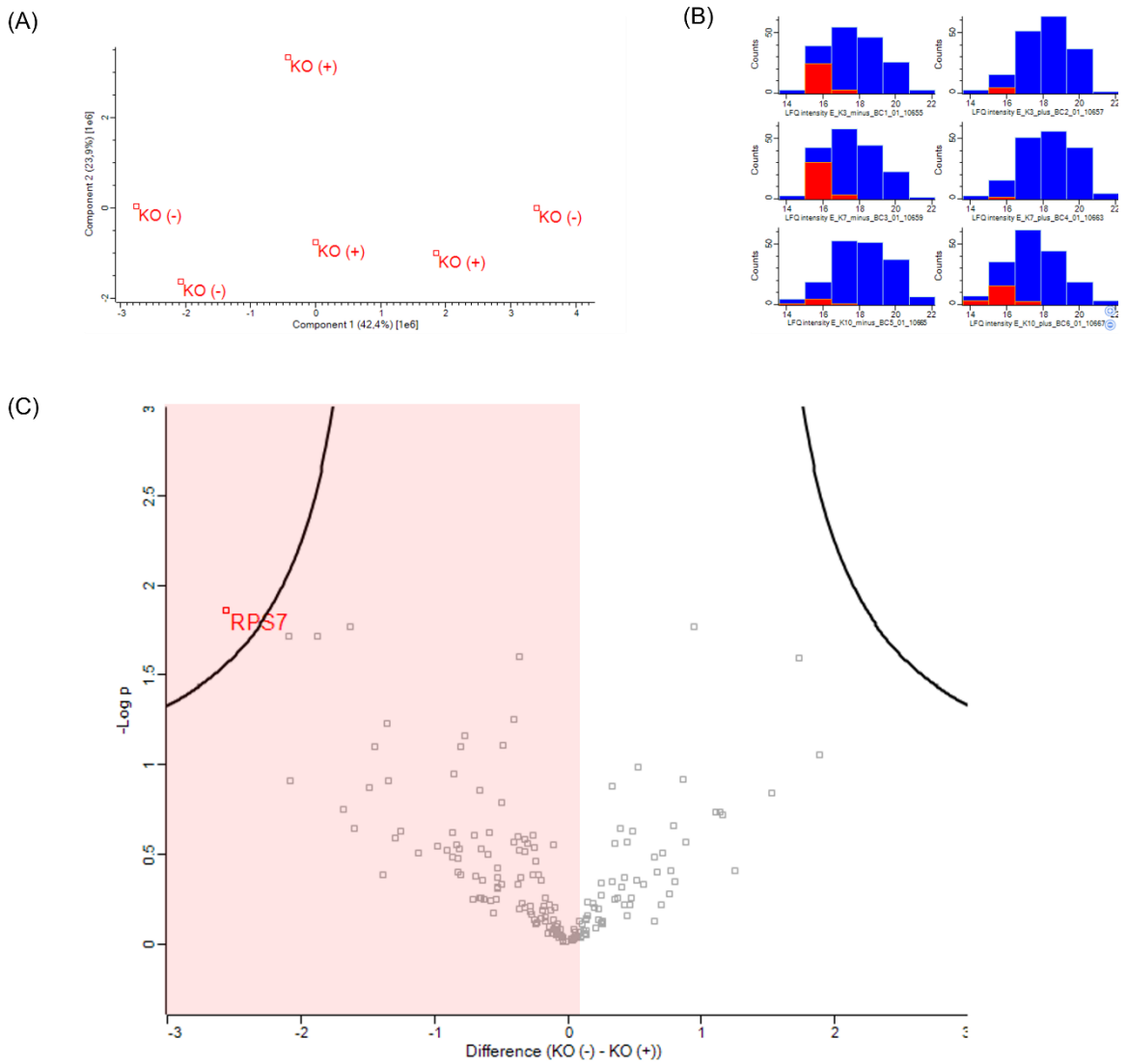

Figure 33: ABPP with TEV linker and eluted ATGL KO* samples with (+) or without (-) ABP *- (A) principle component analysis (PCA) of KO*(+) and KO*(-) samples; (B) log histograms of the log_2 transformed LFQ intensity values (blue) and the imputed values in red ((B) log histograms of the log_2 transformed LFQ intensity values (blue) and the imputed values in red; (C) volcano plot: plotted are the log fold changes of the means of the samples in the two conditions (+) and (-) against the negative log of the p-value of the performed student's t-test – the protein in red is significantly higher in (+) samples compared to (-) samples – proteins higher in treated samples are found in the space colored in red; significance determined by permutation based FDR: FDR 5% and s0 = 1*

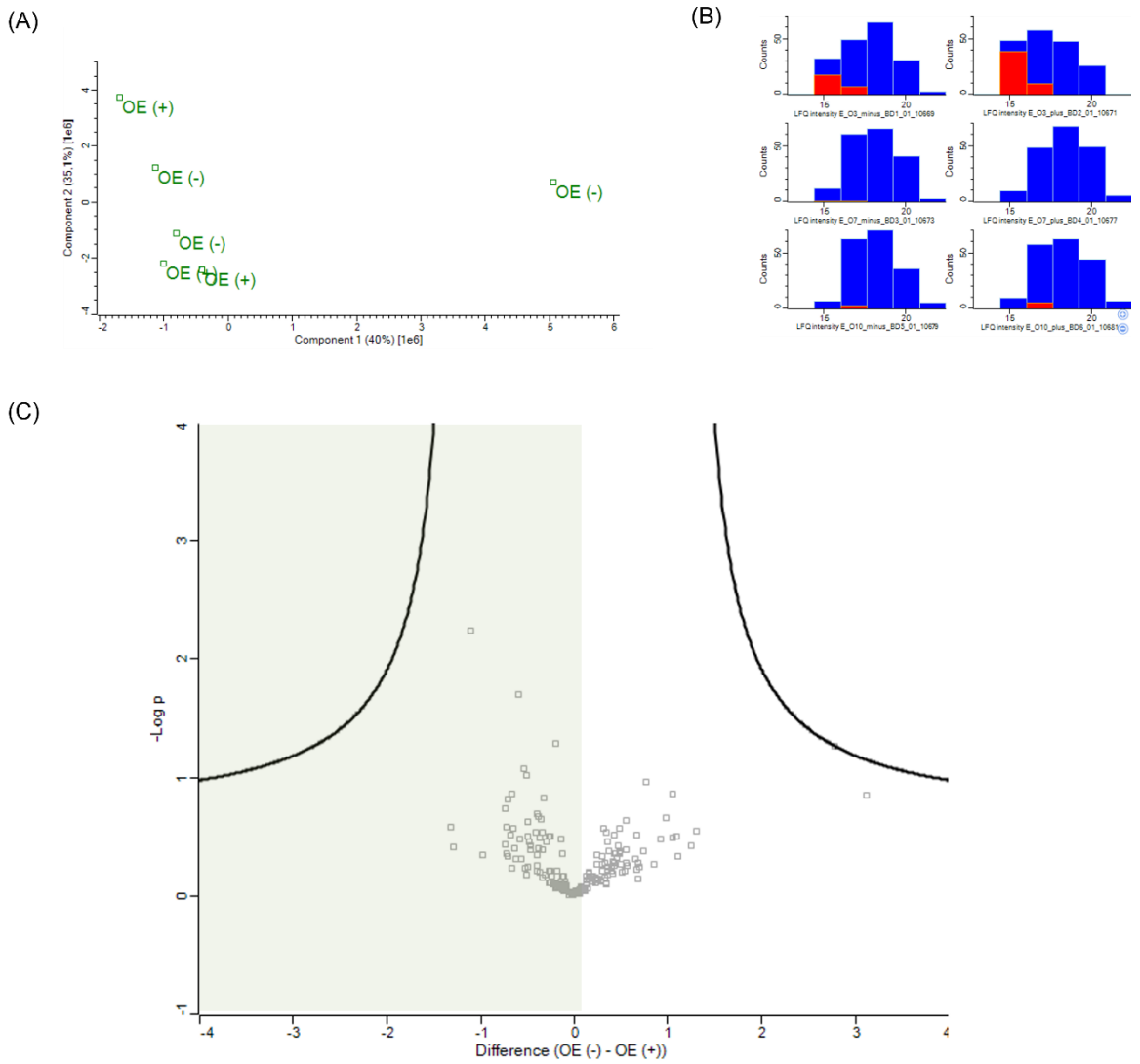

Figure 34: ABPP with TEV linker and eluted ATGL OE samples with (+) or without (-) ABP *- (A) principle component analysis (PCA) of OE(+) and OE(-) samples visualizing the similarity of individual samples; (B) log histograms of the log_2 transformed LFQ intensity values (blue) and the imputed values in red; (C) volcano plot: plotted are the log fold changes of the means of the samples in the two conditions (+) and (-) against the negative log of the p-value of the performed student's t-test – proteins higher in treated samples are found in the space colored in green; significance determined by permutation based FDR: FDR 5% and s0 = 1*

Similar to the DNA linker experiments, in the TEV linker experiments using TEV protease to elute the samples, the ABP-treated samples did not cluster together in the PCA plot, and neither did the non-treated samples (Figures 33 (A) and 34 (A)). Interestingly, the number of protein groups decreased drastically upon filtering for at least three valid values, which suggests that less proteins were eluted from the columns upon TEV protease treatment compared to DNAse treatment of the corresponding samples treated with DNA linker. From the already low number of obtained proteins, none was significantly enriched in ABP-treated samples compared to non-treated samples in the ATGL OE sample set. In the ATGL KO* sample set, however, one protein

group passed the threshold and was higher in (+) samples. However, the protein that was found – 40S ribosomal protein S7 – turned out not to be a serine hydrolase.

In addition to the eluted sample sets from the TEV linker experiment, the on-bead digested proteins of the same experiment were also analyzed.

4.6.2.2. On-bead digest with trypsin

ATGL KO* and ATGL OE sample sets

In the on-bead digest experiment of TEV linker treated ATGL KO* and ATGL OE samples, the initial protein group matrix contained 2377 protein groups. After separation of the matrix into the corresponding sample sets (ATGL KO* and ATGL OE), the individual samples in each sample set were assigned to the corresponding group and the values were $\log_2$ transformed. The filtering for at least three valid values in at least one group yielded a matrix of 1010 protein groups in the ATGL KO* sample set and 934 protein groups in the ATGL OE sample set. Missing values were imputed based on normal distribution of the values (with a 1.6 downshift and width of 0.4). Figures 35-36 show the results of the statistics analyses from Perseus of the ATGL KO* and ATGL OE sample sets, respectively. Each figure shows the volcano plot in which the significant protein groups are depicted in red (ATGL KO*) or green (ATGL OE) (C), the log histograms of each sample in blue with the imputed values in red (B), and a principle component analysis (A). Figures 35 and 36 show that for the first time, the PCA plots appeared to cluster. Even though the samples did not cluster perfectly in this experiment as well, compared to DNA linker experiments they show a tendency towards clustering. One reason why the clustering is – in general – not good might be the problem of many proteins sticking to the agarose beads in a non-specific manner. This might cause a very diverse set of proteins even within the same groups and thus the samples do not cluster well. Since serine hydrolases are enriched in (+) treated samples of this experiment, however, this experiment shows some clustering within the (+) group.

In addition, from the volcano plots it can be seen that several proteins are significantly higher in probe-treated samples compared to non-treated even with FDR set to 1 % – in the ATGL KO* as well as in the ATGL OE sample sets. In the ATGL KO* sample set 22 proteins were found significantly higher in (+) samples, of which 16 belong to the group of serine hydrolases (≈ 73 %). In the ATGL OE sample set 21 proteins were found

significantly higher in ABP-treated samples and 16 of those were annotated as serine hydrolases (≈ 76 %).

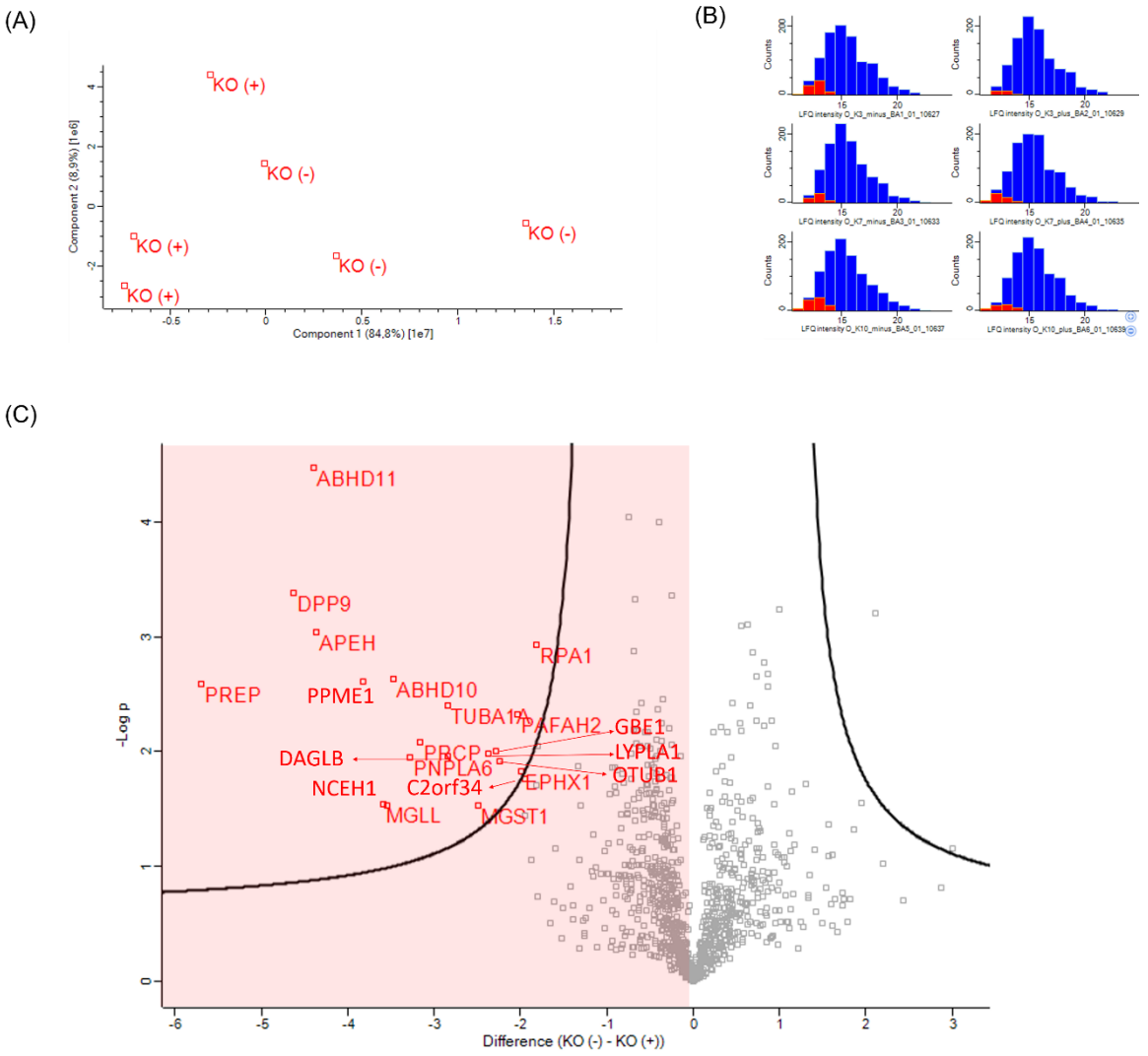

Figure 35: ABPP with TEV linker and on-bead ATGL KO* samples with (+) or without (-) ABP *- (A) principle component analysis (PCA) of KO*(+) and KO*(-) samples; (B) log histograms of the log₂ transformed LFQ intensity values (blue) and the imputed values in red; (C) volcano plot: plotted are the log fold changes of the means of the samples in the two conditions (+) and (-) against the negative log of the p-value of the performed student's t-test – the proteins in red are significantly higher in (+) samples compared to (-) samples – proteins higher in treated samples are found in the space colored in red; significance determined by permutation based FDR: FDR 1% and s0 = 1*

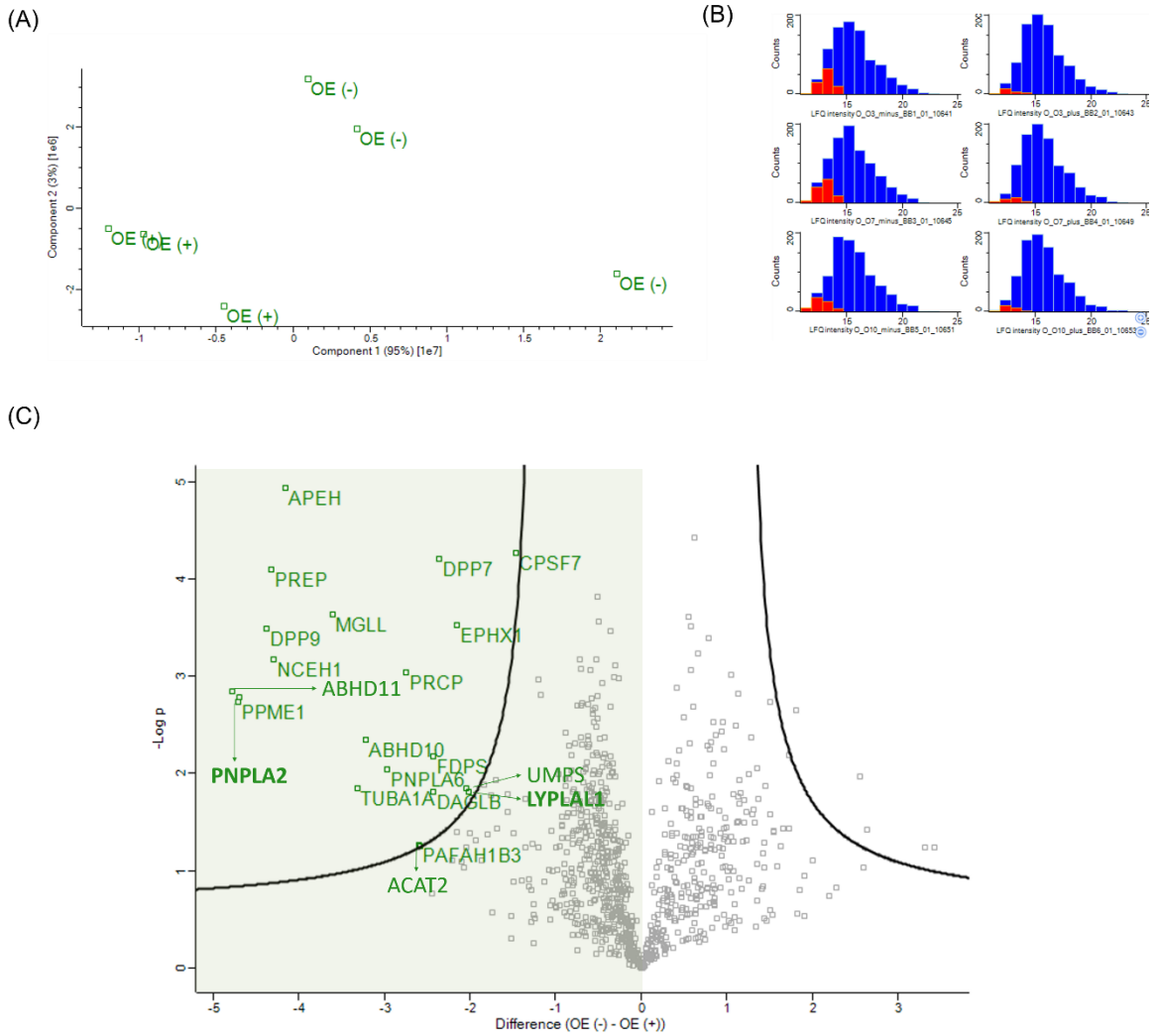

Figure 36: ABPP with TEV linker and on-bead ATGL OE samples with (+) or without (-) ABP *- (A) principle component analysis (PCA) of OE(+) and OE(-) samples; (B) log histograms of the log$_2$ transformed LFQ intensity values (blue) and the imputed values in red; (C) volcano plot: plotted are the log fold changes of the means of the samples in the two conditions (+) and (-) against the negative log of the p-value of the performed student's t-test – the proteins in green are significantly higher in (+) samples compared to (-) samples – proteins higher in treated samples are found in the space colored in green; ATGL (PNPLA2) and LYPLA1 are highlighted in bold; significance determined by permutation based FDR: FDR 1% and s0 = 1*

The obtained serine hydrolases from both sample sets were used to generate a list of serine hydrolases that were enriched in ABP-treated samples in this experiment. 20 serine hydrolases were subsequently compared and subjected to a t-test, in order to find differences in the serine hydrolase profiles between ATGL KO* and ATGL OE cell lines. The result of this comparison is depicted in Table 17. Two serine hydrolases were found (Figure 17, lines shaded in green) that were significantly different between ATGL KO* and ATGL OE samples.

One of the proteins found to be different between ATGL KO* and ATGL OE samples was patatin-like phospholipase domain-containing protein 2 (*PNPLA2*), which is an alternative name for ATGL. ATGL was more than five log fold changes (≈ 50 fold) higher

in the ATGL OE samples than in ATGL KO samples. This result by itself is a proof-of-principle that the experiment worked successfully. Not only were several serine hydrolases enriched, but one of the most important lipid hydrolases, ATGL was identified and the difference between the two sample sets could be determined. This result, however, was to be expected since ATGL was known to be different in those cell lines (confirmed in chapter 4.2. western blot).

More surprisingly, an additional serine hydrolase – lysophospholipase-like protein 1 – was identified to be higher in ATGL OE cell lines. Even though the log fold change between the two conditions was rather small (0.23 corresponding to ~ 17%), this protein is a potentially interesting hit that can be further investigated.

Protein names	Gene names	t.test	Difference (OE) - (KO)
Patatin-like phospholipase domain-containing protein 2	PNPLA2	0,000579	5,69418 (~ 50-fold)
Protein phosphatase methylesterase 1	PPME1	0,416294	0,49683
Epoxide hydrolase 1	EPHX1	0,203063	0,47645
Acetyl-CoA acetyltransferase, cytosolic	ACAT2	0,375075	0,33300
Lysophospholipase-like protein 1	LYPLAL1	0,011699	0,23055 (~17 %)
Dipeptidyl peptidase 7	DPP7	0,915296	0,06767
Neutral cholesterol ester hydrolase 1	NCEH1	0,895867	0,04662
Neuropathy target esterase	PNPLA6	0,990723	-0,00195
Monoglyceride lipase	MGLL	0,950007	-0,04539
Lysosomal Pro-X carboxypeptidase	PRCP	0,516018	-0,21205
Dipeptidyl peptidase 8	DPP8	0,147876	-0,21958
Acylamino-acid-releasing enzyme	APEH	0,437343	-0,23598
UPF0554 protein C2orf43	C2orf43	0,168894	-0,36266
Alpha/beta hydrolase domain-containing protein 11	ABHD11	0,285606	-0,41059
Sn1-specific diacylglycerol lipase beta	DAGLB	0,477929	-0,44137
Prolyl endopeptidase	PREP	0,274801	-0,48779
Platelet-activating factor acetylhydrolase 2	PAFAH2	0,185146	-0,51539
Dipeptidyl peptidase 9	DPP9	0,226537	-0,60684
Mycophenolic acid acyl-glucuronide esterase	ABHD10	0,067174	-0,78586
Ubiquitin thioesterase OTUB1	OTUB1	0,217692	-1,56521

Table 17: Serine hydrolases enriched in ABPP of ATGL KO* and ATGL OE compared

Since the TEV linker experiment with on-bead trypsin digestion of the proteins was the only combination of experiments that yielded several enriched serine hydrolases, this experiment was also performed for ATGL KO and control sample sets.

ATGL KO and control sample sets

In the experiment investigating the serine hydrolase profiles of ATGL KO and control cell lines, the initial protein groups matrix contained 2437 protein groups. After filtering for at least three valid values in at least one group, 1189 protein groups remained in the ATGL KO sample set, while the control sample set contained 1223 protein groups. Figures 37 and 38 show the results of the statistical analysis of ATGL KO and control sample sets, respectively, and contain PCA plots (A), log histograms (B) as well as the volcano plot (C) with significant proteins in red (KO) or blue (control) (C).

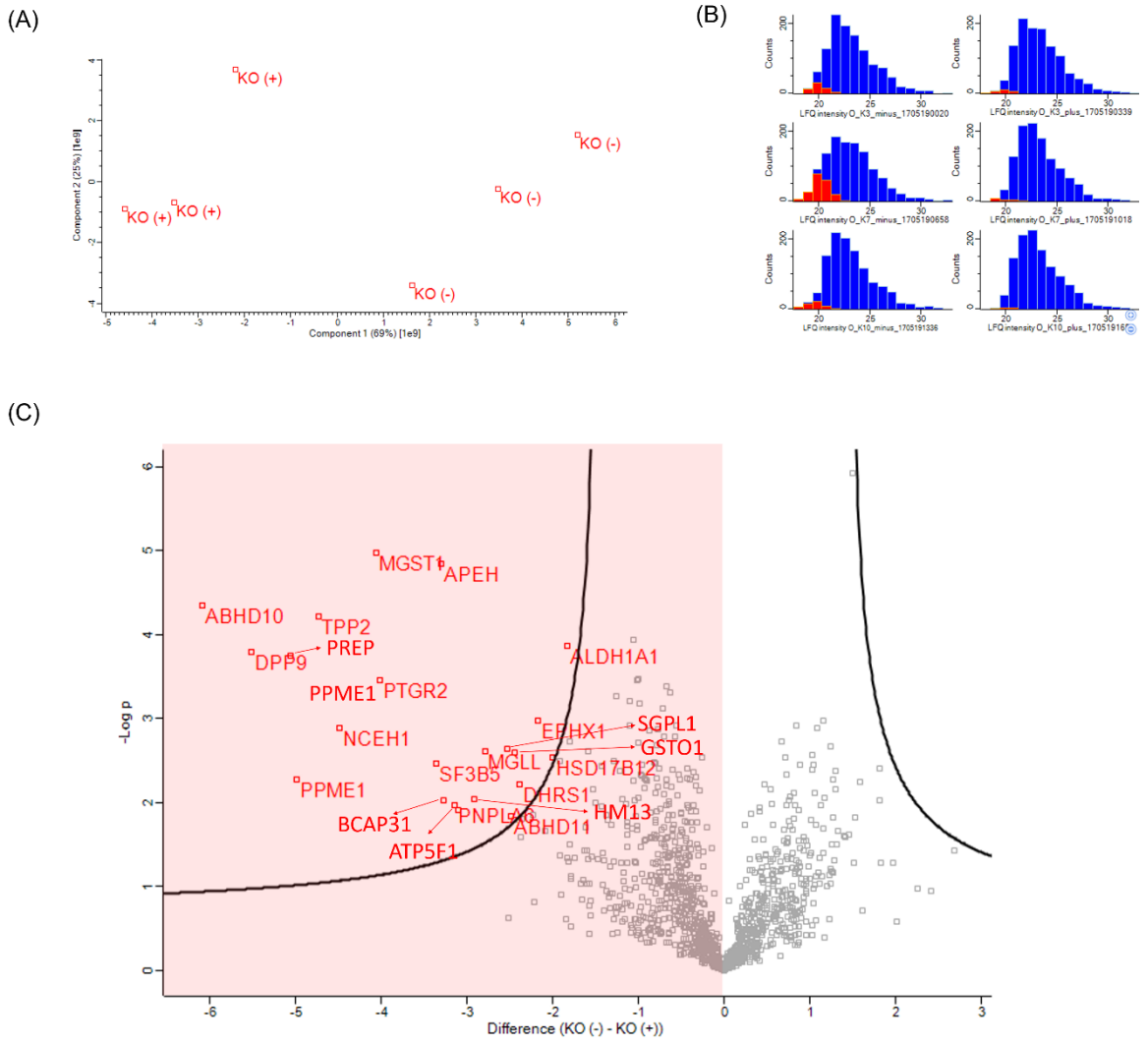

Figure 37: ABPP with TEV linker and on-bead ATGL KO samples with (+) or without (-) ABP *- (A) principle component analysis (PCA) of KO(+) and KO(-) samples; (B) log histograms of the log_2 transformed LFQ intensity values (blue) and the imputed values in red (based on normal distribution); (C) volcano plot: plotted are the difference of the means of the samples in the two conditions (+) and (-) against the negative log of the p-value of the performed student's t-test – the proteins in red are significantly higher in (+) samples compared to (-) samples – proteins higher in treated samples are found in the space colored in red; significance was determined by permutation based FDR: FDR 1% and s0 = 1*

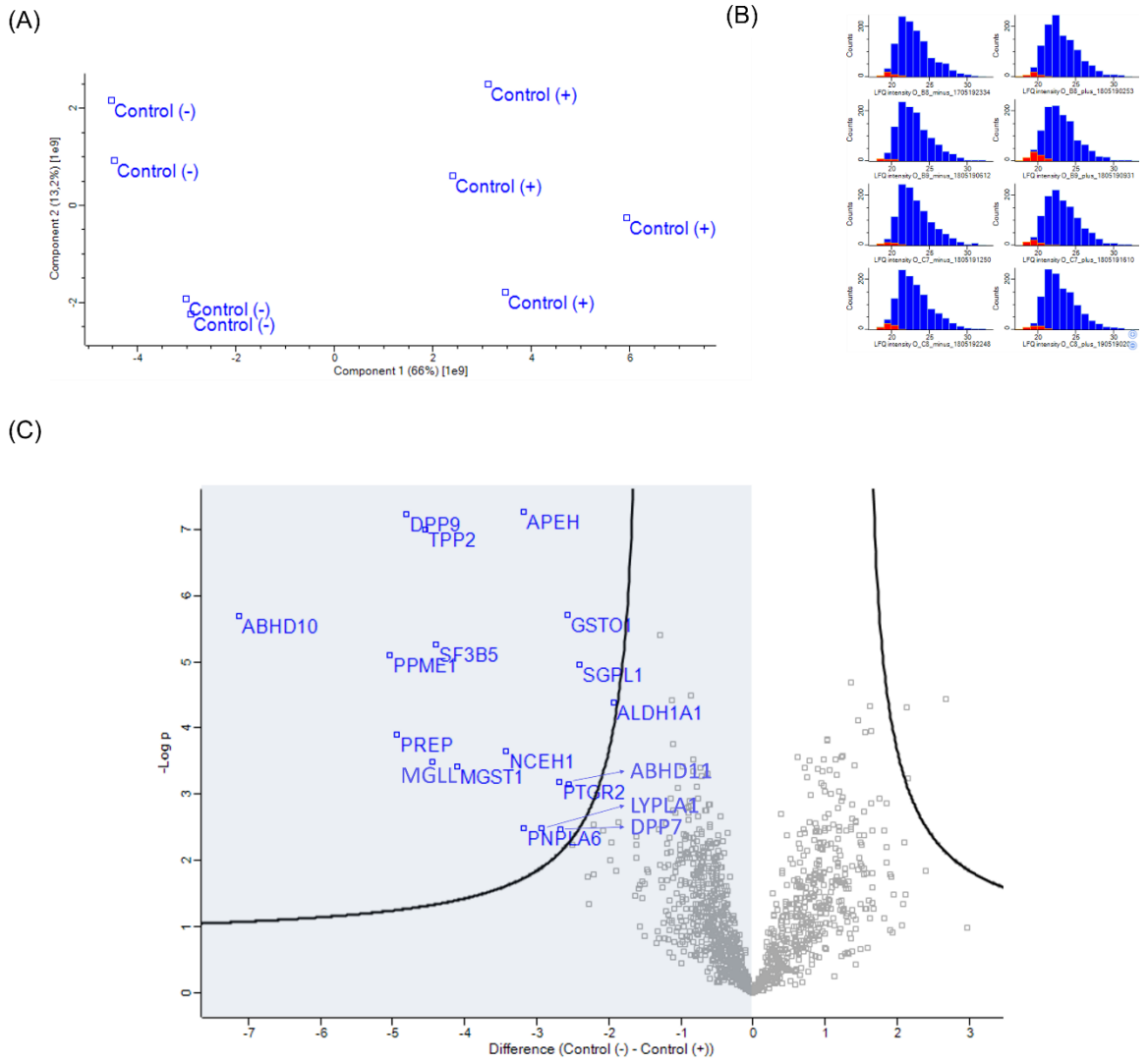

Figure 38: ABPP with TEV-linker and on-bead control samples with (+) or without (-) ABP *- (A) principle component analysis (PCA) of control(+) and control(-) samples; (B) log histograms of the log₂ transformed LFQ intensity values (blue) and the imputed values in red (based on normal distribution); (C) volcano plot: plotted are the difference of the means of the samples in the two conditions (+) and (-) against the negative log of the p-value of the performed student's t-test – the proteins in blue are significantly higher in (+) samples compared to (-) samples – proteins higher in treated samples are found in the space colored in blue; significance determined by permutation based FDR: FDR 1% and s0 = 1*

In both sample sets, the PCA plots confirm that also in this TEV linker and on-bead digest experiment the ABP-treated samples cluster to some degree. The volcano plots were generated again with an FDR of 1 % and s0 value of 1, and even with the more stringent settings like in the other TEV linker on-bead experiment several proteins were significantly higher in the (+) compared to the (-) samples. In the ATGL KO sample set, 22 proteins were significantly higher in the (+) probes, of which 11 were annotated as serine hydrolases (= 50 %). In the control sample set 18 proteins were significantly higher in ABP-treated samples, and 12 of those were serine hydrolases (≈ 67 %).

Again, all of the found serine hydrolases were pooled and a list of 13 serine hydrolases was generated and the probe-treated samples of ATGL KO sample set and the control sample set were compared and a t-test was performed. In table 18 the list of serine hydrolases with the respective difference and significance (t-test) is shown.

Protein names	Gene names	t-test	Difference (Control) - (KO)
Mycophenolic acid acyl-glucuronide esterase	ABHD10	0,9305	0,0186
Alpha/beta hydrolase domain-containing protein 11	ABHD11	0,4629	-0,2483
Acylamino-acid-releasing enzyme	APEH	0,0448	-0,2913 (~22 %)
Dipeptidyl peptidase 2	DPP7	0,7281	0,2287
Dipeptidyl peptidase 9	DPP9	0,8202	-0,0659
Acyl-protein thioesterase 1	LYPLA1	0,4324	0,3267
Monoglyceride lipase	MGLL	0,5573	0,3566
Neutral cholesterol ester hydrolase 1	NCEH1	0,5128	-0,2515
Neuropathy target esterase	PNPLA6	0,9460	-0,0365
Protein phosphatase methylesterase 1	PPME1	0,7046	0,1589
Prolyl endopeptidase	PREP	0,7382	-0,0989
Tripeptidyl-peptidase 2	TPP2	0,5270	-0,1553
Epoxide hydrolase 1	EPHX1	0,8912	-0,1143

Table 18: Serine hydrolases enriched in ABPP of ATGL KO and control cell lines compared

In conclusion, the ABPP experiments using the TEV linker as the bio-orthogonal linker in combination with on-bead digest enabled the successful enrichment and detection of serine hydrolases upon ABP-treatment with the C_6 probe and the here described ABPP workflow. There was, however, no clear-cut serine hydrolase that was higher or lower in ATGL KO cell lines compared to ATGL OE and control cell lines. In each individual experiment, however, there was a serine hydrolase significantly different in the ATGL lacking cell lines compared to ATGL OE or control: acylamino-acid-releasing enzyme, which was higher in ATGL KO cells compared to control cells (~20 %), and lysophospholipase-like protein 1, which was higher in ATGL OE cell lines compared to ATGL KO* (~17 %).

5. Discussion

The aim of this thesis was to employ activity-based proteomic profiling (ABPP) on lung carcinoma cell lines lacking or overexpressing the major triacylglycerol (TAG) hydrolase adipose triglyceride lipase (ATGL). Based on the observed change in the bioactive ether- and lysophospholipid profile upon ATGL absence[68] – a phenotype that cannot be directly linked to impaired ATGL – I intended to determine and compare the serine hydrolase profiles in lung carcinoma cell lines lacking or overexpressing ATGL, to find a potential lipase or acyltransferase within the group of serine hydrolases that may be responsible for the altered lipid profile upon ATGL depletion. It is known from literature that phosphonates with an appropriate leaving group (e.g. fluoride or p-nitrophenol) can be used as serine hydrolase inhibitors that covalently bind to the active site of the enzymes[91,93,98]. Hence, a p-nitrophenyl phosphonate activity-based probe (ABP) termed C_6-probe (Figure 17) was used in combination with one of two different bio-orthogonal linkers (Figures 18 and 19) containing a biotin functional group to enable enrichment of the tagged proteins on streptavidin-agarose beads. The efficiency of serine hydrolase enrichment upon different ABPP approaches (on-bead digestion or elution of proteins prior to digestion) was assessed. The most efficient approach was used for serine hydrolase profile determination in order to compare cell lines overexpressing ATGL with cell lines lacking ATGL as well as ATGL lacking cell lines with respective controls.

Insights of this work

Several of the ABPP approaches that were tested yielded no or only few serine hydrolases that should have been enriched upon ABP treatment. From the successful approaches we conclude that the C_6-probe works properly and that the problem with the unsuccessful experiments lies within the DNA linker or TEV cleavage. In Figures 29-34 the results are depicted in which no enrichment of serine hydrolases was achieved. These experiments include the DNA linker experiments as well as all experiments in which only the proteins that were eluted from the columns upon cleavage of the linker prior to digestion were analyzed.

As for the DNA linker, there were several pitfalls when working with this linker from the beginning. Initially, I performed acetone precipitation of the protein lysates after linker addition instead of using centrifugal filters, in order to save time and consumables.

However, acetone also precipitates DNA[134] and thus probably precipitated the excess of DNA linker to a large degree. After analyzing the data of this experiment and troubleshooting we recognized this error and ascribed the lack of serine hydrolase enrichment to the acetone precipitation error. For further DNA linker experiments I switched to using centrifugal filters. We chose centrifugal filters with larger cutoff (10 kD) at the risk of losing small molecular weight serine hydrolases, due to the DNA linker being substantially larger than the TEV linker, for whose removal 3 kD cutoff centrifugal filters were used. Despite the use of centrifugal filters of appropriate pore size, the DNA linker experiments did not result in enriched serine hydrolases. We noticed that several of the proteins obtained from the DNA linker experiment were DNA-binding or DNA-related proteins and we concluded that the negatively charged backbone of the DNA in the linker interacts with proteins, causing many unspecific proteins to stick to the DNA linker. To this end, we adapted the buffers in DNA linker experiments to contain at least 0.4 M sodium chloride in order for the negatively charged DNA backbone to be coated with counterions in the hope to prevent unspecific binding of proteins to the DNA linker. Despite all those improvements of the initial protocol, the DNA-linker experiments still failed to result in specific enrichments, which can be seen in Figures 29-32 (Chapter 4.6.1.).

The ABPP experiments in which the TEV linker was used in combination with on-bead protein digest yielded a number of serine hydrolases that were enriched based on treatment with the C_6-probe, as seen in figures 35-38. Out of the list of significant proteins, 50-76 % - depending on the experiment – were annotated as serine hydrolases, which is a satisfying result. The serine hydrolases from the respective experiments are listed in Tables 17 and 18. In addition to the high yield of serine hydrolases enriched upon ABP-treatment, as a proof of principle it was observed, that ATGL – a major serine hydrolase – was significantly higher in ATGL overexpressing cell lines compared to the respective ATGL lacking cell lines. This result can also be seen in Table 17. While in the ATGL KO against control cell experiment, a peptidase was found to be higher in ATGL KO cell lines (Table 18), the ATGL KO* against ATGL OE experiment brought forth a potentially more interesting and relevant enzyme: lysophospholipase-like protein 1 (*LYPLAL1)*.

One drawback of the here performed ABPP experiments is that some important lipases such as the hormone sensitive lipase (HSL) were not found in any of the analyzed sample sets and ATGL was not detected in A549 control cells. This indicates that even though numerous serine hydrolases were found by ABPP that would not have been

detected by regular bottom-up proteomics without serine hydrolase enrichment, this approach still bears certain limitations.

The intention of circumventing on-bead digestion of proteins by using a cleavable linker and eluting proteins prior to digestion, unfortunately, did not result in the expected improved results. The TEV linker was designed to be cleavable by TEV protease and upon TEV protease digestion the linker should have been cleaved and only the ABP-tagged proteins eluted. However, this approach did not yield any detected serine hydrolases. The problem here may be the arrangement of the TEV linker sequence linking the biotin and the click-chemistry moiety. We suspect that the cleavage site is too close to the tagged enzyme upon click-chemistry reaction. Since the TEV protease is a large enzyme the cleavage site may be protected by the serine hydrolase and we suspect that the linker was never cleaved off by the TEV protease, resulting in retention of the tagged proteins on the beads. Another observation that would fit this suspicion is that the number of proteins detected in the eluate samples from TEV linker experiments was very low, probably because not many linkers were cleaved only a few unspecific proteins were eluted.

In general, smaller protein matrices were expected, also with on-bead digestion experiments. However, the vast amount of detected proteins is probably due to the fact that agarose beads, in general, are target of unspecific binding of proteins. This might also be the reason why PCA plots did not show strong clustering, as in all samples unspecific proteins were also digested that were found on the agarose beads. The similarity in PCA plots is slightly better for probe-treated samples in which serine hydrolases were enriched, probably because in those samples there are not only the non-specifically bound proteins, but also the enriched serine hydrolases common to the samples within this sample set.

It is possible that even though serine hydrolases were targeted, the abundance of the active enzyme of interest is yet too low to be detected. One example for this can be seen comparing the two TEV linker on-bead digest experiments on ATGL overexpressing cell lines or control cell lines compared to ATGL lacking cells. It was observed that ATGL was targeted by the ABP, and quantified in ATGL OE cell lines, however, in control cell lines, where ATGL is present at a physiological and thus much lower level, it was not quantified. Another major lipase HSL was not readily quantified by our approach either. Hence, the enzyme of interest, causing the altered lysophospholipid levels, might not have been detected as well.

Another possibility is that the enzyme we attempt to find does not share the serine hydrolase catalytic mechanism and thus was not or insufficiently targeted by the ABPP approach. Acyltransferases catalyze the transfer of acyl groups form a donor to an acceptor. Lysophosphatidylcholine acyltransferase 1 (*LPCAT1*) catalyzes the conversion of lysophosphatidylcholine (LPC) to phosphatidylcholine (PC)[135]. An upregulation of LPCAT1 in the control or ATGL overexpression samples, thus, could explain the higher LPC levels in ATGL KO cell lines observed by Tomin *et al.*[68]. However, acyltransferases might not be as susceptible as hydrolases to the serine hydrolase specific ABPs. Even though acyltransferases share a similar protein fold with serine hydrolases, they do not share the same catalytic site loop orientation[136] and thus might not be targeted as efficiently in the here used ABPP approaches.

The significantly higher lysophospholipase-like protein 1 in ATGL OE cell lines is a potentially interesting serine hydrolase, which may be connected to the observed lipid profile differences observed by Tomin *et al.*[68]. LYPLAL1 belongs to the lysophospholipase family[137] and is similar in structure to the acyl protein thioesterases 1 and 2 (APT1/2). LYPLAL1 was found to be associated to several metabolic phenotypes like non-alcoholic fatty liver disease, but is physiological role is largely unknown[138]. Even though LYPLAL1 shows a similar protein fold to APT1 (= LYPLA1), which catalyzes the hydrolysis of lysophosphatidylcholines (LPC), Bürger *et al.* show that LYPLAL1 does not exhibit the suggested phospholipase activity, but rather accepts short-chain substrates[137]. Since the physiological substrates and general role of LYPLAL1 are still unknown, is it impossible to infer a conclusion from this finding without further experimental work.

Conclusion

Overall, it can be concluded that ABPP was successfully employed to enrich and determine serine hydrolases in lung carcinoma cell lines using the C_6-probe (Figure 17) together with the TEV linker (Figure 18) and on-bead trypsin digest of proteins following the in chapter 3.7.5. described ABPP workflow. From the obtained serine hydrolase profiles, it can be observed that most samples share the same serine hydrolases (with a few exceptions), and that the serine hydrolase profiles in between the different sample sets are similar. Even though we found an interesting serine hydrolase – LYPLAL1 – that is higher in ATGL overexpressing compared to ATGL lacking cell lines, more experiments are needed to determine whether this is actually the enzyme we are looking for.

Perspectives

For further ABPP experiments, a new TEV linker will be generated and employed with the cleavage site further away from the enzyme and thus actually be cleavable in order to perform the desired specific elution. Additionally, the ABPP workflow can be employed on 3D-cultured cells, providing a more physiological model of cells as compared to 2D-cultured cells. In order to confirm the higher levels of LYPLAL1 in ATGL overexpressing cell lines immunoblotting with LYPLAL1 antibody or targeted mass spectrometry should be performed.

Another possibility for future experiments would be to change the binding groups of the ABP in a way to be more selective towards acyltransferases rather than hydrolases by designing the probe in a way to mimic an acyltransferase substrate such as Acyl-CoA.

References

1. Bray, F. *et al.* Global cancer statistics 2018: GLOBOCAN estimates of incidence and mortality worldwide for 36 cancers in 185 countries. *CA. Cancer J. Clin.* **68**, 394–424 (2018).
2. Ritchie, H. & Rosner, M. Causes of Death. *Our World in Data* (2018). Available at: https://ourworldindata.org/causes-of-death. (Accessed: 19th July 2019)
3. Yixin Yao, W. D. & WHO. *WHO | World Cancer Report 2014*. *Who* **5**, (2014).
4. Alberg, A. J., Brock, M. V., Ford, J. G., Samet, J. M. & Spivack, S. D. Epidemiology of Lung Cancer 3rd ed : American College of Chest Physicians Evidence-Based Clinical Practice Guidelines. 1–29 (2013). doi:10.1378/chest.12-2345
5. Bhopal, A., Peake, M. D., Gilligan, D. & Cosford, P. Lung cancer in never-smokers: a hidden disease. *J. R. Soc. Med.* **112**, 269–271 (2019).
6. Sun, S., Schiller, J. H. & Gazdar, A. F. Lung cancer in never smokers - A different disease. *Nat. Rev. Cancer* **7**, 778–790 (2007).
7. Samet, J. M. *et al.* Lung Cancer in Never Smokers: Clinical Epidemiology and Environmental Risk Factors. *Clin. Cancer Res.* **15**, 5626–5645 (2009).
8. Smolle, E. & Pichler, M. Non-Smoking-Associated Lung Cancer : A Distinct Entity in Terms of Tumor Biology , Patient Characteristics and Impact of Hereditary Cancer Predisposition. *Cancers (Basel).* 13–17 (2019). doi:10.3390/cancers11020204
9. Inamura, K. Lung Cancer: Understanding Its Molecular Pathology and the 2015 WHO Classification. *Front. Oncol.* **7**, 1–7 (2017).
10. Travis, W. D. *et al.* The 2015 World Health Organization Classification of Lung Tumors. *J. Thorac. Oncol.* **10**, 1243–1260 (2015).
11. Kenfield, S. A., Wei, E. K., Stampfer, M. J., Rosner, B. A. & Colditz, G. A. Comparison of Aspects of Smoking Among Four Histologic Types of Lung Cancer. *Tob Control.* **17**, 198–204 (2008).
12. Yalcin, E. & Monte, S. De. Tobacco nitrosamines as culprits in disease: mechanisms reviewed. **72**, 107–120 (2017).
13. De Sousa, V. M. L. & Carvalho, L. Heterogeneity in Lung Cancer. *Pathobiology* **85**, 96–107 (2018).
14. Henry, N. L. & Hayes, D. F. Cancer biomarkers. *Mol. Oncol.* **6**, 140–146 (2012).
15. Hanahan, D. & Weinberg, R. A. The Hallmarks of Cancer. *Cell* **100**, 57–70 (2000).
16. Caldas, C. & Venkitaraman, A. R. Tumor Suppressor Genes. *Ref. Modul. Life Sci.* 3 (2016). doi:10.1016/b978-0-12-809633-8.07316-7
17. Haschek, W. M., Rousseaux, C. G. & Wallig, M. A. Manifestations of Toxic Cell Injury : Cell Injury /Death and Chemical Carcinogenesis. in (2010). doi:10.1016/B978-0-12-370469-6.00002-7
18. Shortt, J. & Johnstone, R. W. Oncogenes in Cell Survival and Cell Death. *Cold Spring Harb. Perspect. Biol.* 1–10 (2012).
19. Hanahan, D. & Weinberg, R. A. Hallmarks of cancer: the next generation. *Cell* **144**, 646–74 (2011).
20. Fouad, Y. A. & Aanei, C. Revisiting the hallmarks of cancer. *Am. J. Cancer Res.* **7**, 1016–1036 (2017).
21. Sherr, C. J. & Mccormick, F. The RB and p53 pathways in cancer. *Cancer Cell* **2**, 103–112 (2002).
22. Williams, A. B. & Schumacher, B. p53 in the DNA-Damage-Repair Process. *Cold Spring Harb. Perspect. Biol.* 1–15 (2016).
23. Wong, R. S. Y. Apoptosis in cancer : from pathogenesis to treatment. *J. Exp. Clin. Cancer Res.* **30**, 87 (2011).
24. Jafri, M. A., Ansari, S. A., Alqahtani, M. H. & Shay, J. W. Roles of telomeres and telomerase in cancer , and advances in telomerase- targeted therapies. *Genome Med.* (2016). doi:10.1186/s13073-016-0324-x
25. Yao, Y. & Dai, W. Genomic Instability and Cancer. *J Carcinog Mutagen* **5**, 1–3 (2014).
26. Shimada, M. & Nakanishi, M. DNA damage checkpoints and cancer. *J Mol Hist* 253–260 (2006). doi:10.1007/s10735-006-9039-4
27. Tao, W. The Mitotic Checkpoint in Cancer Therapy. *Cell Cycle* **4101**, (2005).
28. Man, Y. *et al.* Tumor-Infiltrating Immune Cells Promoting Tumor Invasion and Metastasis : Existing Theories. *J. Cancer* **4**, (2013).
29. Itoh, Y. & Nagase, H. Matrix metalloproteinases in cancer. *Essays Biochem.* **38**, 21–36 (2002).
30. Lorusso, G. & Rüegg, C. New insights into the mechanisms of organ-specific breast cancer metastasis. *Semin. Cancer Biol.* **22**, 226–233 (2012).

31. Yang, Y., Sun, M., Wang, L. & Jiao, B. HIFs, Angiogenesis, and Cacner. *J. Cell. Biochem.* 967–974 (2012). doi:10.1002/jcb.24438

32. Fraisl, P., Mazzone, M., Schmidt, T. & Carmeliet, P. Regulation of Angiogenesis by Oxygen and Metabolism. *Dev. Cell* **16**, 167–179 (2009).

33. Pavlova, N. N. & Thompson, C. B. The emerging hallmarks of cancer metabolism. *Cell Metab* **23**, 27–47 (2016).

34. Warburg, B. Y. O., Wind, F. & Negelein, E. The Metabolism of Tumors in the Body. *J. Gen. Physiol.* **8**, 519–530 (1927).

35. Commisso, C. *et al.* Macropinocytosis of protein is an amino acid supply route in Ras-transformed cells. *Nature* **497**, 633–637 (2013).

36. Long, J. *et al.* Lipid metabolism and carcinogenesis, cancer development. *Am. J. Cancer Res.* **8**, 778–791 (2018).

37. Currie, E., Schulze, A., Zechner, R., Walther, T. C. & Farese, R. V. Cellular Fatty Acid Metabolism and Cancer. **18**, 153–161 (2013).

38. Munir, R., Lisec, J., Swinnen, J. V & Zaidi, N. Lipid metabolism in cancer cells under metabolic stress. *Br. J. Cancer* (2019). doi:10.1038/s41416-019-0451-4

39. Santos, C. R. & Schulze, A. Lipid metabolism in cancer. *FEBS J.* **279**, 2610–2623 (2012).

40. Beloribi-djefa, S., Vasseur, S. & Guillaumond, F. Lipid metabolic reprogramming in cancer cells. *Oncogenesis* (2016). doi:10.1038/oncsis.2015.49

41. Bozza, P. T. & Viola, J. P. B. Lipid droplets in inflammation and cancer. *Prostaglandins, Leukot. Essent. Fat. Acids* **82**, 243–250 (2010).

42. Abramczyk, H., Surmacki, J. M., Kopec, M. & Olejnik, A. The role of lipid droplets and adipocytes in cancer. Raman imaging of cell cultures: MCF10A, MCF7, MDA-MB-231 compared to adipocytes in cancerous human breast tissue. *Analyst* (2015). doi:10.1039/c4an01875c

43. Tansey, J. T., Sztalryd, C., Hlavin, E. M., Kimmel, A. R. & Londos, C. The Central Role of Perilipin A in Lipid Metabolism and Adipocyte Lipolysis. *Life* **56**, 379–385 (2004).

44. Olzmann, J. A. & Carvalho, P. Dynamics and functions of lipid droplets. *Nat. Rev. Mol. Cell Biol.* doi:10.1038/s41580-018-0085-z

45. Zhang, X. *et al.* Inhibition of intracellular lipolysis promotes human cancer cell adaptation to hypoxia. *Elife* 1–24 (2017).

46. Onal, G., Kutlu, O., Gozuacik, D. & Dokmeci Emre, S. Lipid Droplets in Health and Disease. *Lipids Health Dis.* **16**, 1–15 (2017).

47. Lass, A., Zimmermann, R., Oberer, M. & Zechner, R. Lipolysis - A highly regulated multi-enzyme complex mediates the catabolism of cellular fat stores. *Prog. Lipid Res.* **50**, 14–27 (2011).

48. Lord, C. C. & Brown, J. M. Distinct roles for alpha-beta hydrolase domain 5 (ABHD5/CGI-58) and adipose triglyceride lipase (ATGL/PNPLA2) in lipid metabolism and signaling. *Adipocyte* 123–131 (2012).

49. VandeKopple, M. J. *et al.* HILPDA regulates lipid metabolism, lipid droplet abundance, and response to microenvironmental stress in solid tumors. *Mol. Cancer Res.* (2019). doi:10.1158/1541-7786.MCR-18-1343

50. Zechner, R., Kienesberger, P. C., Haemmerle, G. & Zimmermann, R. Adipose triglyceride lipase and the lipolytic catabolism of cellular fat stores. *J. Lipid Res.* **50**, (2009).

51. Zhang, H. *et al.* PEDF and PEDF-derived peptide 44mer stimulate cardiac triglyceride degradation via ATGL. *J. Transl. Med.* 1–12 (2015). doi:10.1186/s12967-015-0432-1

52. Das, S. K. *et al.* Adipose Triglyceride Lipase Contributes to Cancer-Associated Cachexia. *Science (80-.).* **333**, (2011).

53. Arner, P. & Langin, D. Lipolysis in lipid turnover , cancer cachexia , and obesity-induced insulin resistance. *Trends Endocrinol. Metab.* **25**, 255–262 (2014).

54. Schreiber, R., Xie, H. & Schweiger, M. Of mice and men: The physiological role of adipose triglyceride lipase. *Mol. Cell Biol. Lipids* **1864**, 880–899 (2019).

55. Zaidi, N. *et al.* Lipogenesis and lipolysis: the pathways exploited by the cancer cells to acquire fatty acids. *Prog Lipid Res* **52**, 585–589 (2013).

56. Tirinato, L. *et al.* An Overview of Lipid Droplets in Cancer and Cancer Stem Cells. *Stem Cells Int.* **2017**, (2017).

57. Haemmerle, G. *et al.* Loss of adipose triglyceride lipase is associated with human cancer and induces mouse pulmonary neoplasia. *Oncotarget* **7**, (2016).

58. Vegliante, R., Di Leo, L., Ciccarone, F. & Ciriolo, M. R. Hints on ATGL implications in cancer: Beyond bioenergetic clues. *Cell Death Dis.* **9**, (2018).

59. Di Leo, L. *et al.* Forcing ATGL expression in hepatocarcinoma cells imposes glycolytic rewiring through PPAR- α / p300-mediated acetylation of. *Oncogene* 1860–1875 (2019). doi:10.1038/s41388-018-0545-0

60. Becerra, P. S. & Notario, V. The effects of PEDF on cancer biology: mechanisms of action and therapeutic potential. *Nat Rev Cancer* **13**, 258–271 (2013).

61. Frühbeck, G., Mendez-Gimenez, L., Fernandez-Formoso, J.-A., Fernandez, S. & Rodriguez, A. Regulation of adipocyte lipolysis. *Nutr. Res. Rev.* 63–93 (2014). doi:10.1017/S095442241400002X

62. Nomura, D. K. *et al.* Monoacylglycerol lipase regulates a fatty acid network that promotes cancer pathogenesis. *Cell* **140**, 49–61 (2011).

63. Nieman, K. M. *et al.* Adipocytes promote ovarian cancer metastasis and provide energy for rapid tumor growth. *Nat. Med.* **17**, (2011).

64. Yang, D. *et al.* Utilization of adipocyte-derived lipids and enhanced intracellular trafficking of fatty acids contribute to breast cancer progression. *Cell Commun. Signal.* **16**, 1–12 (2018).

65. Zagani, R., El-assaad, W., Gamache, I. & Teodoro, J. G. Inhibition of adipose triglyceride lipase (ATGL) by the putative tumor suppressor G0S2 or a small molecule inhibitor attenuates the growth of cancer cells. *Oncotarget* **6**, (2015).

66. Mayer, N. *et al.* Development of small molecule inhibitors targeting adipose triglyceride lipase. *Nat Chem Biol* **9**, 1–13 (2014).

67. Die Österreichische Forschungsförderungsgesellschaft. FFG Projektdatenbank - Atglistatin - Preclinical Development of Small Molecule Inhibitors Targeting Human Adipose Triglyceride Lipase. Available at: https://projekte.ffg.at/projekt/1831216. (Accessed: 26th July 2019)

68. Tomin, T. *et al.* Deletion of Adipose Triglyceride Lipase Links Triacylglycerol Accumulation to a More-Aggressive Phenotype in A549 Lung Carcinoma Cells. *J. Proteome Res.* **17**, 1415–1425 (2018).

69. Long, J. Z. & Cravatt, B. F. The Metabolic Serine Hydrolases and Their Functions in Mammalian Physiology and Disease. *Chem Rev* (2011). doi:10.1371/journal.pone.0178059

70. Bender, M. L. & Kezdy, F. J. Mechanism of Action of Proteolytic Enzymes. *Annu. Rev. Biochem.* (1964).

71. Blow, D. M. Structure and Mechanism of Chymotrypsin. *Acc. Chem. Res.* **678**, 672–678 (1976).

72. Polgar, L. Catalytic Mechanisms of Serine and Threonine Peptidases. in *Handbook of Proteolytic Enzymes* 2524–2534 (2013). doi:10.1016/B978-0-12-382219-2.00560-3

73. Dodson, G. & Wlodawer, A. Catalytic triads and their relatives. *Elsevier Sci.* **0004**, 347–352 (1998).

74. Ollis, D. L. *et al.* The alpha/beta hydrolase fold. *Protein Eng.* (1992). doi:10.1093/protein/5.3.197

75. Lord, C. C., Thomas, G. & Brown, J. M. Mammalian alpha beta hydrolase domain (ABHD) proteins: lipid metabolizing enzymes at the interface of cell signaling and energy metabolism. *Biochim. Biophys. Acta* **1831**, 792–802 (2016).

76. Sugiura, T. & Waku, K. 2-Arachidonoylglycerol and the cannabinoid receptors. *Chem. Phys. Lipids* **108**, 89–106 (2000).

77. Wang, D. *et al.* Human carboxylesterases: a comprehensive review. *Acta Pharm. Sin. B* **8**, 699–712 (2018).

78. Blankman, J. L., Simon, G. M. & Cravatt, B. F. A Comprehensive Profile of Brain Enzymes that Hydrolyze the Endocannabinoid 2-Arachidonoylglycerol. *Chem. Biol.* **14**, 1347–1356 (2007).

79. Botos, I. & Wlodawer, A. The expanding diversity of serine hydrolases. *Curr. Opin. Struct. Biol.* **17**, 683–690 (2007).

80. Ishida, T. & Kato, S. Theoretical Perspectives on the Reaction Mechanism of Serine Proteases : The Reaction Free Energy Profiles of the Acylation Process. *J. Am. Chem. Soc.* 12035–12048 (2003). doi:10.1021/ja021369m

81. Simon, G. M. & Cravatt, B. F. Activity-based Proteomics of Enzyme Superfamilies: Serine Hydrolases as a Case Study. *J. Biol. Chem.* **285**, 11051–11055 (2010).

82. Anderson, N. L. & Anderson, N. G. Proteome and Proteomics: new technologies, new concepts, and new words. *Electrophoresis* **19**, 1853–61 (1998).

83. Clark, D. P. & Pazdernik, N. J. Proteomics: The Global Analysis of Proteins. in *Molecular Biology* 459–487 (Academic Press Elsevier, 2013).

84. Willyard, C. New human gene tally reignites debate. *Nature* **558**, 354–355 (2018).

85. Pertea, M. The Human Transcriptome: An Unfinished Story. *Genes (Basel).* 344–360 (2012). doi:10.3390/genes3030344

86. Jensen, O. N. Modification-specific proteomics: characterization of post-translational modifications by mass spectrometry. *Curr. Opin. Chem. Biol.* **8**, 33–41 (2004).

87. Harper, J. W. & Bennett, E. J. Proteome complexity and the forces that drive proteome imbalance. doi:10.1038/nature19947

88. Overview of Post-Translational Modifications (PTMs). Available at: https://www.thermofisher.com/at/en/home/life-science/protein-biology/protein-biology-learning-center/protein-biology-resource-library/pierce-protein-methods/overview-post-translational-modification.html#/legacy=www.piercenet.com. (Accessed: 2nd August 2019)

89. Maithal, K. Proteomics-A new player in the post-genomic era. *Indian J. Biochem. Biophys.* **39**, 291–302 (2002).

90. Karpievitch, Y. V, Polpitiya, A. D., Anderson, G. A., Smith, R. D. & Dabney, A. R. Liquid Chromatography Mass Spectrometry-Based Proteomics: Biological and Technological Aspects. *Ann. Appl. Stat.* **4**, 1797–1823 (2011).

91. Schittmayer, M. & Birner-Gruenberger, R. Lipolytic Proteomics. *Mass Spectrom. Rev.* 570–582 (2012). doi:10.1002/mas

92. Schittmayer, M. & Birner-Gruenberger, R. Functional proteomics in lipid research: Lipases , lipid droplets and lipoproteins. *J. Proteomics* **72**, 1006–1018 (2009).

93. Liu, Y., Patricelli, M. P. & Cravatt, B. F. Activity-based protein profiling: The serine hydrolases. *PNAS* **96**, 14694–14699 (1999).

94. Birner-Gruenberger, R. *et al.* The Lipolytic Proteome of Mouse Adipose Tissue. *Mol. Cell. Proteomics* 1710–1717 (2005). doi:10.1074/mcp.M500062-MCP200

95. Viertler, M., Schittmayer, M. & Birner-Gruenberger, R. Activity based subcellular resolution imaging of lipases. *Bioorg. Med. Chem.* **20**, 628–632 (2012).

96. Greenbaum, D., Medzihradszky, K. F., Burlingame, A. & Bogyo, M. Epoxide electrophiles as activity-dependent cysteine protease profiling and discovery tools. *Chem. Biol.* **7**, 569–581 (2000).

97. Kumar, S. *et al.* Activity-based probes for protein tyrosine phosphatases. *PNAS* **101**, 7943–7948 (2004).

98. Schmidinger, H. *et al.* Novel Fluorescent Phosphonic Acid Esters for Discrimination of Lipases and Esterases. *ChemBioChem* **16**, 1776–1781 (2005).

99. Kolb, H. C., Finn, M. G. & Sharpless, K. B. Click Chemistry: Diverse Chemical Function from a Few Good Reactions. *Angew. Chemie* **40**, 2004–2021 (2001).

100. Liang, L. & Astruc, D. The copper(I)-catalyzed alkyne-azide cycloaddition (CuAAC) “click” reaction and its applications. An overview. *Coord. Chem. Rev.* **255**, 2933–2945 (2011).

101. Rostovtsev, V. V, Green, L. G., Fokin, V. V & Sharpless, K. B. A Stepwise Huisgen Cycloaddition Process: Copper(I)-Catalyzed Regioselective “Ligation” of Azides and Terminal Alkynes. *Angew. Chemie* **41**, (2002).

102. Zheng, T., Rouhanifard, S. H., Jalloh, A. S. & Wu, P. Click Triazoles for Bioconjugation. *Top Heterocycl. Chem.* **28**, 163–183 (2012).

103. Kennedy, D. C. *et al.* Cellular Consequences of Copper Complexes Used To Catalyze Bioorthogonal Click Reactions. *J. Am. Chem. Soc.* 17993–18001 (2011).

104. Hang, H. C., Yu, C., Kato, D. L. & Bertozzi, C. R. A metabolic labeling approach toward proteomic analysis of mucin-type O-linked glycosylation. *PNAS* **100**, 14846–14851 (2003).

105. Sletten, E. M. & Bertozzi, C. R. From Mechanism to Mouse: A Tale of Two Bioorthogonal Reactions. *Accounts* **44**, 666–676 (2011).

106. Saxon, E. & Bertozzi, C. R. Cell Surface Engineering by a Modified Staudinger Reaction. *Science (80-.).* **287**, 2007–2010 (2000).

107. Agard, N. J., Prescher, J. A. & Bertozzi, C. R. A Strain-Promoted [3 + 2] Azide - Alkyne Cycloaddition for Covalent Modification of Biomolecules in Living Systems. *J. Am. Chem. Soc.* **126**, 15046–15047 (2004).

108. Staudinger, H. & Meyer, J. Über neue organische Phosphorverbindungen III. Phosphinmethylenderivate und Phosphinimine. (1919).

109. Shadmehr, M. Design and Synthesis of Triazabutadiene-based Fluorogenic Probes for Tyrosine Specific Labeling of Proteins. (University of Arizona, 2019). doi:10.13140/RG.2.2.29711.23209

110. Codelli, J. A., Baskin, J. M., Agard, N. J. & Bertozzi, C. R. Second-Generation Difluorinated Cyclooctynes for Copper-Free Click Chemistry. *J. Am. Chem. Soc.* 11486–11493 (2008).

111. Ning, X., Guo, J., Wolfert, M. A. & Boons, G. Visualizing Metabolically Labeled Glycoconjugates of Living Cells by Copper-Free and Fast Huisgen Cycloadditions. *Angew. Chemie* 2253–2255 (2008). doi:10.1002/anie.200705456

112. Jewett, J. C., Sletten, E. M. & Bertozzi, C. R. Rapid Cu-Free Click Chemistry with Readily Synthesized Biarylazacyclooctynones. *J. Am. Chem. Soc.* 3688–3690 (2010).

113. Sletten, E. M. & Bertozzi, C. R. A Hydrophilic Azacyclooctyne for Cu-Free Click Chemistry. *Org. Lett.* **10**, 3097–3099 (2008).

114. Yao, J. Z. *et al.* Fluorophore Targeting to Cellular Proteins via Enzyme-Mediated Azide Ligation and Strain-Promoted Cycloaddition. *J. Am. Chem. Soc.* (2012). doi:10.1021/ja208090p

115. Snyder, L. R., Kirkland, J. J. & Dolan, J. W. *Introduction to Modern Liquid Chromatography*. (2011).

116. Catherman, A. D., Skinner, O. S. & Kelleher, N. L. Top Down proteomics: Facts and perspectives. *Biochem. Biophys. Res. Commun.* **445**, 683–693 (2014).

117. Shi, Y., Xiang, R., Horváth, C. & Wilkins, J. A. The role of liquid chromatography in proteomics. *J. Chromatogr. A* **1053**, 27–36 (2004).

118. Hage, D. S. Chromatography. in *Principles and Applications of Clinical Mass Spectrometry* (eds. Rifai, N., Horvath, A. R. & Wittwer, C. T.) 216 (Elsevier, 2018).

119. Han, X., Aslanian, A. & Yates, J. R. Mass Spectrometry for Proteomics. *Curr. Opin. Chem. Biol.* **12**, 483–490 (2009).

120. Michalski, A. *et al.* Mass Spectrometry-based Proteomics Using Q Exactive, a High-performance Benchtop Quadrupole Orbitrap Mass Spectrometer. *Mol. Cell. Proteomics* **10**, (2011).

121. Gross, H. *Massenspektrometrie*. (Springer Spektrum, 2019).

122. Fenn, J. B. *et al.* Electrospray Ionization for Mass Spectrometry of Large Biomolecules. *Science (80-.).* **246**, 64–71 (1989).

123. Bruins, A. P. Mechanistic aspects of electrospray ionizatoin. *J. Chromatogr. A* **794**, 345–357 (1998).

124. Domon, B. & Aebersold, R. Mass Spectrometry and Protein Analysis. *Tools Biochem.* **312**, 212–218 (2006).

125. Angel, T. E. *et al.* Mass spectrometry based proteomics: existing capabilities and future directions. *Chem. Soc. Rev.* **41**, 3912–3928 (2012).

126. Zhang, Z., Stenoien, D. L. & Paša-Tolić, L. High-throughput proteomics. *Annu. Rev. Anal. Chem.* **7**, 427–454 (2014).

127. Cox, J. & Mann, M. MaxQuant enables high peptide identification rates, individualized p.p.b.-range mass accuracies and proteome-wide protein quantification. *Nat. Biotechnol.* **26**, 1367–1372 (2008).

128. Cox, J. *et al.* Accurate proteome-wide label-free quantification by delayed normalization and maximal peptide ratio extraction, termed MaxLFQ. *Mol. Cell. Proteomics* **13**, 2513–2526 (2014).

129. Tyanova, S. *et al.* The Perseus computational platform for comprehensive analysis of (prote)omics data. *Nat. Methods* **13**, 731–740 (2016).

130. Alves, G. & Yu, Y.-K. Improving Peptide Identification Sensitivity in Shotgun Proteomics by Stratification of Search Space. *J. Proteome Res.* **12**, 2571–2581 (2013).

131. Knudsen, G. M. & Chalkley, R. J. The effect of using an inappropriate protein database for proteomic data analysis. *PLoS One* **6**, (2011).

132. Rengachari, S. *et al.* Conformational plasticity and ligand binding of bacterial monoacylglycerol lipase. *J. Biol. Chem.* **288**, 31093–31104 (2013).

133. Tomin, T. Dissertation Role of adipose triglyceride lipase (ATGL) in cancer metabolism submitted by Doctor of Philosophy (PhD) Medical University of Graz. (2018).

134. Bryzgunova, O. *et al.* A reliable method to concentrate circulating DNA. *Anal. Biochem.* **408**, 354–356 (2011).

135. Law, S. H. *et al.* An updated review of lysophosphatidylcholine metabolism in human diseases. *Int. J. Mol. Sci.* **20**, 1–24 (2019).

136. Jiang, Y., Morley, K. L., Schrag, J. D. & Kazlauskas, R. J. Different Active-Site Loop Orientation in Serine Hydrolases versus Acyltransferases. *ChemBioChem* **12**, 768–776 (2011).

137. Bürger, M. *et al.* Crystal structure of the predicted phospholipase LYPLAL1 reveals unexpected functional plasticity despite close relationship to acyl protein thioesterases. *J. Lipid Res.* **53**, 43–50 (2012).

138. Watson, R. A. *et al.* Lyplal1 is dispensable for normal fat deposition in mice. *Dis. Model. Mech.* 1481–1488 (2017). doi:10.1242/dmm.031864

List of Figures

List of Tables